



PhD-FSTM-2023-005
The Faculty of Science, Technology and Medicine

DISSERTATION

Defence held on 23/02/2023 in Luxembourg

to obtain the degree of

DOCTEUR DE L'UNIVERSITÉ DU LUXEMBOURG EN BIOLOGIE

by

Redouane SLIMANI

Born on 13th of November 1989 in Levallois-Perret (France)

STUDY OF EARLY MELANOMA BRAIN METASTASIS MECHANISMS USING IN VITRO AND IN VIVO MODELS OF TUMOR INVASION

Dissertation defence committee

Dr Michel Mittelbronn, dissertation supervisor

*Head of the National Centre of Pathology and Luxembourg Centre of Neuropathology (LCNP), Luxembourg Health Laboratories (LNS), Luxembourg Institute of Health (LIH)
Affiliated Professor, Université du Luxembourg*

Dr Ulrike Naumann

*Gruppenleiter Forschung Labor für Molekulare Neuro-Onkologie im Hertie-Institut
Professor, Universitätsklinikum Tübingen*

Dr Stephanie Kreis, Chair

*Head of the Doctoral School in Science and Engineering (DSSE)
Associate professor, Université du Luxembourg*

Dr Kavi Devraj

Associate Professor, Hyderabad, Telangana, India

Dr Felix Kleine-Borgmann, Vice Chair

Scientist and Physician, Medical Faculty Saarland University, Luxembourg Institute of Health (LIH), Laboratoire National de Santé (LNS), Luxembourg Center of Neuropathology (LCNP)



A dissertation by
Redouane SLIMANI
submitted to the University of Luxembourg
in partial fulfilment of the requirements for the degree of

DOCTOR of PHILOSOPHY

Approved by the Dissertation Defense Committee:

Chair of committee: Prof. Dr. Stephanie KREIS

Committee members: Prof. Dr. Ulrike NAUMANN

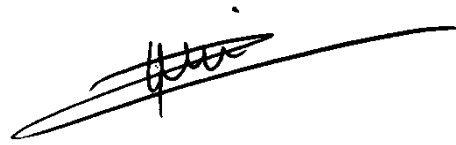
Dr. Kavi DEVRAJ

Dr. Felix KLEINE-BORGMANN

Supervisor: Prof. Dr. Michel MITTELBRONN

Affidavit

I hereby confirm that the PhD thesis entitled “STUDY OF EARLY MELANOMA BRAIN METASTASIS MECHANISMS USING IN VITRO AND IN VIVO MODELS OF TUMOR INVASION” has been written independently and without any other sources than cited. All necessary ethical approvals have been obtained in accordance with the Luxembourgish law (on the use of clinical samples and on the Care and Use of laboratory animals, where applicable).

A handwritten signature in black ink, appearing to read 'Redouane Slimani', is written over a long, horizontal, slightly curved line that serves as a baseline for the signature.

Luxembourg, 30 November 2022

Redouane Slimani

Acknowledgments

My gratitude goes first of all to Prof. Dr. Michel Mittelbronn, who accepted to supervise my research and who allowed me to form myself as a young researcher by involving me in multiple projects. His demand for rigor and consistency as well as his remarks allowed me to methodically define the subject and to pursue my investigations to a point, I hope, that is satisfactory.

I would like to extend my sincere gratitude to Prof. Dr. Stephanie Kreis, Prof. Dr. Ulrike Naumann, and Dr. Kavi Devraj for having so generously accepted to be part of the thesis jury, for devoting their time and expertise to read and review my work. I thank them in advance for all their valuable contributions that will further enrich this research study.

I would like to address a special thanks to Dr. Felix Kleine-Borgmann, a wise mentor, as valuable as a colleague as he is a friend. I would like to express all my gratitude to him for his proofreading, his wise advice, his encouragement and his unfailing support as well as for our stimulating exchanges.

A very special thanks goes to Anaïs Carpentier and Vanessa Barthélémy who have put their expertise at my disposal while being always benevolent and encouraging.

I also wish to thank all the members of the LCNP group – Dr. Tanja Müller, Dr. Ann-Christin Hau, Dr. Victoria El Khoury, Dr. Katrin Frauenknecht, Dr. Manuel Buttini, Dr. Pierre Garcia, Dr. Kristopher Schmit, Dr. Tony Heurtaux, Dr. David Bouvier and Jean-Jacques Gérardy, as well as all the members of the DoCR led by Dr. Simone Niclou at LIH.

I would like to warmly thank my friends and fellow doctoral students – Dr. Yolanda Pires, Dr. Carina Fabian, Dr. Lia Pinto Marzetti, Andrea Scaffidi, Alice Benoit, Frida Lind-Holm Mogensen, Lara Hass – for their attentive listening, for their benevolent questions about my

work, for the exchanges that nourished my reflection and helped me in the elaboration of my thoughts. I thank them for having contributed to the intellectual emulation climate which was a source of perseverance and additional motivation.

I would like to warmly thank my family-in-law, Ornella, Christian and my little Nad who encouraged and supported me in my efforts.

I do not forget the exciting hours spent in the presence of Prof. Dr. Frank Hertel, either by observing him at work or during our exchanges.

Cristabella, this thesis is dedicated to you. It would have had neither meaning nor existence without you. For the journey we have shared so far, for everything that has made us what we are today, I will never thank you enough.

To Cristabella,

“With you I realized that I had found the person who could
share my heights without being horrified by my
abysses” – Fabrizio de André

Table of contents

PART I. INTRODUCTION	1
1. BLOOD-BRAIN BARRIER – BIOLOGICAL AND THEORETICAL BACKGROUND	2
1.1. NEUROVASCULAR UNIT AND BLOOD-BRAIN BARRIER – AN OVERVIEW	2
1.2. CELLULAR AND FUNCTIONAL CONSTITUENTS OF THE BBB	5
1.3. OTHER CELLULAR CONSTITUENTS OF THE BBB	11
1.4. BBB – CHARACTERISTIC FEATURES OF A PHYSICAL BARRIER	14
1.5. BBB CROSSING AT THE CELLULAR AND MOLECULAR LEVELS	21
2. IN VITRO BBB MODELS	29
2.1. REPLICATING THE BBB IN VITRO	29
2.2. STATIC IN VITRO BBB MODELS	30
3. BRAIN METASTASIS	33
4. MELANOMA.....	36
4.1. CLASSIFICATION OF CUTANEOUS MELANOMA	36
4.2. MELANOMA INCIDENCE AND PREVALENCE	37
4.3. RISK FACTORS FOR MELANOMA SKIN CANCER	38
4.4. BRAIN METASTASIS IN MELANOMA	39
4.5. RISK FACTORS FOR BRAIN METASTASIS IN MELANOMA.....	40
4.6. THERAPEUTIC STRATEGIES FOR BRAIN METASTASIS	41
5. BBB DISRUPTION	42
6. AIM OF THE THESIS.....	45
PART II. MATERIALS AND METHODS	47
1. IN VITRO MODEL.....	48

1.1. CELL CULTURE	48
1.2. TESTING OF CULTURE MEDIA	48
1.3. PROLIFERATION ASSAY.....	49
1.4. MIGRATION AND INVASION ASSAY	49
1.5. hicBBB FORMATION PROTOCOL	50
1.6. TIME-LAPSE OBSERVATION OF TUMOR CELLS CROSSING THE hicBBB MODEL...	52
1.7. hicBBB IN VITRO MODEL PERMEABILITY TEST	52
1.8. FACS SORTING OF FLUORESCENT TUMOR CELLS	53
1.9. ANTIBODY ARRAY	53
1.10. IMMUNOFLUORESCENCE	54
1.11. IMMUNOCYTOCHEMISTRY	55
1.12. TEER MEASUREMENT WITH THE CELLZSCOPE2	55
1.13. ELECTRON MICROSCOPY	56
1.14. 3'-END RNA-Seq.....	58
1.15. STATISTICAL ANALYSIS	60
2. IN VIVO MODEL	61
2.1. LEFT HEART VENTRICLE INJECTION ASSISTED BY ULTRASOUND DEVICE	61
2.2. IMMUNOFLUORESCENCE BRAIN SLICES SCREENING	62
PART III. RESULTS	64
1. hicBBB CELLS IDENTIFICATION AND DESCRIPTION	65
1.1. hicBBB CELLS IDENTIFICATION BY IF	65
2. TUMOR MODEL IDENTIFICATION	69
2.1. IDENTIFICATION OF THE A375 CELL LINE BY ICC	69
2.2. hicBBB CELLS AND A375 MELANOSOME OBSERVATION BY ELECTRON MICROSCOPY	71

3. MIGRATORY AND INVASIVE POTENTIAL OF THE A375 CELL LINE AND PROLIFERATION POTENTIAL OF THE CELLS FROM THE IN VITRO hicBBB MODEL AND FROM THE A375 CELL LINE	74
4. MEDIUM DETERMINATION FOR THE hicBBB MODEL	77
5. FORMATION OF THE hicBBB MODEL.....	81
5.1. OBSERVATION OF THE hicBBB BY CONFOCAL MICROSCOPY.....	81
5.2. TEER MEASUREMENT OF THE NEWLY FORMED hicBBB	82
5.3. PERMEABILITY OF THE hicBBB USING A FLUORESCENT TRACER	83
6. EXPOSURE OF THE hicBBB MODEL TO TUMOR CELLS.....	86
6.1. TEER MEASUREMENT OF THE hicBBB WHEN EXPOSED TO A375 CELLS.....	86
6.2. MEASUREMENT OF THE hicBBB PERMEABILITY WHEN EXPOSED TO A375 CELLS ..	87
6.3. IN VITRO TRACKING OF A375 CELLS CROSSING THE hicBBB MODEL	88
7. OBSERVATION BY ANTIBODY ARRAY OF THE hicBBB REACTION TO THE PRESENCE OR ABSENCE OF TUMOR CELLS	91
7.1. MMP ARRAY EXPOSED TO CONDITIONED MEDIUM	91
7.2. ANGIOGENESIS ARRAY EXPOSED TO CONDITIONED MEDIUM	92
7.3. CYTOKINE ARRAY EXPOSED TO CONDITIONED MEDIUM	95
8. RESISTANT CELLS AND FLOW CYTOMETRY SORTING.....	98
9. 3' RNA-Seq OF A375 CELLS THAT CROSS THE hicBBB MODEL	101
9.1. PCA CLUSTERING OF SAMPLES	101
10. IN VIVO MODEL OF THE METASTASIS PROCESS TO THE BRAIN.....	103
10.1. ULTRASOUND IMAGING OF AN INJECTION INTO THE LEFT VENTRICLE OF THE HEART.....	103
10.2. BRAIN SCREENING STRATEGY USING CONFOCAL MICROSCOPY.....	105
10.3. SAMPLE PREPARATION FOR EM IMAGING	107
10.4. EM OBSERVATION OF A MOUSE CONTROL SAMPLE	108
10.5. STEM OBSERVATION OF MOUSE BRAIN TISSUE INJECTED WITH A375 CELLS ...	108

PART IV. DISCUSSION AND OUTLOOK	111
1. IN VITRO hicBBB MODEL DISCUSSION.....	111
1.1. hicBBB MODEL FORMATION.....	112
1.2. IDENTIFICATION OF POTENTIAL A375 MARKERS AND DETECTION OF MELANOSOMES BY ELECTRON MICROSCOPY.....	113
1.3. hicBBB MODEL SUITABILITY ASSESSMENT.....	114
1.4. STUDY OF EARLY STAGE INVASION OF THE hicBBB BY TUMOR CELLS	116
1.5. hicBBB MODEL – CONCLUSION AND OUTLOOK.....	116
2. IN VIVO MODEL OF EARLY BRAIN INVASION OF BLOOD-BRAIN BARRIER	119
2.1. TRAINING FOR MODEL EXPLOITATION	119
2.2. INJECTION OF A375 CELLS AND DETECTION OF THEIR FLUORESCENT SIGNAL IN THE BRAIN	120
2.3. IN VIVO MODEL – CONCLUSION AND OUTLOOK.....	121
PART V. APPENDIX.....	123
1. DETAILS OF THE MEDIA COMPOSITION.....	124
2. ANTIBODY ARRAY DETAILS	125
3. INVASION POTENTIAL OF THE hicBBB CELL LINES.....	126
4. MEAN VALUES OF TEER MEASUREMENTS DURING 72 HOURS OF COCULTURE	127
5. EFFECT OF TNF α ON TEER	128
6. SAMPLES QC REPORT FOR 3'END mRNA-SEQUENCING.....	129
VI. REFERENCES.....	137
Publication bibliography.....	138

List of illustrations, figures, tables

<i>Figure 1 Max Lewandowsky during a brain surgical procedure</i>	3
<i>Figure 2 Schematic drawing of the transcellular and paracellular pathways in the BBB crossing process</i>	5
<i>Figure 3 Schematic illustration of endothelial cell tight junctions and adherens junctions</i>	16
<i>Figure 4 Schematic illustration of the diffusion of molecules and of their transport through the BBB</i>	28
<i>Figure 5 From melanocyte to melanoma metastasis: the pathway to the brain</i>	44
<i>Figure 6 Schematic illustration of the culture media testing</i>	49
<i>Figure 7 Schematic illustration of the hicBBB in vitro model formation protocol</i>	50
<i>Figure 8 Schematic representation of TEER measurement using the cellZscope2</i>	56
<i>Figure 9 Schematic representation of sample processing for electron microscopy</i>	58
<i>Figure 10 Schematic representation of the library preparation for the 3' mRNA-Seq from Lexogen</i>	59
<i>Figure 11 Schematic representation of the in vivo model of the metastatic process to the brain</i>	62
<i>Figure 12 Immunofluorescence identification of hCMEC/D3 cells in the in vitro hicBBB model</i>	66
<i>Figure 13 Immunofluorescence identification of SV40-HBVP cells in the in vitro hicBBB model</i>	67
<i>Figure 14 Immunofluorescence identification of SVGA cells in the in vitro hicBBB model</i> .	67
<i>Figure 15 Search for a specific A375 cell line marker</i>	70
<i>Figure 16 Scanning transmission electron microscope (STEM) observation of hCMEC/D3 cells and SV-40 HBVP cells</i>	72
<i>Figure 17 Scanning transmission electron microscope (STEM) observation of SVGA and A375 cells</i>	73

Figure 18 Migration potential of the A375 cell line	74
Figure 19 Invasion potential of the A375 cell line	75
Figure 20 Cell proliferation assessment of the in vitro hicBBB model and the A375 cell line	76
Figure 21 SVGA viability in a gradient of mixed media	77
Figure 22 SV40-HBVP viability in a gradient of mixed media	77
Figure 23 hCMEC/D3 viability in a gradient of mixed media	77
Figure 24 hicBBB cells viability in different media	78
Figure 25 Microscopic observation of the hicBBB Z-stack by IF	81
Figure 26 Assessment of hicBBB formation using TEER measurement	83
Figure 27 Changes in the permeability of the hicBBB model at different time points	84
Figure 28 Impact of the presence of A375 melanoma cells on the in vitro hicBBB model assessed by TEER	87
Figure 29 Impact of the presence of A375 melanoma cells on the in vitro hicBBB model assessed by permeability assay	87
Figure 30 Live in vitro tracking by confocal microscopy of A375 mCherry cells crossing the in vitro hicBBB model	89
Figure 31 3D fluorescent microscopic reconstruction of the hicBBB in the presence of A375 mCherry cells	90
Figure 32 Summary analysis of the MMP array exposed to hicBBB-conditioned medium in the presence or absence of A375 melanoma cells	91
Figure 33 Summary analysis of the angiogenesis array exposed to hicBBB-conditioned medium	93
Figure 34 Summary analysis of the angiogenesis array exposed to hicBBB-conditioned medium in the presence of A375 melanoma cells	93
Figure 35 Summary analysis of the cytokines array exposed to hicBBB-conditioned medium	95

Figure 36 Summary analysis of the cytokines array exposed to hicBBB-conditioned medium in the presence of A375 melanoma cells	95
Figure 37 Migration potential of A375 mono and double treatment-resistant cell lines ...	98
Figure 38 Invasion potential of A375 mono and double treatment-resistant cell lines	99
Figure 39 FACS sorting of treatment-resistant and non-treatment-resistant A375 melanoma cells that have crossed the in vitro hicBBB model	100
Figure 40 PCA of FACS-sorted A375 cell samples after 3' RNA-Seq	101
Figure 41 Description of the performing of an injection into the left ventricle of a mouse heart and verification of the needle placement using trypan blue	103
Figure 42 Ecographic images of the left ventricular area of a mouse heart before (left) and during (right) injection	105
Figure 43 Images captured by fluorescence confocal microscopy of a potential A375 mCherry cell identified in the brain parenchyma of a mouse 10 days after injection	106
Figure 44 Images captured by fluorescence confocal microscopy of a potential A375 mCherry cell identified in the brain parenchyma of a mouse 10 days after injection	107
Figure 45 STEM observation of a brain capillary in a control sample	108
Figure 46 STEM observation of potential melanoma cells after invasion of the capillaries in a mouse brain 10 days post injection	109
Figure 47 Invasion potential of the hicBBB cell lines	127
Figure 48 Mean values of TEER measurements during 72 hours of coculture	128
Figure 49 Disruption of hicBBB by TNFα	129
Figure 50 Disruption of hCMEC/D3 and SVGA coculture by TNFα	129

Table 1 Summary table of the different types of melanoma	37
Table 2 Antibody array reference table	54
Table 3 Antibody reference table for IF and WB	54
Table 4 Secondary antibody reference table	55
Table 5 Table of alternative compositions of the EM resins.....	57
Table 6 ab134004 Human MMP Antibody Array - Membrane (10 targets)	125
Table 7 ab133998 Human Cytokine Antibody Array Membrane (80 targets)	125
Table 8 ab134000 Human Angiogenesis Antibody Array - Membrane (20 targets).....	126
Table 9 ab211061 Human MAPK Phosphorylation Antibody Array (Membrane 17 Targets)	126

List of abbreviations

aa	Amino acid
AJ	Adherens junction
Ang-1	Angiopoietin-1
Angptl4	Angiopoietin-like protein 4
AP	Area postrema
BBB	Blood-brain barrier
BMEC	Brain microvascular endothelial cell
BRAFi	BRAF inhibitor
CBF	Cerebral blood flow
CEC	Cerebral endothelial cell
CLEM	Correlative light-electron microscopy
CLDN	Claudin
CMC	Cerebral microcirculation
CO	Cardiac output
CSF	Cerebrospinal fluid
CVR	Cerebrovascular resistance
Da	Dalton
EC	Endothelial cells
ECM	Extracellular matrix

EGM-2	Endothelial Cell Growth Medium-2 BulletKit
FAK	Focal adhesion kinase
FIB-SEM	Focused ion beam scanning electron microscope
FGF	Fibroblast growth factor
FN	Fibronectin
γ-GT	Gamma-glutamyltranspeptidase
GDNF	Glial cell line derived neurotrophic factor
GJ	Gap junctions
GLUT-1	Glucose transporter-1
hCMEC/D3	Immortalized human cerebral microvascular endothelial cells
hicBBB	Human immortalized cells blood-brain barrier
ICC	Immunocytochemistry
IF	Immunofluorescence
IGF	Insulin growth factor
IHC	Immunohistochemistry
ISF	Interstitial fluid
JAM	Junctional adhesion molecule
kDa	Kilodalton
MCT1	Monocarboxylate transporter 1
MITF	Microphthalmia-associated transcription factor

MS	Multiple sclerosis
NanoSIMS	Nanoscale secondary ion mass spectrometry
NBD	Nucleotide binding domains
NPC	Neural progenitor cell
NVU	Neurovascular unit
O.N.	Overnight
PCA	Principal component analysis
PFA	Paraformaldehyde
P-gp	P-glycoproteins
PLL	Poly-L-Lysine
PM	Pericytes medium
PRR	Pattern-recognition receptor
PV-1	Plasmalemmal vesicle associated protein
RFU	Raw fluorescence unit
RMT	Receptor-mediated transcytosis
RNA-Seq	RNA sequencing
SD	Standard deviation
SFO	Subfornical organ
STEM	Scanning transmission electron microscope
TEER	Transendothelial electrical resistance

TEM	Transendothelial migration
TGFβ	Transforming growth factor beta
TJ	Tight junction
TMD	Transmembrane domains
UVR	Ultraviolet radiation
VE	Vascular endothelial
VEGF	Vascular endothelial growth factor
VSMC	Vascular smooth muscle cells
WT	Wild Type
YS	Yolk sac
ZO	Zonula occludens

List of contributions

Dr. Felix KLEINE-BORGMANN	Animal protocol; electron microscope; confocal microscope
Anaïs CARPENTIER	Sample preparation for electron microscopy and imaging
LuxGen	3' RNA-Seq and data analysis

List of publications

1. Schumacher, Leonie; Slimani, Rédouane; Zimare, Laimdota; Ehlers, Jakob; Kleine Borgmann, Felix; Fitzgerald, Julia C. et al. (2023): TGF-Beta Modulates the Integrity of the Blood Brain Barrier In Vitro, and Is Associated with Metabolic Alterations in Pericytes. In *Biomedicines* 11 (1). DOI: 10.3390/biomedicines11010214.

Adaptation of the PBMVEC and HBVP cells coculture model from the laboratory of Prof. Dr. Ulrike Naumann to the CellZscope2 system; study of the impact of TGF β on pericytes as well as on the integrity of the *in vitro* model using TEER; production of coculture samples for the study of tight junctions by cryo-fracture electron microscopy.

2. Borgmann, Felix Kleine; Klamminger, Gilbert Georg; Mombaerts, Laurent; Klein, Karoline; Jelke, Finn; Mirizzi, Giulia et al. (2021): PATH-43. RAMAN SPECTROSCOPY AS A TOOL IN NEUROSURGERY. In *Neuro Oncol* 23 (Supplement 6), vi125-vi125.

Development of a standardized protocol for brain tumor analysis by Raman spectroscopy; measurement of fresh, fixed and frozen tissues using a Raman spectrometer; creation of an informative form to improve the communication between the operating theatre and the pathology department; development of a standardized procedural protocol for the analysis of the relevant visible chemical elements present in the data.

3. Jelke, Finn; Mirizzi, Giulia; Borgmann, Felix Kleine; Husch, Andreas; Slimani, Rédouane; Klamminger, Gilbert Georg et al. (2021): Intraoperative discrimination of native meningioma and dura mater by Raman spectroscopy. In *Scientific Reports* 11 (1), p. 23583. DOI: 10.1038/s41598-021-02977-7.

Development of a standardized protocol for brain tumor analysis by Raman spectroscopy; measurement of fresh, fixed and frozen tissues using a Raman spectrometer; creation of an informative form to improve the communication between the operating theatre and the pathology department; development of a standardized procedural protocol for the analysis of the relevant visible chemical elements present in the data.

4. Klamminger, Gilbert Georg; Gérardy, Jean-Jacques; Jelke, Finn; Mirizzi, Giulia; Slimani, Rédouane; Klein, Karoline et al. (2021): Application of Raman spectroscopy for detection of histologically distinct areas in formalin-fixed paraffin-embedded glioblastoma. In *Neuro Oncol Adv* 3 (1), vdab077. DOI: 10.1093/nojnl/vdab077.

Development of a standardized protocol for brain tumor analysis by Raman spectroscopy; measurement of fresh, fixed and frozen tissues using a Raman spectrometer; creation of an informative form to improve the communication between the operating theatre and the pathology department; development of a standardized procedural protocol for the analysis of the relevant visible chemical elements present in the data.

5. Klamminger, Gilbert Georg; Klein, Karoline; Mombaerts, Laurent; Jelke, Finn; Mirizzi, Giulia; Slimani, Rédouane et al. (2021): Differentiation of primary CNS lymphoma and glioblastoma using Raman spectroscopy and machine learning algorithms. In *Free Neuropathol* 2, p. 26. DOI: 10.17879/freeneuropathology-2021-3458.

Development of a standardized protocol for brain tumor analysis by Raman spectroscopy; measurement of fresh, fixed and frozen tissues using a Raman spectrometer; creation of an informative form to improve the communication between the operating theatre and the pathology department; development of a standardized procedural protocol for the analysis of the relevant visible chemical elements present in the data.

6. Klamminger, Gilbert Georg; Mombaerts, Laurent; Klein, Karoline; Jelke, Finn; Mirizzi, Giulia; Slimani, Redouane et al. (2021): PATH-44. RAMAN SPECTROSCOPY AS A DIAGNOSTIC TOOL IN NEUROPATHOLOGY. In *Neuro Oncol* 23 (Supplement 6), vi125-vi125.

Development of a standardized protocol for brain tumor analysis by Raman spectroscopy; measurement of fresh, fixed and frozen tissues using a Raman spectrometer; creation of an informative form to improve the communication between the operating theatre and the pathology department; development of a standardized procedural protocol for the analysis of the relevant visible chemical elements present in the data.

7. Kleine Borgmann, Felix; Husch, Andreas; Slimani, Redouane; Jelke, Finn; Mirizzi, Giulia; Klein, Karoline et al. (2019): PATH-29. POTENTIAL OF RAMAN SPECTROSCOPY IN ONCOLOGICAL NEUROSURGERY. In Neuro Oncol 21 (Supplement 6), vi149-vi149. DOI: 10.1093/neuonc/noz175.625.

Development of a standardized protocol for brain tumor analysis by Raman spectroscopy; measurement of fresh, fixed and frozen tissues using a Raman spectrometer; creation of an informative form to improve the communication between the operating theatre and the pathology department; development of a standardized procedural protocol for the analysis of the relevant visible chemical elements present in the data.

8. Kleine Borgmann, Felix; Husch, Andreas; Slimani, Redouane; Jelke, Finn; Mirizzi, Giulia; Klein, Karoline et al. (2019): PATH-31. BUILDING A RAMAN SPECTROSCOPY REFERENCE DATABASE FOR TUMOR IDENTIFICATION AND CLASSIFICATION. In Neuro Oncol 21 (Supplement 6), vi149-vi150. DOI: 10.1093/neuonc/noz175.627.

Development of a standardized protocol for brain tumor analysis by Raman spectroscopy; measurement of fresh, fixed and frozen tissues using a Raman spectrometer; creation of an informative form to improve the communication between the operating theatre and the pathology department; development of a standardized procedural protocol for the analysis of the relevant visible chemical elements present in the data.

Abstract

Of all skin cancers, melanoma is the most fatal. Of all cancer types, melanoma is also the cancer with the highest level of brain tropism. Approximately 50% of patients with stage IV melanoma are diagnosed with melanoma brain metastases. A percentage that rises when postmortem patients are also taken into account. Following lung cancer and breast cancer, melanoma is the leading cause of malignant metastasis to the central nervous system. Of all metastatic brain tumors, melanoma represents 6-12% of cases. The overall survival rate following a diagnosis of melanoma brain metastases has been historically low. However, over the past ten years, advances in targeted therapies as well as in immunotherapies have significantly improved the survival rate of patients with advanced melanoma. Melanoma brain metastases most frequently occur at the junction between the gray and the white matter and in the frontal lobe. In order to reach the brain parenchyma, metastases must cross the brain vasculature. The specific properties of the blood vessels that perfuse the central nervous system are referred to as the blood-brain barrier. They allow these vessels to finely regulate the flow of cells, ions and molecules between the bloodstream and the brain parenchyma in order to preserve brain homeostasis for the proper functioning of neurons and the protection of the brain against toxic and pathogenic agents. Abnormalities in this functional interfacing barrier that separates the brain from the bloodstream are a critical element in the development and progression of several neurological pathologies. A poor understanding of the early mechanisms of metastasis crossing the blood-brain barrier constitutes an obstacle to the development of effective preventive therapeutic strategies as well as a particularly challenging domain of interest as it is one of the most crucial and least documented steps in the metastasizing process to the brain. Here, we focused on the ideation and consequent creation of effective *in vitro* and *in vivo* models to help identify and characterize as meticulously as possible, the players that are implicated in the crossing of melanoma metastases through the blood-brain barrier to reach the brain parenchyma. We used human immortalized cells (endothelial cells, pericytes and astrocytes) in triple coculture to recreate a blood-brain barrier *in vitro* and be able to investigate eventual changes in the gene expression of the tumor cells crossing the model. In parallel, we have set up an *in vivo* murine model to recreate the process of brain metastasis by injecting melanoma tumor cells into the left ventricle of the heart and thus be able to study the early stages of blood-brain

barrier invasion. The analysis of the murine tissues was performed by Correlative light-electron microscopy (CLEM) and the results obtained revealed the presence of cells in the brain that present artifacts that have the same appearance as melanosomes. Experiments using focused ion beam scanning electron microscopes (FIB-SEM) as well as nanoscale secondary ion mass spectrometry (NanoSIMS) may be conducted to take the investigation further.

Key words: blood-brain barrier, early stages of brain melanoma metastases, *in vitro* live cell imaging, electron microscopy, transendothelial electrical resistance

PART I. INTRODUCTION

1. BLOOD-BRAIN BARRIER – BIOLOGICAL AND THEORETICAL BACKGROUND

1.1. NEUROVASCULAR UNIT AND BLOOD-BRAIN BARRIER – AN OVERVIEW

It is commonly acknowledged that the German researchers Paul Ehrlich and Edwin Goldmann began conducting the first experiments on the brain barrier in 1885. Nevertheless, the first mentions of a brain-specific protection system were brought up as early as 1695 by the English physician Humphrey Ridley in “The Anatomy of the Brain: Containing Its Mechanism and Physiology; Together With Some New Discoveries and Corrections of Ancient and Modern Authors, Upon That Subject”. Humphrey was most probably the first to describe an impermeability of the cerebral vasculature to mercury after an injection of this chemical element into the blood (Liddelow 2011). It was two hundred years later that Paul Ehrlich injected a mouse intraperitoneally with coerulein S, a vital dye, and observed that all of the animal’s organs were stained with the exception of the brain. He then deduced that there was a lack of affinity between the dye and the brain (Valent et al. 2016). In 1909, Ehrlich’s former student, Edwin Goldmann, further worked on this study and noted that trypan blue, an azo dye, when injected intravenously, failed to stain brain tissue (Goldmann 1909). For years, the unsuccessful passage of dyes from the blood to the central nervous system (CNS) has been attributed to the lack of sufficient extracellular space to allow their penetration. In 1913, Goldmann’s next experiment refuted this hypothesis. Indeed, the scientist demonstrated that when injected directly into the cerebrospinal fluid (CSF) of the CNS, trypan blue stained exclusively the brain, thus proving the affinity between the dye and the brain tissue. Combined, these experiments demonstrated the existence of a barrier restricting the exchange between the blood and the brain (Goldmann 1913).

The term “blood-brain barrier” (Bluthirnschranke) was coined in 1909 by the German-Jewish neurologist Max Heinrich Lewandowsky (Lewandowsky 1909) . However, the location of the BBB in brain capillaries was not established until tight junctions between endothelial cells

were discovered (Reese and Karnovsky 1967). Nowadays, this barrier is known to be an adaptive interface whose primary function is to maintain CNS homeostasis, crucial for the functioning of neurons and glial cells.



Figure 1 Max Lewandowsky during a brain surgical procedure

Image with open license reproduced from Marcinowski (2020), shows Max Lewandowsky, second from the left, in the process of performing a brain puncture (Marcinowski 2020).

In recent years, the connection between cerebral microvascular endothelial cells (BMECs), vascular smooth muscle cells (VSMCs), microglia, astrocytes, oligodendrocytes, pericytes and neurons termed the neurovascular unit (NVU) (**Figure 2**), has gained increasing popularity among the scientific community (Hawkins and Davis 2005; Bautch and James 2009; Kugler et al. 2021).

As conceptualized by Harder et al. (2002), the NVU is a dynamic network that connects the neuronal and vascular systems of the brain, thus constituting a BBB capable of maintaining brain homeostasis (Harder et al. 2002). In addition to the cells of the NVU, there is the extracellular matrix (ECM) that provides an architectural bedding and physiological guidance to the BBB actors and facilitates cell adhesion and mechanosensing between the cells and the ECM. The NVU ECM basement membrane, which envelops endothelial cells, fulfills the

specific purpose of pericyte embedding and has distinct characteristics from the ECM of the brain parenchyma (Appelt-Menzel et al. 2017; Sweeney et al. 2016; Thurgur and Pinteaux 2019).

The vasculature of the brain is crucial as it provides oxygenated red blood cells and nutrients to the entire brain and also evacuates waste. Each component is tightly interconnected, creating a highly efficient and meticulously orchestrated system that regulates brain perfusion. The finely regulated vascular microenvironment is responsible for ensuring normal CNS function. Two biological barriers enable the exchanges between the circulating blood and the CNS: the blood-cerebrospinal fluid (CSF) barrier, which consists of the epithelial cells of the choroid plexus that are in direct contact with the CSF, and the BBB, which consists of endothelial cells. These two barriers together with the avascular arachnoid barrier, which envelops the brain under the dura mater, form a protective biological interface between the brain and the rest of the body.

At the BMEC level, the BBB is the first intermediate barrier that separates the brain parenchyma from the bloodstream and is the privileged area, due to its direct proximity, where neurons are supplied with nutrients. Therefore, the BBB operates as a highly selective rampart that separates neurotransmitters from the CNS and the pool of neuroactive agents from the peripheral nervous system, thus preventing any cross talk. The most notable quality of the BBB is that of providing the brain with protection against bloodborne pathogens and preventing exogenous drugs and molecules from entering the CNS (Kadry et al. 2020).

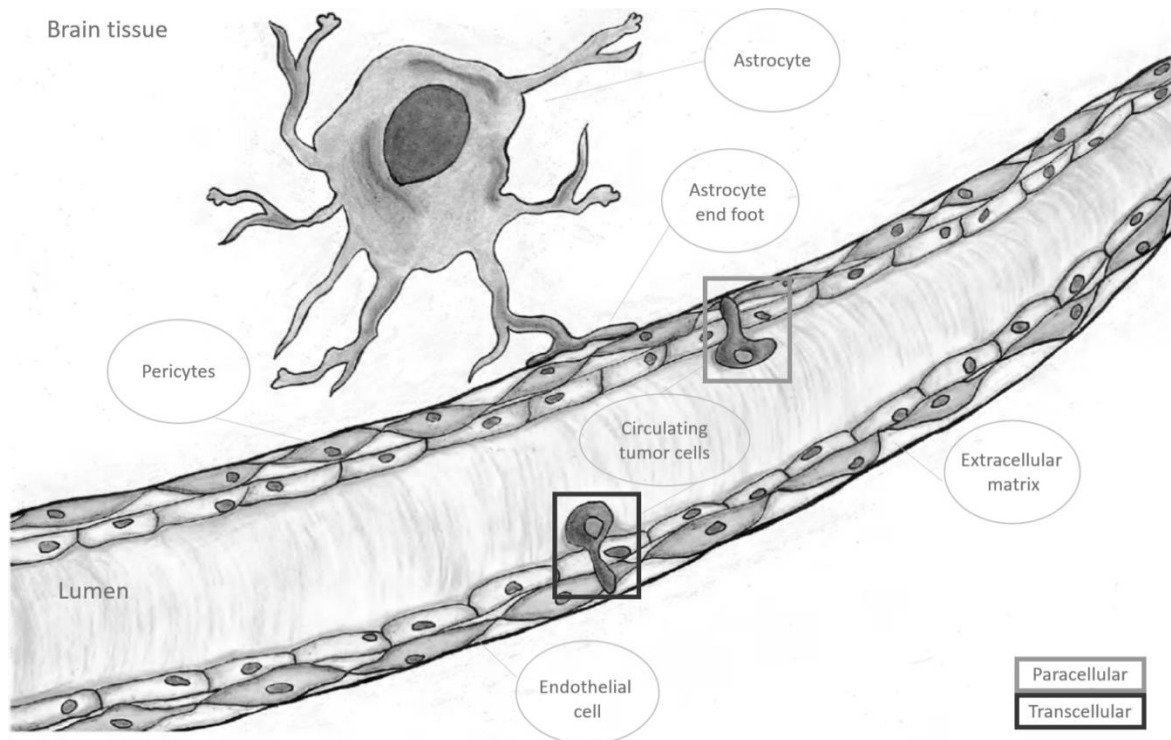


Figure 2 Schematic drawing of the transcellular and paracellular pathways in the BBB crossing process

Schematic drawing by Nathalie Marrama depicting metastases crossing the BBB via the transcellular and paracellular pathways.

1.2. CELLULAR AND FUNCTIONAL CONSTITUENTS OF THE BBB

1.2.1. ENDOTHELIAL CELLS

Endothelial cells (ECs) are modified squamous epithelial cells of mesodermal origin that line the blood vessel walls. The circulatory system, in its entirety, is paved by ECs. ECs are essential in vessel physiology and they coordinate the flow of nutrients and cells in and out of the vascular system.

Large arteries and veins may be lined with dozens of ECs, whereas capillaries can be lined with a single EC that folds in on itself forming the vessel lumen (Lammert and Axnick 2012) . With a gap of less than a 1/4 micron between the lumen and the brain parenchyma,

morphologically CNS microvascular ECs are exceptionally thin cells (Coomber and Stewart 1985).

Depending on the organ, endothelial cells possess specific properties and characteristics, which result in structural and functional heterogeneity in the vascular beds, depending on the requirements of the subjacent tissue (Gifre-Renom et al. 2022). Tissues' metabolic function necessitates angiogenesis. The development of new blood vessels is induced by energy requirements and is followed by morphological and phenotypic changes within ECs (Lidonnici et al. 2022).

Based on their morphology, the organs' endothelial cells are categorized into three types: discontinuous, fenestrated, and continuous. Discontinuous endothelial cells are characterized by large intercellular spacings, fenestrated endothelial cells are characterized by fenestras and pores, whereas continuous endothelial cells are characterized by tight junctions between cells (Stan 2007; Okada et al. 2017). The rate of molecular exchange between blood and tissue varies according to the morphology of the endothelial cell. Discontinuous, fenestrated, and continuous endothelial cells respectively provide different rates of molecular exchange between blood and tissue.

Because of their low permeability, which is even lower than that of the continuous peripheral endothelium, brain endothelial cells are phenotypically unique. In addition, the ECs of the CNS blood vessels are one of the components of the BBB, which tightly regulates the molecular exchange between the bloodstream and the brain parenchyma, essential for maintaining brain homeostasis. CNS endothelial cells have a higher expression of tight junctions (TJ) compared to other ECs in the body, which binds them strongly together, and they also have low levels of transcytosis to limit molecular exchange (Daneman and Prat 2015). Furthermore, CNS endothelial cells restrict the access of immune cells into the brain parenchyma through the expression of lower levels of E-selectin (Marchetti and Engelhardt 2020). A consequence of their limited permeability is the expression of transporters that intervene to facilitate the absorption of nutrients and the clearance of metabolic waste (Sanchez-Covarrubias et al. 2014). In addition, they show the highest density of pericytes, which are cells that envelop blood vessels and are in close contact with astrocyte end-feet. Together, these cells form the BBB (Daneman and Prat 2015).

1.2.1.1. CAVEOLAE IN ENDOTHELIAL CELLS

First visualized by electron microscopist George Palade in 1953 (Palade 1953), caveolae are intricate complexes of invaginated plasma membranes that superficially resemble coated pits. In 1955, Eichi Yamada suggested the explanatory Latin term “caveolae”, which means “little caves” (Yamada 1955). From a structural point of view, caveolae are composed of cholesterol, glycosylphosphatidylinositol-anchored proteins, integral membrane proteins caveolin-1 and caveolin-2, and sphingolipids. Caveolae abound in many cell types, particularly in adipocytes and endothelial cells. Caveolae abound in many cell types, particularly in adipocytes and endothelial cells. In the latter, caveolae may participate in the passage of albumin through the cell monolayer, thus playing a role in endocytosis (Nassey and Lamaze 2012).

Morphological studies revealed the presence of thin layers of proteins embedded within the caveolae, called “stomatal diaphragms”, whose function is not yet known. The plasmalemma vesicle-associated protein (PV-1) is an essential structural element in the formation of stomatal diaphragms.

A connection between caveolae, microfilaments and microtubules has been observed within endothelial cells. Arteriolar and capillary endothelia have an average of 5 caveolae per sq mm (Nassey and Lamaze 2012; Zhou et al. 2021). In comparison with the endothelium of vessels in other parts of the body, the cerebrovascular endothelium has a decreased number of vesicles indicating a reduced transcellular transport of solutes. Conversely, areas that are devoid of BBB, such as the area postrema and the subfornical organ (SFO), show an increase in permeability and a considerably higher number of endothelial caveolae (Kadry et al. 2020).

1.2.1.2. MITOCHONDRIA IN ENDOTHELIAL CELLS

Mitochondria are crucial regulators of metabolism in most cell types. They are linked to a wide range of regulatory mechanisms that are involved in cell proliferation as well as apoptosis and signaling to the nucleus.

The subcellular location of these membrane-bound cell organelles in the brain endothelium is in proximity to the nucleus, but they occasionally may be present in the cytoplasm (Kluge et al. 2013).

Mitochondrial concentration per cell varies considerably across endothelial beds, for example brain ECs have more mitochondria than liver ECs. Glucose is an absolute necessity for ECs, which produce adenosine triphosphate (ATP) primarily by glycolysis, hence the low concentration of mitochondria is consistent with a function in regulating signaling responses to environmental factors rather than in ATP production.

The murine cerebral microvascular endothelium shows a higher mitochondrial density compared with that observed in the endothelia of other tissues. The higher mitochondrial concentration supplies the energy necessary to maintain the ionic balance on the vascular side of the BBB. Interestingly, there is a decrease in the concentration of endothelial mitochondria in the SFO, which is located outside the BBB (Kluge et al. 2013).

1.2.2. PERICYTES

Pericytes were first identified at the end of the 19th century by C.J. Eberth and C. Rouget. They have been described as cells being spatially separated and connected to the capillary wall (Attwell et al. 2016), localized within the basement membrane with extensions spreading from the cell body to cover the EC lining of the vessels.

It was in 1923 that K.W. Zimmermann termed these cells “pericytes”, a term that included other cell subtypes such as vascular smooth muscle cells (VSMC), and proceeded to describe them as cells with a large nucleus and a reduced cytoplasmic space (Zimmermann 1923).

Recent and ongoing studies mainly focus on the operating mechanisms of pericytes and their role in the homeostasis of the organism.

Variations in pericyte density are related to their location in the tissue, the type of tissue, and the width of the vessels.

Differences in their structure have been observed depending on whether they are located in arterioles or venules (Brown et al. 2019).

Pericytes are especially present in CNS capillaries, with a ratio of one pericyte to one endothelial cell up to one pericyte to three endothelial (Brown et al. 2019; Uemura et al. 2020; Bonkowski et al. 2011). Their location as well as their number inside the brain capillaries seem to indicate that pericytes have a significant role there, a role that is yet to

be determined. Nowadays, it is hypothesized that pericytes respond to angiogenic factors such as the vascular endothelial growth factor (VEGF) and the transforming growth factor beta (TGF β), thereby regulating vascular permeability and remodeling (Armulik et al. 2005), and that they have contractile capacities that enable them to control the blood stream in capillaries (Peppiatt et al. 2006).

It has been acknowledged that pericytes play a major role in ECs differentiation during embryonic vascular development, even before the appearance of astrocytes (Armulik et al. 2011). Pericytes recruitment and interaction with the endothelium are essential for the formation, maturation and maintenance of the BBB. It has been shown that pericytes regulate the formation of tight junctions and vesicular trafficking in ECs by inhibiting the expression of molecules that increase vascular permeability and the infiltration of immune cells into the CNS (Birbrair et al. 2014; Jo et al. 2013; Daneman et al. 2010).

Pericytes are of critical importance to the BBB function due to their location at the interface in between glial cells and ECs. Consequently, they operate as chemical sensors to allow communication between the two cell types.

1.2.3. ASTROCYTES

Earlier researches tended to imply that BMECs role in the formation of the BBB was not an intrinsic characteristic of these cells and that the CNS environment with its astrocytes, microglia and neurons originated NVU barrier attributes. Some studies later suggested that mature astrocytes play a key role in the BBB formation, astrocytes' function remains therefore enigmatic. Within the NVU, astrocytes are situated in a strategic position at the interface between the neurons and the ECs. This allows them to control CBF depending on the neuronal metabolic needs and synaptic exchanges.

Astrocytes are abounding cells in mammals' brain and implicated in numerous homeostatic and metabolic mechanisms, which include: separation of the neuronal parenchyma into different compartments; neural environment ion homeostatic balance; regulation of the pH; recapture of neurotransmitters and regulation of glucose balance in the brain environment; signals' transmission between the neurons and the NVU (Cabezas et al. 2014; Verkhratsky et al. 2016) .

BMECs and astrocytes must work in concert in order to meet the brain oxygen and glucose metabolic needs. Neurovascular coupling (NVC) is a signaling mechanism that occurs when astrocytes originate an interaction that regulates blood circulation by tightly wrapping brain capillaries with their end-feet (Verkhatsky et al. 2016). By releasing neurotransmitters, like for example glutamate, astrocytes are able to adapt NVC signaling cascade, which allows glial cells to manage NVU attributes thus modulating blood perfusion. One of astrocytes characteristics is their heterogeneity, which relies on the brain area where they are located and on their connection with the different cellular types. Depending on their location in the brain, astrocytes express various ion channels' quantities and types, this has an impact on their electrophysiology, which also includes their resting membrane potential. Astrocytic heterogenous nature explains the brain's one-of-a-kind structure, this may be the reason for the BBB peculiar molecular structure and function (Abbott et al. 2006). Structurally, in the CNS, vascular basement membrane comprises two layers of extracellular matrix (ECM) proteins: the endothelial and parenchymal basement membranes. These ensure the separation between astrocytes and ECs. Moreover, the vascular basement membrane is partly responsible for vessel formation and development, and preservation of the BBB. Via the endothelial and parenchymal basement membranes, the association between ECM molecule network and integrins establishes an interaction between the ECs and their microenvironment. Through their close contact with the brain vasculature, astrocytes are able to balance the brain homeostasis regulating the Ca^{2+} concentration (Szokol et al. 2015). Neurovascular coupling possesses a high concentration of specialized molecules, which includes the water channel protein aquaporin-4 (AQP4) in astrocytic membranes, the potassium channel Kir4.1, and the purinergic G protein-coupled P2Y receptors, implying its important role in the signaling at the gliovascular interface and in the balancing of water and ion metabolism in the CNS in pathological as well as non-pathological conditions (Petzold and Murthy 2011).

Additionally, astrocytes are involved in the formation of BBB properties such as TJs and polarized localization of membrane transporters such as glucose transporter (GLUT1). Astrocytes interact with neighboring astrocytes via gap junctions (GJ), these gather building a syncytium capable of delivering a well-orchestrated reaction to stimuli, for example mediating vessel compliance (Langen et al. 2019). The existing synergy between the BMECs and astrocytes within the BBB is crucial to the formation and preservation of BBB properties.

Astrocytes secrete angiogenic factors such as vascular endothelial growth factor (VEGF), glial cell line derived neurotrophic factor (GDNF) (Kotliarova and Sidorova 2021), fibroblast growth factor (FGF) and angiopoietin-1 (Ang-1) (Michinaga and Koyama 2019), which have an important role during formation and maintenance of BBB and ECs properties. Additionally, ECs are capable to modulate astrocytic phenotype by expressing growth factors.

1.3. OTHER CELLULAR CONSTITUENTS OF THE BBB

1.3.1. MICROGLIA

Microglia are non-neuronal immune cells accounting for 5 to 20% of all glial cells. Microglial cells originate in the yolk sac (YS), from precursor cells expressing erythro-myeloid CSF1R+, a colony stimulating factor 1 receptor common to resident macrophages. They colonize the neuroepithelium early on, where they continue their differentiation following a unique pathway in the CNS environment (Ginhoux et al. 2013). During their lifespan, they retain a regenerative capacity that allows them to maintain their cell pool and to respond to specific demands. After birth, a subpopulation of microglial cells seems to originate from a hematopoietic source via the infiltration of monocytes in the parenchyma (Ginhoux and Garel 2018; Ginhoux et al. 2013). Constantly exploring their environment by means of the rapid movements of their cytoplasmic extensions and endowed with a broad activity potential, they metamorphose in response to the environment stimuli they experience (Kaur et al. 2001). Microglial cells are essential in the organization of the CNS and in the execution of higher nervous functions. However, they are best known for their involvement in traumatic situations. Microglial cells express all the pattern-recognition receptors (PRRs) identified so far, and are therefore particularly well equipped to detect disturbances in their environment, whether caused by the presence of an unusual compound or the abnormal concentration and/or shape of a molecule (Weinstein et al. 2010). The detection of the disturbance induces the transition from the resting state to the activated state, the objective being firstly, to eliminate the source of the disturbance and secondly, to promote remodeling and regeneration of the impacted tissue.

In the presence of a danger signal, microglial cells adopt an amoeboid shape that facilitates both their division and movement. Microglial pattern-recognition receptors are activated by “danger signals” or by chemokines expressed by under stress, damaged or dying cells. They form a protective shield around the damaged area, this aims to limit the extent of the damage. The response following activation depends on the encounter with the initiating stimulus, the reason for this is that microglial cells oscillate between two response modes: a classical activation mode and an alternative one with a healing vocation (Boche et al. 2013). When in a proinflammatory state, microglia have the ability to alter the tightness of the BBB, attract leukocytes – mainly granulocytes, lymphocytes, and monocytes, facilitate their movement into the extracellular matrix, present antigens, trigger the activation of specific immunity responses and neutralize disruptive agents. Microglia also has the potential to cause irreversible collateral damage to the CNS, this collateral damage capacity is tempered by the environment immunosuppressive properties, attributable to neurons (Matsudaira and Prinz 2022). Thus, promoting angiogenesis and stimulating the generation of new oligodendrocytes, astrocytes, and even neurons from stem cells still present in the adult nerve parenchyma, microglia has the potential to participate in the healing of injured tissue and the restoration of homeostasis (da Fonseca, Anna Carolina Carvalho et al. 2014).

1.3.2. NEURONS

The neuron is the brain’s primary working unit. It is a specialized cell that transmits information to other nerve cells, muscle cells and glandular cells. The brain’s characteristics are principally based on the structural and functional features of the interconnectivity between neurons.

Anatomically, in mammals, each neuron of the brain consists of a soma, dendrites and an axon. The nucleus and cytoplasm are located in the soma. The axon arises from the soma and develops several small ramifications before forming nerve endings. Axons can range in length from less than a centimeter to a meter or even longer. Dendrites originate from the soma and their role is to receive information from adjacent neurons. The brain, depending on the mammalian species, can contain between 100 million and 100 billion neurons (Goaillard et al. 2019).

The role of neurons in the formation and regulation of the BBB has received increasing interest in recent years, along with the popularization of the concept of neuro-glial-vascular unit. Studies have shown that the formation of tight junctions (TJ) between endothelial cells occurs when blood vessels invade the brain, while gliogenesis has not yet taken place (Banerjee and Bhat 2007). The formation of tight junctions would therefore be initiated by neural progenitor cells (NPCs) rather than by differentiated glia, at least in an initial phase (Homem et al. 2015). However, there is a paucity of data available to corroborate this hypothesis. A study conducted on BMECs cultured *in vitro* showed that gamma-glutamyltranspeptidase (γ -GT) activity in ECs is higher when cocultured with neurons than with astrocytes (Tontsch and Bauer 1991). Another study determined that ECs from brain capillaries cultured with neural progenitors had a decreased paracellular permeability and an increased transendothelial electrical resistance (TEER) (Weidenfeller et al. 2007). These studies hint at the involvement of neurons in the formation of BBB properties in ECs. Moreover, neural tissue intense metabolic activity suggests that the cerebral microcirculation (CMC) reacts to the metabolic needs of the tissue it supplies. Finally, BBB rupture can occur during pathologies that modify cerebral blood flow, such as cancer metastases, ischemia or hemorrhage (Petty and Wettstein 2001; Schulz et al. 2019).

1.3.3. ECM

Also called basement membrane, the extracellular matrix is produced by endothelial cells and pericytes. At the level of the adult BBB, it forms a continuous extracellular network 30 to 40 nm thick, composed of structural proteins: type IV collagen, laminin, fibronectin, elastin, thrombospondin and various proteoglycans (Baeten and Akassoglou 2011; Lu et al. 2011; Bonnans et al. 2014). It interacts with endothelial cells via laminin and other matrix proteins, interacting with integrin receptors on endothelial cells, thereby anchoring endothelial cells (Baeten and Akassoglou 2011). In addition to its structural role, degradation of the extracellular matrix and alteration of adhesion receptors are associated with increased paracellular permeability of the BBB during ischemic shock (Del Zoppo et al. 2006). Finally, the loss of basement membrane stability under the effect of metalloproteases or collagenases is frequently observed in the pathological manifestations at the origin of BBB

rupture, suggesting its importance in maintaining the properties of this barrier (Salimi and Klein 2019).

1.4. BBB – CHARACTERISTIC FEATURES OF A PHYSICAL BARRIER

1.4.1. BBB FUNCTION

The BBB has various responsibilities such as controlling molecular transit and withstanding toxins, thus reducing neurons' apoptosis; regulating ion concentration for a most favorable neuronal signaling; keeping a low protein level within the brain parenchyma, thus restraining proliferation and maintaining neuronal connectivity; separating the neurotransmitters from the CNS and neuroactive agents' pool from the peripheral nervous system, preventing cross talk, and allowing non-synaptic signaling in the brain; allowing immunosurveillance and response with low inflammation and cellular damage (Kaplan et al. 2020; Figueira et al. 2019; Tenreiro et al. 2016).

The BBB offers a well-regulated microenvironment by means of transporters and ion channels that maintain ideal ion balance for neuronal activity. Consequently, it regulates ion and fluid flow between the CNS and the vasculature. In addition to this, the BBB enables ion transporters and channels to generate an interstitial fluid (ISF) which is a physiological medium that supports neuronal as well as synaptic activity, supplies the brain with nutrients and is responsible of waste efflux (Dalvi et al. 2014).

One of the NVU's functions is the transit and diffusion regulation via the BMECs. Due to their gaseous nature, oxygen and carbon dioxide diffuse without restraint through the lipid membranes, these latter are also the point of entry to lipophilic compounds, such as found in drugs and alcohol. Hydrophilic molecules' transit is controlled by several precise transport systems situated on the luminal and abluminal membranes that allow nutrients' provision and toxic agents outflow.

Furthermore, the BBB can be also seen as a metabolic barrier, an association of intracellular enzymes such as monoamine oxidase and cytochrome P450, which are able to lyse neuro-

toxic agents, and extracellular enzymes such as peptidases and nucleosidases, which can enzymatically process peptides as well as ATP (Figueira et al. 2019).

From a constitution point of view, the brain ISF is very much alike blood plasma, with the exception of its lower protein, K^+ and Ca^{2+} content and increased Mg^{2+} concentration. In consequence of that, the BBB acts as a protection, preserving the brain from ion variations that can occur e.g. after food intake or physical activity (Sweeney et al. 2019).

The NVU maintains the separation between CNS neurotransmitters and adjacent tissue and blood peripheral neuroactive agents, thus avoiding cross talk. Neurotransmitters transit from the CNS to the blood relies mainly upon Na^+ coupled and Na^+ independent amino acid (aa) pumps. The BBB restricts the influx of some aa like e.g. glutamate and glycine, and at the same time, allows the influx of indispensable aa (Pardridge 2007).

The endothelium is in control of the CNS microenvironment by virtue of its important surface, which is of approximately 20 m^2 , and of its close diffusion distance between glial cells and the capillary network. The choroid plexus epithelium also participates in this regulation mechanism by removing brain metabolites and larger compounds from the CSF and the ISF. Hydrophilic nutrients and metabolites that are necessary to the maintenance of the nervous system machinery are allowed to pass through the BBB with the help of specific active transporters. The expression of the latter is responsible for BBB polarity (Ballabh et al. 2004).

When intact, the BBB keeps large molecules from reaching the brain via regular paracellular and/or transcellular pathways. In the event of a breach in the BBB, large proteins like e.g. albumin, reach the brain parenchyma and can be responsible for detrimental pathological effects. Blood contains a large number of proteins and their activators, such as factor X^a , which is able to induce the transformation of prothrombin into thrombin, or such as reaction activators, which convert plasminogen into plasmin. When the resulting proteins manage to reach the brain parenchyma, reactions such as seizures, glial cell activation, glial cell division and cell apoptosis can occur. Therefore, the BBB can be regarded as a sentinel challenging comers and preventing surprise attacks (Kaplan et al. 2020; Hawkins and Davis 2005; Ballabh et al. 2004).

The BBB interendothelial space is characterized by the presence of junctional complexes like adherens and tight junctions, which follow one another in a precise order from the lumen of the capillary. The role of these complexes is not limited to restricting the passage of solutes, they are also involved in the polarization of ECs by limiting the diffusion of lipids and proteins between the apical and basolateral membranes. The formation of these complexes involves the interaction between transmembrane and cytosolic proteins linked to each other and to the intracellular actin network. These junctions are also involved in the transmission of intracellular signals and in other cellular functions such as growth, cytoskeleton reorganization and apoptosis (Luissint et al. 2012; Stamatovic et al. 2016)

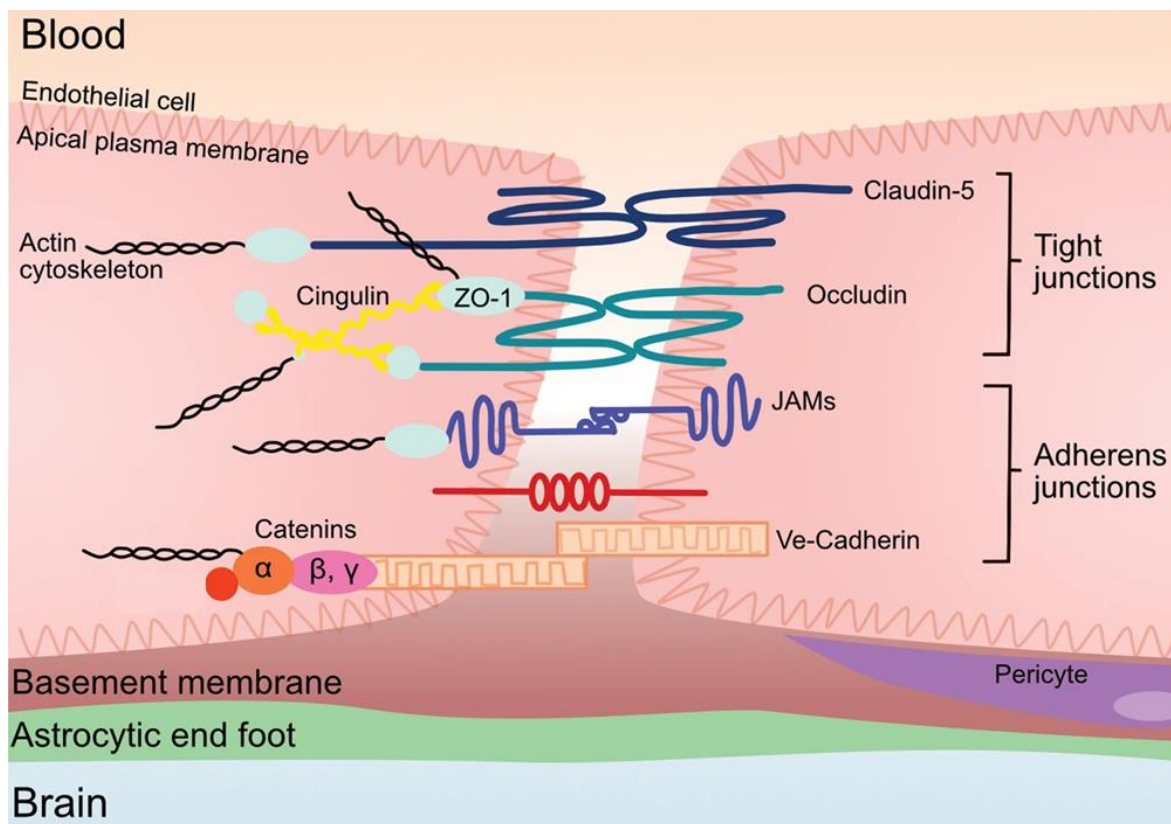


Figure 3 Schematic illustration of endothelial cell tight junctions and adherens junctions

Simplified version of a schematic illustration with open license reproduced from Knox et al. (2022) (Knox et al. 2022) depicting the interactions between the main proteins forming adherens and tight junctions. Claudins and occludins form the backbone of tight junctions by homophilic dimerization with their homologues from the adjacent cell. Tight junctions also include cytoplasmic proteins like the Zonula Occludens proteins (ZO-1, -2 and -3), which serve as recognition proteins for the placement of tight junctions and are also involved in signal transduction. Cingulin is a double stranded myosin-like protein that binds to ZO-1 via its globular part. Actin has binding sites on Zos: occludins and claudins. Tight junctions rely on

an intercellular contact zone, made of adhesion molecules such as junctional adhesion molecules (JAMs), as well as on the presence of adherent junctions, made of cadherins and catenins.

1.4.2. TIGHT JUNCTIONS

Tight junctions are made of transmembrane and cytoplasmic proteins (Furuse 2010). The association of these proteins with each other and with the cytoskeleton actin allows the formation of junctional complexes that effectively seal the intercellular spaces.

1.4.2.1. OCCLUDINS

Among the transmembrane proteins of tight junctions, occludin was one of first to be described (Furuse et al. 1993). The cellular localization of this 65-kDa protein is directly linked to its degree of phosphorylation: the least phosphorylated forms are located on the cytoplasm and tight junctions basolateral membrane, whereas the most phosphorylated form is exclusively present on the tight junctions (Sakakibara et al. 1997). Its presence in the BBB tight junctions is correlated with an increase in transendothelial resistance (TER) and a decrease in paracellular permeability (Hirase et al. 1997), however, this does not seem to be essential for their establishment since occludin-deficient mice show a normal organization of tight junctions (Saitou et al. 2000). Occludin is therefore involved in the regulation of TJs rather than in the establishment of barrier properties (Luissint et al. 2012).

1.4.2.2. CLAUDINS

Claudins (CLDN) are proteins specific to tight junctions. There are 24 different claudins' types with molecular weights that range from 21 to 28 kDa (Furuse 2010). They have 4 transmembrane domains that carry a highly conserved homologous domain at their carboxy-terminus that allows them to interact with several cytoplasmic proteins such as Zonula occludens (ZO)-1, -2 and -3 (Greene et al. 2019; Itoh and Bissell 2003). Claudins form dimers with their adjacent cell homologus, allowing a stronger adhesion between the two membranes compared to the one obtained by occludin (Huber et al. 2001; Itoh et al. 1999). At the level of the mammalian BBB ECs, CLDN-3, CLDN-5, and CLDN-12 are expressed with

CLDN-5 showing the highest expression level (Jia et al. 2014; Lippoldt et al. 2000; Wolburg and Lippoldt 2002). Mice deficient in CLDN-5 are characterized by an increase in BBB permeability to small molecules, confirming the role of this protein in the restriction of paracellular passage (Nitta et al. 2003; Ohtsuki et al. 2008).

1.4.2.3. JUNCTIONAL ADHESION MOLECULES

Junctional adhesion molecules (JAMs) belong to the immunoglobulin superfamily (IgSF). JAMs are small proteins of around 30 to 50 kDa in size, capable of binding to ZO-1, cingulin and occludin. (Bazzoni et al. 2000; Ebnet et al. 2004) They can establish homo- and/or heterodimeric interactions with each other, on either side of the membranes of two adjacent cells (Wolburg and Lippoldt 2002; Martin-Padura et al. 1998). They form intercellular junctions that reduce the permeability of the BBB (Sharma and Westman 2004; Martin-Padura et al. 1998) and play an important role in the formation of tight junctions and in the acquisition of cell polarity (Ebnet et al. 2004; Ebnet et al. 2018).

1.4.2.4. CYTOPLASMIC ACCESSORY PROTEINS

In addition to the three transmembrane proteins described above, cytoplasmic proteins like ZO-1, -2 and -3 are membrane-associated guanylate kinases that provide structural support to TJs by enabling their organization and connection with the actin cytoskeleton (González-Mariscal et al. 2003; Odenwald et al. 2017). ZO-1 (220 kDa) was the first to be identified by Stevenson et al. Its presence in the TJ protein complex is important because when absent, an increased endothelial permeability is observed (Odenwald et al. 2017; Abbruscato et al. 2002; Mark and Davis 2002). Since it is able to translocate into the nucleus under stress and proliferation conditions, ZO-1 also plays the role of a signaling molecule (Gottardi et al. 1996). ZO-2 (160 kDa) and ZO-3 (130 kDa) were later identified through their co-precipitation with ZO-1 in cultured epithelia extracts (Gumbiner et al. 1991; Haskins et al. 1998).

The phosphoprotein 7H6 owes its name to the monoclonal antibody that allowed its isolation by Zhong et al. In 1993 (Zhong et al. 1993). Its molecular weight varies between 155 kDa and 175 kDa depending on the species. 7H6 plays a major role in the assembly and regulation of tight junctions in BBB epithelial and endothelial cells, via a direct interaction with ZO-1 (Satoh

et al. 1996). 7H6 protein only localizes at tight junctions only if it is phosphorylated (Zhong et al. 1993).

Cingulin is a dipeptide (140 kDa) located on the TJ cytoplasmic side, able to interact with ZO-1, ZO-2 and JAMs via its amino terminus, and with ZO-3 and myosin via its amino and carboxy-terminal ends (Cordenonsi et al. 1999; Vasileva et al. 2020). Cingulin may play a role in the transduction of the mechanical force generated by the contraction of actin and myosin to which it is connected, influencing permeability at the paracellular level (Vasileva et al. 2020).

The AHNAK protein is a so-called “giant” phosphoprotein because of its molecular weight (700 kDa). It migrates from the cytoplasm to the plasma membrane during the establishment of intercellular contacts within the epithelia and has an important role in calcium homeostasis (Gentil et al. 2005; Sundararaj et al. 2021). Gentil et al., 2005 has demonstrated its expression in ECs of cerebral capillaries, where it is associated with ZO-1.

Actin, although not belonging to the tight junction proteins, is involved in the establishment and maintenance of the junctional complex. Actin globular form polymerizes into filaments (F-actin), whose dynamics provide the cytoskeleton with the necessary infrastructure to maintain cell morphology (Fanning et al. 1998). In 1991, Rubin et al. Studied the organization of F-actin marked with rhodaminephalloidin in cultured ECs: TEER increase is associated with the redistribution of F-actin (Rubin et al. 1991). In the absence of TJs, F-actin is dispersed and distributed in ECs cytoplasm (Yan et al. 2019). Conversely, when ECs have tight junctions, F-actin is mainly localized at the plasma claudin and occludin (Itoh et al. 1999), and plays an important role in the regulation of BBB permeability in physiological and pathological conditions (Lai et al. 2005).

All of the aforementioned proteins interact to restrict the intercellular space, however BBB TJs have other additional functions. Far from just forming static assemblies, these highly dynamic structures are finely regulated by the brain environment (Wolburg et al. 2009), creating heteromeric signaling complexes that allow the control of gene expression, proliferation and cell differentiation (González-Mariscal et al. 2008). Signaling at TJs is bidirectional: they receive signals that regulate their assembly and function, and they transmit information back to the cell interior to regulate gene expression and ensuing cellular responses (Haas et al. 2020).

1.4.3. ADHERENS JUNCTIONS

Present all along the vascular tree, adherens junctions (AJ) perform various functions: initiation and stabilization of cell-cell adhesion, organization of the actin cytoskeleton and regulation of intracellular signaling. They represent the first contact between adjacent ECs, a precondition for the formation of TJs and the establishment of cell polarization (Bazzoni and Dejana 2004).

AJs are composed of the transmembrane protein cadherin and the intracellular protein catenin. Cadherin is a glycoprotein with a single transmembrane domain and interacts homotypically in the presence of Ca^{2+} to enable adhesion of adjacent cells. ECs express cadherin-5, which is also called vascular endothelial (VE)-cadherin (Dejana et al. 1995). VE-cadherin is expressed by all the ECs of the vascular system. It binds via its carboxyterminal end to catenins and plays a central role in junction stabilization (Vestweber et al. 2009). Catenins serve as link between TJs and AJs enabling their communication, and also between the junctional complex and the actin cytoskeleton. At the BBB level, β - and γ -catenins bind AJs to actin (Hussain et al. 2022).

1.4.4. INTEGRINS

Cell adhesive interactions are involved in multiple physiological processes such as formation and development of the embryo, cicatrization, wound repair, progression of pathologies such as cancer metastases. Cell adhesion, the capacity that cells have to connect and cooperate with each other and their environment, is conveyed by the bindings between cell surface receptors and extracellular glycoproteins (Haas et al. 2020; Michael Bachmann et al. 2019).

Integrins are heterodimeric transmembrane cell adhesion glycoproteins constituted of the two subunits, α and β . They belong to a family of approximatively 23 members. Integrins cytoplasmic domains comprise on average 60 aa (Michael Bachmann et al. 2019).

Among the integrins that are fibronectin receptors, the $\alpha 5\beta 1$ integrin is the most recurrent one on most cells. Integrins like fibronectin, take actively part in signal transduction. $\alpha 5\beta 1$ integrin conveys cell to substrate signals such as ECM formation and remodeling, adhesion and migration (Danen et al. 2002).

At the intracellular level, cell adhesive interactions can trigger cell migration and proliferation, assembly and structure of F-actin cytoskeleton, as well as formation of adhesion plaques, pH cytoplasmic variations and Ca^{2+} concentration, and finally gene expression (Bachir et al. 2017).

1.5. BBB CROSSING AT THE CELLULAR AND MOLECULAR LEVELS

1.5.1. TRANSCYTOSIS

Most often observed in epithelial cells, transcytosis is a biological mechanism occurring in numerous other cell types. It refers to a type of transcellular transport during which high molecular weight molecules are conveyed across the cell cytoplasm from the apical plasma membrane to the basolateral one (Pulgar 2018).

Successive stages in this process are endocytosis, intracellular vesicular trafficking and exocytosis. These stages may imply adsorptive or receptor mediated internalization. Molecules with a positive charge may be attracted to the cell membranes that are negatively charged leading to internalization by adsorptive endocytosis (Pulgar 2018).

Essentially all endothelial cells feature receptor-mediated transcytosis (RMT). In the BBB, there are multiple receptors, like for example the insulin receptor, able to generate RMT, while others, like the albumin receptors, are not present (Pulgar 2018).

Vesicular transport is a crucial cellular activity, responsible for macromolecules intracellular transport process. Cerebral endothelium presents three sorts of endocytic vesicles: potocytosis vesicles, clathrin-coated pits and caveolae (Parkar et al. 2009). Following vesicle internalization, the intracellular mechanism starts with the early endosome, which form a compartment that operates as a sorting platform (Kiss and Botos 2009).

In BMECs, endocytosis takes place in both basolateral and apical domains of the plasma membrane, originating two distinct early endosomal compartments (Thompson et al. 2007; Haqqani et al. 2018).

1.5.2. CARRIER-MEDIATED TRANSPORT

At the level of the BBB endothelium, there are different categories of transporter proteins expressed by CNS ECs that facilitate the transport of nutrients into the CNS parenchyma such as glucose (Devraj et al. 2011), aa (Zaragozá 2020) (whether non-polar and neutral, polar and neutral, acidic and polar or basic and polar), monocarboxylic acids (Settergren et al. 1976) such as lactate, pyruvate and ketone bodies. Nutrients' concentration gradient decreases from the blood into the brain. This transport mechanism does not require energy and is therefore regulated by the brain metabolic needs and by the plasma substrates concentrations (Drioli and Giorno 2016; León 2016).

1.5.2.1. GLUCOSE TRANSPORT

Glucose is the main source of energy required for brain activity, the transport of this hexose is thus of paramount importance (Simpson et al. 2007). In addition, glucose transporter-1 (GLUT-1) is the most commonly glucose transporter expressed at the level of BBB and is specific to its endothelium (Pardridge et al. 1990; Devraj et al. 2011). GLUT-1 transports D-glucose but not L-glucose and is also able to transport other hexoses such as D-mannose, D-galactose and D-xylose (Lund-Andersen 1979). The density of GLUT-1 in the abluminal membrane of the BBB ECs is three times higher than the one in the luminal membrane (Simpson et al. 2007).

1.5.2.2. AMINO ACID TRANSPORT

Amino acid transport is required for protein synthesis in general and for neurotransmitters' production, moreover, it is of particular importance in the CNS. In fact, the CNS does not autonomously produce most of the essential aa it uses, for this reason, the brain aa metabolic needs are fulfilled via the bloodstream. There are two groups of aa transporters that coexist at BBB ECs level, these are characterized by their substrate specificity and their sodium dependence (Hawkins et al. 2006):

- Transporters responsible for aa facilitated diffusion, independent of Na⁺ ions, and present within the ECs luminal and abluminal membranes (Zaragozá 2020). These transporters form the following four different systems: L1, γ⁺,

n, and xG. The first two systems are present within the luminal and abluminal membranes, whereas the last two are present exclusively within the luminal side. The L1 system represents the main pathway for the transport of neutral amino acids (Naa), which are essential to the brain. The γ + system is the main provider of cationic amino acids (Caa) such as lysine, arginine and ornithine. The xG system represents the main transport pathway for glutamate and aspartate. The n system mediates glutamine and asparagine transport (Zaragozá 2020).

- Na^+ ion-dependent amino acid transporter systems are located exclusively in the ECs abluminal membrane and they are responsible for the active aa transport from the brain parenchyma to the blood, and are therefore part of the efflux mechanisms (Zaragozá 2020). These are the alanine-preferring (A) system, alanine, serine, cysteine-preferring (ASC) system, large neutral amino acids (LNAA) system, excitatory amino acid transporter (EAAT) system and nitrogen-rich amino acids (N) systems.

1.5.2.3. MONOCARBOXYLIC ACIDS TRANSPORT

The transport of monocarboxylic acids is carried out by the monocarboxylate transporter 1 (MCT1), present within the luminal and abluminal ECs membranes (Kido et al. 2000). MCT1 is specifically involved in the transport of lactate and ketone bodies, which represent a source of energy for the brain in specific situations, such as fasting and lactation. Plasma concentrations of MCT-1 substrates regulate its expression (Simpson et al. 2007).

1.5.3. WATER AND ION TRANSPORT

1.5.3.1. WATER TRANSPORT

Ions are essential for neuronal activity and the functioning of various channels and transporters. The distribution of ions is linked to water homeostasis. Aquaporins (AQPs) are a family of channels that, depending on their subtype, facilitate the flow of water and/or

solutes like glycerol and urea, across the membranes of different cell types (Badaut et al. 2002). They can form fenestras (pores) allowing bidirectional water transport following the principles of osmolarity. So far, 13 aquaporins have been described in humans (Sorani et al. 2008). The water channel protein aquaporin 4 (AQP 4) is the most abundantly expressed aquaporin at BBB level. AQP 4 is localized in astrocytic end-feet that are in contact with cerebral capillaries (Nielsen et al. 1997). It is closely associated with K^+ ion transport (Wolburg et al. 2009). At BBB level, AQP 4 appears to play an important role under pathological conditions (Deng et al. 2014). Studies conducted on *in vivo* models showing AQP4 deficiency or delocalization, suggest that this protein is involved in cerebral edema formation (Papadopoulos and Verkman 2007).

1.5.3.2. ION TRANSPORT

Ion transport requires the involvement of different ion channels, localized at the luminal and abluminal membranes of the BBB ECs. The active ion transporter Na^+/K^+ ATPase is mainly located on the abluminal side of the BBB ECs and is responsible for the active influx of sodium to the brain parenchyma in exchange for potassium (Betz 1986; Hladky and Barrand 2016). The Na^+/K^+ ATPase pump allows the balance of the sodium gradient at BBB level, providing the conditions for Na^+ -dependent transports. Due to K^+ ions crucial role in nerve impulse transmission, their concentration in brain interstitial fluid must be stable. K^+ ions balance is achieved by removing excess K^+ by astrocytes and by transport of K^+ from the brain to the blood. Astrocytes use mechanisms such as Na^+/K^+ ATPase uptake to carry out K^+ clearance from the interstitial fluid. Subsequently, K^+ ions reach the blood compartment through K^+ channels (Breschi et al. 2013).

The Cl^-/HCO_3^- exchangers, are expressed at both the luminal and abluminal membranes of ECs. Cl^-/HCO_3^- exchanger is involved in the entry of chloride ions into the ECs in exchange of hydrogen carbonate ions secretion.

For all of the aforementioned reasons, both Na^+/K^+ ATPase and Cl^-/HCO_3^- exchangers proteins play a role in pH regulation (Hladky and Barrand 2016).

1.5.4. EFFLUX TRANSPORT

In addition to its physical properties, the BBB presents metabolic characteristics which limit and/or prevent the entry of numerous specific molecules in the CNS. Efflux transporters are proteins that sit in cell membranes and participate in CNS protection by limiting the passage and/or by expelling potentially toxic molecules. For this reason, the activity of efflux transporters reduces the penetration of numerous pharmaceutical molecules into the CNS, thus limiting the effectiveness of drugs that specifically target the brain. There are several efflux transporters families and subfamilies present at BBB level, the most important being the family of adenosine triphosphate (ATP)-binding cassette (ABC) (Kusuhara and Sugiyama 2005).

1.5.4.1. THE ABC FAMILY OF EFFLUX TRANSPORTERS

In humans, ABC efflux transporters are a superfamily of 49 proteins, grouped into 7 subfamilies (ABCA to ABCG) according to their structural homology (Vasiliou et al. 2009). Efflux transporters use the energy released by ATP hydrolysis to transport molecules across membranes, into or out of the cell, against their electrochemical gradient (Löscher and Potschka 2005a). Most ABC family transporters are membrane proteins consisting of four main domains:

- Two cytosolic ATP-binding domains called “nucleotide binding domains” (NBDs), at which level ATP hydrolysis takes place to ensure substrate transport.
- Two transmembrane domains called “transmembrane domains” (TMDs), each one of them comprises 4 to 6 transmembrane α -helices. The two TMDs form the channel through which the transits the molecule that is being transported and ensure ABC protein specificity for its substrates. This is the reason why TMDs vary from one ABC protein to another.

Along to these core domains, other optional domains can be added to the basic structure, such as regulatory domains and/or an additional transmembrane domain (Vasiliou et al. 2009). The mechanism of ABC efflux transporters' action involves the binding of a substrate to their TMD domains. This leads to ATP binding to the two NBDs domains. As a consequence,

ATP is hydrolyzed to provide the energy necessary to move the substrate across the membrane (Linton and Higgins 2007).

ABC proteins are involved in the transport of an important number of biological substances like for example peptides, hormones, sugars and ions, but also in the transport of toxic substances like heavy metals and drugs. By preventing the entry and efflux of many lipophilic substances present in the blood, ABC efflux transporters ensure the protection of the BBB, and thus, the protection of the CNS from several xenobiotics (Potschka 2010).

At the BBB level, the major efflux transporters are the following: P-glycoproteins (P-gp or ABCB1 or MDR multidrug resistance 1), multidrug resistance-associated proteins (MRPs or ABCCs) and breast cancer resistance protein (BCRP or ABCG2) (Staud and Pavek 2005; Abbott et al. 2010).

The first ABC efflux transporter ever discovered was P-gp in 1976 (Juliano and Ling 1976). It is a 170 kDa-phosphorylated glycoprotein encoded by the MDR1 gene. It was discovered through the appearance of multidrug resistant tumors (Juliano and Ling 1976; Kartner et al. 1983). P-gp is also expressed in multiple healthy human tissues such as intestine, kidney, placenta (Staud et al. 2010), furthermore, it can be found in astrocytes (Declèves et al. 2000) and pericytes (Bendayan et al. 2006).

One of P-gp characteristics is its ample range of substrates, which vary in pharmacokinetics as well as in molecular structure and weight. P-gp substrates consist of amphiphilic or hydrophobic molecules, with a molecular weight that varies from 250 to 4000 Da (Seelig 2020).

1.5.4.2. THE MULTIDRUG RESISTANCE PROTEINS MRPs/ABCCs

The MRPs subfamily consists of at least 13 members, 9 of which (MRP1-9) take part in the active transport of molecules. These proteins are transporters of organic anions but can also carry organic molecules. The MRPs generally found in brain ECs are MRPs 1 to 6 (Morris et al. 2017).

MRP1 efflux pump has a wide spectrum of substrates, which includes hydrophobic compounds, glutathione conjugated lipophilic molecules, glucuronate or sulfate. It is

estimated that approximately 20% of drug candidates are MRP1 substrates (Johnson and Chen 2017).

At the cerebral capillaries level, pericytes in culture seem to be able to express some of these MRPs (Santos et al. 2019).

1.5.4.3. THE BREAST CANCER RESISTANCE PROTEIN BCRP/ABCG2

BCRP (ABCG2) was first discovered in a highly resistant to mitoxantrone breast cancer cell line (Doyle et al. 1998). It is a glycoprotein membrane with a molecular weight of 72kDa and is considered a half ABC transporter, with a single NBD and a single TMD. In cells, BCRP can form homodimers or multimers.

BCRP distribution and expression in tissues is often close to that of P-gp, suggesting that these two transporters act in synergy to protect cells from xenobiotics contained in the bloodstream. Additionally, BCRP and P-gp have overlapping wide substrates ranges (Löscher and Potschka 2005b). In a study on P-gp-deficient mice, the expression of BCRP in the cerebral microvessels appeared threefold upregulated compared to the one of wild-type (WT) mice. The results of this study suggest that BCRP overexpression may be a compensatory mechanism for the absence of P-gp (Cisternino et al. 2004).

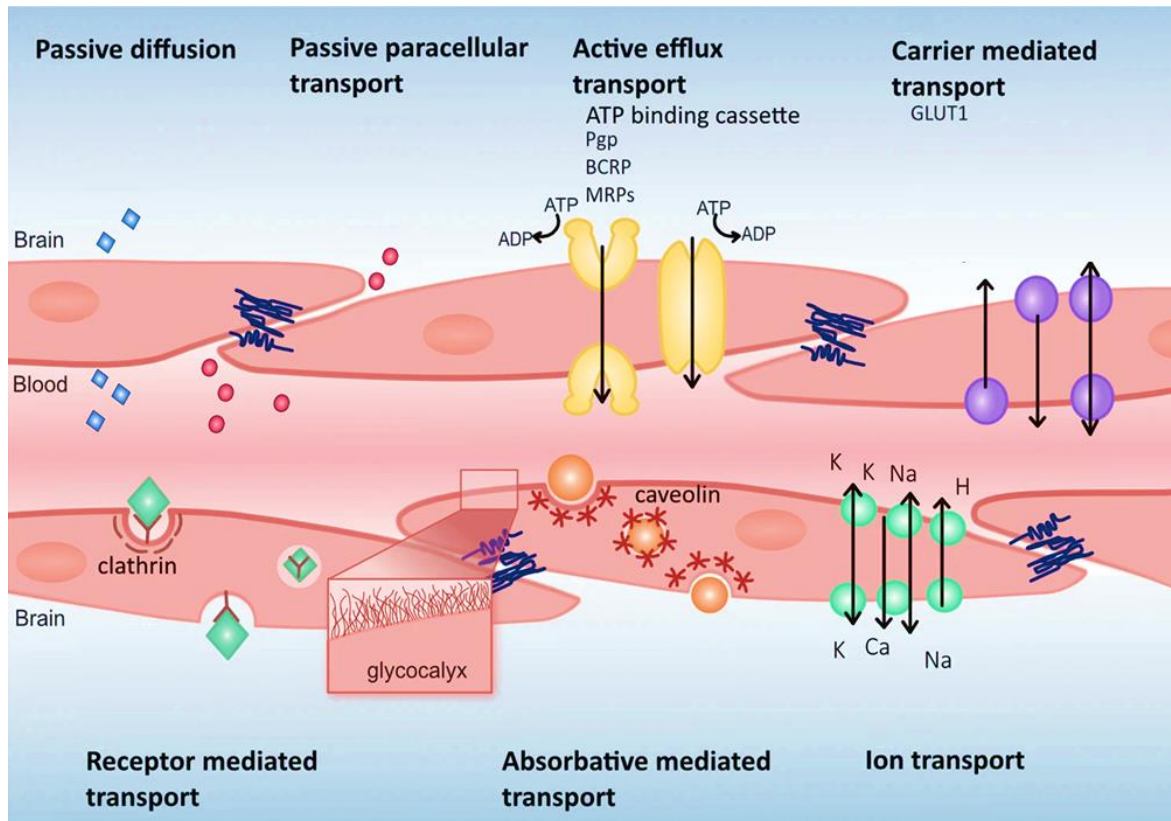


Figure 4 Schematic illustration of the diffusion of molecules and of their transport through the BBB

Simplified version of a schematic illustration with open license reproduced from Knox et al. (2022) (Knox et al. 2022) of the passive diffusion and passive paracellular transport that allow small molecules to cross the BBB. The active efflux transport prevents molecules to cross the BBB by hydrolyze of ATP. Carrier mediated transport allow important molecules like glucose and aa to cross the BBB. Ion transport allows the passage of ions K⁺, Ca²⁺, Na⁺, which are essential for glial cells homeostasis.

2. IN VITRO BBB MODELS

2.1. REPLICATING THE BBB IN VITRO

The first *in vitro* cultures of cerebral endothelial cell (CEC) were established in the 1970s to study the passage or transport of molecules from the blood to the brain or inversely, and used bovine, murine and porcine brain capillaries whose isolation was followed by the enzymatic digestion process to eliminate the basement membrane and the brain pericytes (Helms et al. 2016). The cerebral and blood compartments could then be reconstituted by placing the CECs on a porous plastic membrane, previously coated with ECM components. However, these kind of primary cells are difficult to obtain and to maintain in culture, and important variations between different extractions cannot be avoided (Bhalerao et al. 2020; Dehouck et al. 1994). For this specific reason, transformed cell models have been developed. These models have undeniably facilitated cell culture approaches, however, they have the disadvantage of using cell lineages that sometimes show important changes in their metabolism and physiology. For example, some lineages display a partial loss or decrease in the expression of TJ, resulting in high paracellular permeabilities (Bhalerao et al. 2020). Primary CEC cultures show another limitation, which is that their BBB properties are sometimes lost (Dehouck et al. 1994). To improve these models, glial cells or brain pericytes were then added to the bottom of the wells to create a coculture model (Bicker et al. 2014). *In vivo*, cultured CECs physical and metabolic properties are enhanced and/or maintained by soluble and diffusible factors that are secreted by glial cells or pericytes (Dehouck et al. 1994). Later, some studies have allowed the development of triculture models consisting in culturing CECs in the presence of both glial cells and brain pericytes (Bicker et al. 2014). However, when using these models, there are parameters other than the nature of the cells that should not be neglected, for example, the matrix composition, the membrane porosity, ECs origin and heterogeneity.

2.1.1. THE EXTRACELLULAR MATRIX

The membrane is coated with the extracellular matrix (ECM) which must mimic that present in the cerebral microvessels for the CECs to be able to adhere to it and proliferate. *In vivo*, the ECM is very heterogeneous. It is synthesized by the CECs, pericytes and glial cells (Banerjee et al. 2016; Engelhardt and Sorokin 2009). The artificial matrices commonly used can be made of collagen, matrigel, poly-L-lysine, or fibronectin and thus influence the properties of CECs *in vitro* (Banerjee et al. 2016).

2.1.2. SPECIFICITY OF THE TRANSWELL MEMBRANE

The pores' size of the membrane used in experiments is a crucial point. Pores of 0.4 μm in diameter are used to estimate the passage of small molecules through the BBB. Larger pores are required to be able to study the passage of larger molecules such as peptides, proteins, nanoparticles or even cells. However, ECs have the intrinsic property of migrating. Precautions need to be taken when culturing CECs on large pore membranes to prevent them from passing through them and colonizing the bottom membrane part (Helms et al. 2016), generating double layer models where CECs are not only present on the membrane but also underneath (Vandenhoute et al. 2016). For obvious reasons, this would have an impact on the experiment's results, especially on those centered on permeability (Vandenhoute et al. 2016; Helms et al. 2016).

2.2. STATIC IN VITRO BBB MODELS

Before presenting the main static BBB models, it is important to determine what makes a relevant and reliable static BBB model. The European Centre for the Validation of Alternative Methods (ECVAM), which is composed of experts in various fields, including the field of BBB, has assessed a list of criteria that a BBB model must have (Prieto et al. 2004):

- CECs should have the same morphology and the same markers that are observed *in vivo* such as TJ and AJ proteins, efflux pumps like P-gp, BCRP, receptors for transferrin, LDL, etc., enzymes like cytochrome P450, etc.

- When grown on a membrane, CECs must display low paracellular permeability to small molecules. Tracers such as lucifer yellow and Texas red are generally used to test the paracellular permeability. Another criterion also considered is the measurement of the transendothelial electrical resistance (TEER) provided by the cells. However, this technique is not easy to reproduce and the results obtained heavily rely upon the device used and upon the manipulator, which makes it difficult to compare models with each other.
- The models are intended to be used by other laboratories and/or pharmaceutical companies, therefore they must be reproducible, reliable and easy to culture.

2.2.1. HUMAN MODEL

Used extensively in the study of multiple sclerosis, the human cerebral microvascular endothelial cell line/D3 (hCMEC/D3) allowed the identification of the mechanisms of interaction and extravasation of immune cells across the BBB (Prat et al. 2000; Larochelle et al. 2015). hCMEC/D3 is undoubtedly the most commonly used cell line in studies of the human BBB (Weksler et al. 2013; Weksler et al. 2005). The line was derived from temporal lobe microvessels isolated from a patient with epilepsy. The cells were immortalized by transduction with a lentiviral vector containing the catalytic subunit of human telomerase (hTERT) and the SV40 virus T antigen. hCMEC/D3 has most of the properties of BBB ECs, namely the expression of specific receptors, transporters, enzymes and proteins involved in signaling pathways critical for BBB. However, under culture conditions, a low expression of the TJ key protein claudin-5, is reported (Weksler et al. 2013). This may explain hCMEC/D3 high permeability for low molecular weight molecules (Helms et al. 2016). These properties may be improved by adding specific growth factors to the culture media. Thus, only tracers with a high molecular weight and taken up by membrane receptors and/or transporters can be studied using this cell line. Furthermore, coculture and triculture that use astrocytes and pericytes have little influence on hCMEC/D3 homeostasis (Mkrtchyan et al. 2009).

More recent human BBB lines have been established such as TY10, TY08, BB19, human brain microvascular endothelial cells (HBMEC), NIKM-6, human brain endothelial cell line (HCEC),

HBEC-5i, and HBMEC-3, however, hCMEC/D3 remains the most characterized one (Banerjee et al. 2016).

Static models are used to better understand BBB physiology. Their use has led to significant advances in the treatment of brain metastasis (Larochelle et al. 2015). However, each BBB *in vitro* model possesses its own peculiarities. The choice of the ECs model is closely related to the question raised by the study.

3. BRAIN METASTASIS

The phase in the metastatic cascade in which metastatic cancer cells invade tissue by infiltrating and crossing the vascular endothelial lining is termed transendothelial migration (TEM), transmigration or diapedesis. Cancer cells' TEM is to some degree analogous to the adhesion mechanism of leukocytes.

The probability of success of cancer cells in transmigrating and generating metastases is remarkably low (Chambers et al. 2002; Fidler 1970), which has been hypothesized to be caused by a deficiency of a number of integrins that are needed for adhesion and TEM (Madsen and Sahai 2010). After a circulating metastatic cell attaches to the endothelium, a sequence of events takes place that enables the adhered cells to cross the endothelial monolayer. Additionally, the uncoupling of several endothelial cell-cell junctional complexes is necessary for metastatic migrating cells to pass through the endothelium and invade adjacent tissue. TEM can be divided into two pathways: Paracellular TEM which guides migrating cells to the cell-cell junctional complexes where the uncoupling of adhesion molecules permits the cell to transit through the endothelial cell layer; TEM that entails the migration of cells through the cytoplasm of endothelial cells by a transient reconfiguration of the actin cytoskeleton (Mamdouh et al. 2009; Reymond et al. 2013).

In addition to their role in adhesion, multiple integrin complexes promote the TEM of cancer cells. $\alpha\beta3$ integrin complex is essential for the TEM of metastatic cells and has been demonstrated to be significantly expressed in cancer cells undergoing TEM. In a set of metastatic cancer cell lines, depletion and blocking of $\alpha\beta3$ through siRNA knockdown and specific antibodies decreased TEM, but seemed to have no effect on adhesion (Bauer et al. 2007). It has been further demonstrated that $\alpha\beta3$ -expressing cancer cells bind to the platelet endothelial cell adhesion molecule 1 (PECAM1), which supports the adhesion and transmigration of cancer cells across the endothelium (Weber et al. 2016).

Several endothelial cell-cell adhesion receptors have been linked to the transmigration of metastatic cancer cells. Langer et al. (2011) used both global and endothelium-specific JAM-C knockout mice to demonstrate that JAM-C participates in the passage of cancer cells across the endothelium and in metastatic spreading (Langer et al. 2011).

Adhesion and TEM of metastatic melanoma cells have been linked to the CD146 molecule (Wang et al. 2020; Melnikova and Bar-Eli 2009). Through the use of CD146 knockout mice, it was determined that endothelial CD146 on the host was needed for VEGF-induced focal adhesion kinase (FAK) activation. The latter is essential for the transmigration of melanoma cells during hematogenous dissemination (Jouve et al. 2015). CD146 expression in melanoma has also been shown to be essential for adhesion and TEM, with shRNA knockdown reducing both processes *in vitro* and *in vivo* (Melnikova and Bar-Eli 2009). In addition, endothelial cells from CD146-deficient mice expressed significantly less VEGFR2 and VE-cadherin than endothelial cells from control mice, indicating that CD146 may have a role in regulating the EC phenotype (Jouve et al. 2015).

It has been demonstrated that a number of factors released by cancer cells promote the transmigration of metastatic cancer cells. Work conducted by Padua et al. (2008) have shown that the transforming growth factor (TGF) induces the transcription of angiopoietin-like protein 4 (Angptl4) in metastatic cancer cells. Additionally, Padua et al. (2008) observed that Angptl4 released by metastatic cancer cells triggered the uncoupling of endothelial cell-cell junctions and caused an increase in endothelial permeability, thereby supporting the extravasation of cancer cells into the lungs (Padua et al. 2008). Huang et al. (2011) observed that the binding of Angptl4 to VE-cadherin, $\alpha\beta 1$ and claudin-5 is partly involved in the impairment of the endothelium during tumor cell extravasation. In the latter study, activation of the Rac1 GTPase was also detected, which supports endothelial cell uncoupling by promoting the actin cytoskeleton remodeling (Huang et al. 2011).

Colon cancer cell secretion of CCL2, followed by its binding to CCR2 from endothelial cells, has been shown to trigger JAK-STAT and p38 MAPK signaling pathway. This has led to the disruption of E-selectin-dependent endothelial junctions and consequent extravasation of the metastatic cancer cells (Wolf et al. 2012). Moreover, coordinated activation of E-selectin by monocytes and metastatic tumor cells led to VE-cadherin phosphorylation and cell-cell decoupling which promotes cancer cell transmigration (Tremblay et al. 2006). Additionally, transmigration and metastatic spread of Lewis lung cancer cells were greatly inhibited in the absence of endothelial E and P selectin expression (Kim et al. 2017).

Cancer cells also secrete metalloproteinases such as MMP1, MMP2, MMP9, ADAM12, and other proteases that help break down endothelial cell junction and adhesion complexes, allowing the cancer cell to pass ECs (Reymond et al. 2013; Albrechtsen et al. 2013).

In the course of TEM, metastatic cancer cells deploy a number of additional mechanisms, including the recruitment of multiple blood cell elements to support their transmigration. According to research by Evani et al. (2013), when exposed to the blood flow, monocytes cluster with breast cancer cells and improve the adhesion to endothelial cells activated by TNF α (Evani et al. 2013) . Furthermore, platelets also promote emperipolesis and TEM of circulating cancer cells, which is evidenced by rats' models showing that platelet depletion significantly reduces the development of metastatic lesions(Gasic et al. 1968; Kim et al. 1998; Labelle et al. 2011). As well as promoting metastasis, platelet recruitment by circulating cancer cells has been shown to reduce the ability of immune cells to identify and eliminate metastatic tumor cells. Platelets act as a barrier in cancer cell clusters and prevent identification and elimination by natural killer cells, allowing cancer cells to escape and survive.

Metastatic cancer cells trigger endothelial cell necroptosis, which is an inducible type of apoptosis, in order to successfully achieve transmigration. Cancer cells that express amyloid precursor protein (APP) trigger endothelial death receptor 6 (DR6), which causes the death of endothelial cells (Strilic et al. 2016).

4. MELANOMA

“As to the remote and exciting causes of melanosis, we are quite in the dark, nor can more be said of the methodus medendi. We are hence forced to confess the incompetency of our knowledge of the disease under consideration, and to leave to future investigators the merit of revealing the laws which govern its origin and progress....and pointing out the means by which its ravages may be prevented or repressed” - Thomas Fawcington, The Manchester Royal Infirmary, 1826.

Melanomas are malignant tumors that originate from melanocytes. Of all skin cancers, melanoma is the most fatal. Of all cancer types, melanoma is also the cancer with the highest level of brain tropism. Approximately 50% of patients with stage IV melanoma are diagnosed with melanoma brain metastases. A percentage that rises when postmortem patients are also counted. Following lung cancer and breast cancer, melanoma is the leading cause of malignant metastasis to the central nervous system. Of all metastatic brain tumors, melanoma represents 6-12% of cases (Janavicius et al. 2020). The overall survival rate following a diagnosis of melanoma brain metastases has been historically low (Bander et al. 2021). However, over the past ten years, advances in targeted therapies as well as in immunotherapies have significantly improved the survival rate of patients with advanced melanoma (Bander et al. 2021). Melanoma brain metastases most frequently occur at the junction between the gray and the white matter and in the frontal lobe (Redmer 2018).

4.1. CLASSIFICATION OF CUTANEOUS MELANOMA

The most commonly used anatomical classification separates melanomas into the following five major types (Scolyer et al. 2011):

- Acral lentiginous melanoma (ALM);
- Hutchinson’s malignant lentigo or precancerous melanosis of Dubreuilh or LM (lentigo maligna);

- Mucosal lentiginous melanoma (MLM);
- Nodular melanoma (NM);
- Superficial spreading melanoma (SSM), which is the most common type of most frequent melanoma.

Melanoma	Lentiginous			Superficial spreading melanoma (SSM)	Nodular melanoma (NM)
	Lentigo maligna melanoma (LM)	Acral lentiginous melanoma (ALM)	Mucosal lentiginous melanoma (MLM)		
Frequency in %	5 to 10	2 to 10	1	60 to 70	10 to 20
Horizontal epidermic feature	Lentiginous	Lentiginous	Lentiginous	Pagetoid, visible lateral to the invasive contingent	Absent
Vertical invasive feature	Rare	Inconstant	Frequent	Very frequent	Always
Area of occurrence	Elderly subject, face, neckline	Palms, soles, fingers, toes	Mouth, gland, vulva		
Aspect	Macula, then layer pigmented then very late tumor	Macula, late tumor	Pigmented macula then ulcerating tumor often partially achromic	Pigmented macula then tumor	A tumor of immediate onset and often of rapid growth

Table 1 Summary table of the different types of melanoma

The table shows the different types of melanoma, indicating for each type the frequency in %, the horizontal epidermal feature, the vertical invasive feature, the area of occurrence, the aspect.

The frequency distribution of the histological type of melanoma is dependent on environmental factors such as sun exposure and ethnicity.

4.2. MELANOMA INCIDENCE AND PREVALENCE

According to the American National Institute of Health (NIH), the rate of new melanoma of the skin cases and related deaths was 21.5 per 100,000 men and women per year. The death rate being 2.1 per 100,000 men and women per year. These rates are age-adjusted and based on 2015–2019 cases and 2016–2020 deaths.

Moreover, the probability (incidence) is that approximately 2.1 percent of men and women are going to be diagnosed with melanoma skin cancer during their lifetime, based on 2017–2019 data.

As for the prevalence of this cancer, in 2019, there were approximately 1,361,282 individuals suffering from melanoma of the skin in the United States.

In 2022, the number of skin melanoma new cases in the United States was estimated by the NIH to be around 99,780 and the correspondent number of deaths was estimated to be around 7,650. The overall 5 year relative survival rate was around 93.7% between the end of 2012 and 2018.

All of the above is variable depending on the regions of the world, and is correlated with latitude (UV exposure) and ethnic characteristics of the populations. The highest incidence is found in light skin phototype populations in regions with high UV exposure. It is estimated that the total number of patients diagnosed with melanoma will continue to increase in the coming decades, this is mainly due to the increase in life expectancy and the aging of the population as well as for example, to risky behaviors and the gradual thinning of Earth's ozone layer (Saginala et al. 2021).

4.3. RISK FACTORS FOR MELANOMA SKIN CANCER

Melanoma skin cancer can be genetically determined as well as influenced by UVR exposure. Exposure to ultraviolet radiation (UVR) has been known to be a risk factor for melanoma for many years. UVR exposure includes solar exposure as well as artificial sources, such as tanning beds. Phototype is another risk factor. It classifies individuals according to the reaction of their skin to UVR exposure and depends on skin, eye and hair color. The probability to develop skin melanoma is inversely correlated with the pigmentation level (Carr et al. 2020).

As aforementioned, there is also a genetic component to melanoma. CDKN2A gene is a tumor suppressor gene and its mutation predisposes to the development of melanoma. Its prevalence is about 2%, higher in cases of multiple melanomas or of a family history of melanoma. The BRCA1 gene is another tumor suppressor gene, its mutation predisposes to melanoma. It is responsible for a wide spectrum of neoplasia such as mesothelioma, renal cell carcinoma, basal cell carcinoma, as well as benign melanocytic tumors. With less than 1%, its prevalence appears to be lower than CDK2NA gene mutations. The majority of melanomas arise de novo (70%) and are not nevus associated (30%) (Carr et al. 2020).

4.4. BRAIN METASTASIS IN MELANOMA

Melanoma is the third most common cancer-causing brain metastases after lung cancer and breast cancer, accounting for 6 to 14% of all brain metastases. About 57% of autopsies of patients with melanoma of the skin showed brain metastases (Ostrom et al. 2018; Schiff and van den Bent 2018). The 5-years survival rates for a patient with a stage IV melanoma ranges from 8% to 18% (Pisani et al. 2020 Apr).

There are significant differences in the frequency of brain metastases occurrence depending on the type of primary cancer. Lung cancer (small cell and non-small cell), renal cancer, breast cancer (especially HER2-positive and triple negative) and melanoma are among the primary cancers that metastasize. Melanoma cells have been shown to have a very strong angiotropism (Barnhill et al. 2009).

Pericytic mimicry, or the spread of tumor cells on the abluminal surface of capillaries, is promoted by angiotropism (Lugassy et al. 2013). Melanoma cells that continuously move outside of blood vessels to secondary sites represent an instance of extravascular migratory metastasis. Melanoma cells can propagate through this pathway to local or distant areas. Of interest, tumor cells have been shown to migrate at speeds ranging from 0.01 $\mu\text{m}/\text{min}$ to 2 $\mu\text{m}/\text{min}$, or from 0.5 cm to 105 cm/year. Due to the faster amoeboid migration of cancer cells, these distances may become considerably greater (Lugassy et al. 2013; Bentolila et al. 2016). In the course of human cancer, these rates are consistent with the time gap between the detection of the primary tumor and the development of visible metastases foci.

Furthermore, it has been shown that the angiotropic interplay of melanoma cells with endothelial cells results in the change of expression of certain genes that are related to cancer cell migration, EMT, embryonic and stem cell features, and pericyte recruitment.

4.5. RISK FACTORS FOR BRAIN METASTASIS IN MELANOMA

Several studies in the literature investigate the risk factors for the development of brain metastases in melanoma. The results are highly variable and can be explained by different numbers and methodologies.

In a retrospective study of 2014, Gumusay et al. found the following risk factors for brain metastases in melanoma: location of the primary tumor in the head and neck, a Breslow index higher than 4 mm, histological ulceration, and N2 or N3 (lymph nodes containing tumoral cells) involvement (Gumusay et al. 2014).

The ulceration and the location of the primary tumor in the head and neck were also found to be significant risk factors for the development of brain metastases (Zakrzewski et al. 2011).

For Daryanani et al., tumor location in the head and neck appeared to be a risk factor for brain metastasis as well as a Breslow index higher than 4 mm, male sex, young age, and a mitotic index higher than 5 mitoses per field. For these authors, ulceration does not appear to be a risk factor (Daryanani et al. 2005).

Sampson et al. reported a 20-year retrospective study of 6,953 melanoma patients, 702 of whom had brain metastases. Male gender, mucosal or skin location of the primary tumor on the trunk, head, and neck, melanoma with high Breslow scores or ulcers, and histologic subtype (lentiginous or nodular acral) were associated with the development of brain metastases (Sampson et al. 1998).

In a study of the clinicopathological correlation of BRAF and NRAS mutations in patients with metastatic melanoma, these mutations appear to be risk factors for brain metastases with a higher proportion of metastases compared to subjects without mutations (Ren et al. 2022).

Thanks to advances in molecular biology, several somatic mutations have been identified in melanoma that represent therapeutic targets (Hodis et al. 2012).

Mutations in the BRAF gene are the most frequent mutations, they are found in approximately 50% of cases. The two most frequent mutations are V600E and V600K. These mutations are mostly found in melanomas of skin that has received intermittent UVR exposure (Gutiérrez-Castañeda et al. 2020).

The NRAS mutation was first described in 1984 (Padua et al. 1984) and is found in 15-20% of melanomas (Mehnert and Kluger 2012).

It has been shown that PTEN is correlated with metastatic melanoma (Goel et al. 2006).

The NF1 gene is a tumor suppressor gene, and its mutations, most often responsible for loss of function, are found in 12 to 18% of melanomas. They are responsible for activation of the MAP-kinase pathway leading to loss of Ras inhibition and cell proliferation (Larribère and Utikal 2016).

4.6. THERAPEUTIC STRATEGIES FOR BRAIN METASTASIS

In the case of a patient with brain metastases, three situations must be distinguished (Tawbi et al. 2018): In the case of a single brain metastasis (or 1 to 5 maximum), the first-line treatment to be favored is local treatment with surgery or stereotaxis depending on the location, size and number of metastases. If local treatment is incomplete, it is recommended to add a systemic treatment according to the mutation status of the tumor. In the case of multiple brain metastases, and especially if there are also extra-brain metastases, treatment is based on a systemic therapy chosen according to the mutation status of the tumor. Association with a local treatment is to be considered according to the location, the benefit/risk ratio and the clinical symptoms. For palliative and/or symptomatic situations: patient global management and palliative radiotherapy and care (Arora et al. 2022).

5. BBB DISRUPTION

Following an injury or a disease, the brain endothelium and ECM go through substantial alterations such as TJs disruption, ECM remodeling, ECM proteins enzymatic degradation by reactive oxygen species (ROS) and matrix metalloproteinases (MMP). These changes may contribute to a leakage of the BBB allowing proteins, immune cells and potential neurotoxins derived from the circulatory system to enter the brain. These changes may also lead to the synthesis of ECM molecules that are normally absent in a physiological state (Summers et al. 2013; Arvanitis et al. 2020; Ahluwalia et al. 2020). Dysfunctions in maintaining BBB and TJ integrity may result from TJ protein phosphorylation as well as from RhoA GTPase pathway, both of which can generate changes in the permeability of the BBB leading to its impaired functioning (Luissint et al. 2012).

CNS homeostasis relies, among other things, on the complex regulation of transcytosis at the BBB level, hence, changes in these pathways can be partly responsible for the pathogenesis of pathogenesis of multiple cerebrovascular diseases (Abbott et al. 2010; Ballabh et al. 2004; Zhao et al. 2015). BBB disruption and the subsequent mechanisms implicated in its dysfunction are closely related to the nature of the CNS disorder, the latter can be acute or chronic. In the case of CNS acute disorders like ischemia, BBB disruption consequent inflammatory mechanisms are resultant from the primary injury. Acute conditions, such as cerebral vascular accident for example, can implicate the following responses : Vasculitis, degradation of the ECM, infiltration of immune cells into the brain parenchyma, structural alterations in TJs causing structural changes in ECs (Sandoval and Witt 2008). BBB disruption in multiple chronic neurodegenerative CNS disorders, such as Alzheimer's disease, Parkinson's disease, Huntington's disease, manifests as capillary leakage of molecules derived from the circulatory system into the CNS, ECs degeneration leading to disruption of AJs and TJs, and anarchic cellular infiltration into the CNS (Sweeney et al. 2018). Whether acute or chronic, CNS disorders put NVU function in jeopardy and compromise the activity of resident brain cells like neurons and microglia.

Melanoma Initiation and Progression

Metastatic Process towards the Brain

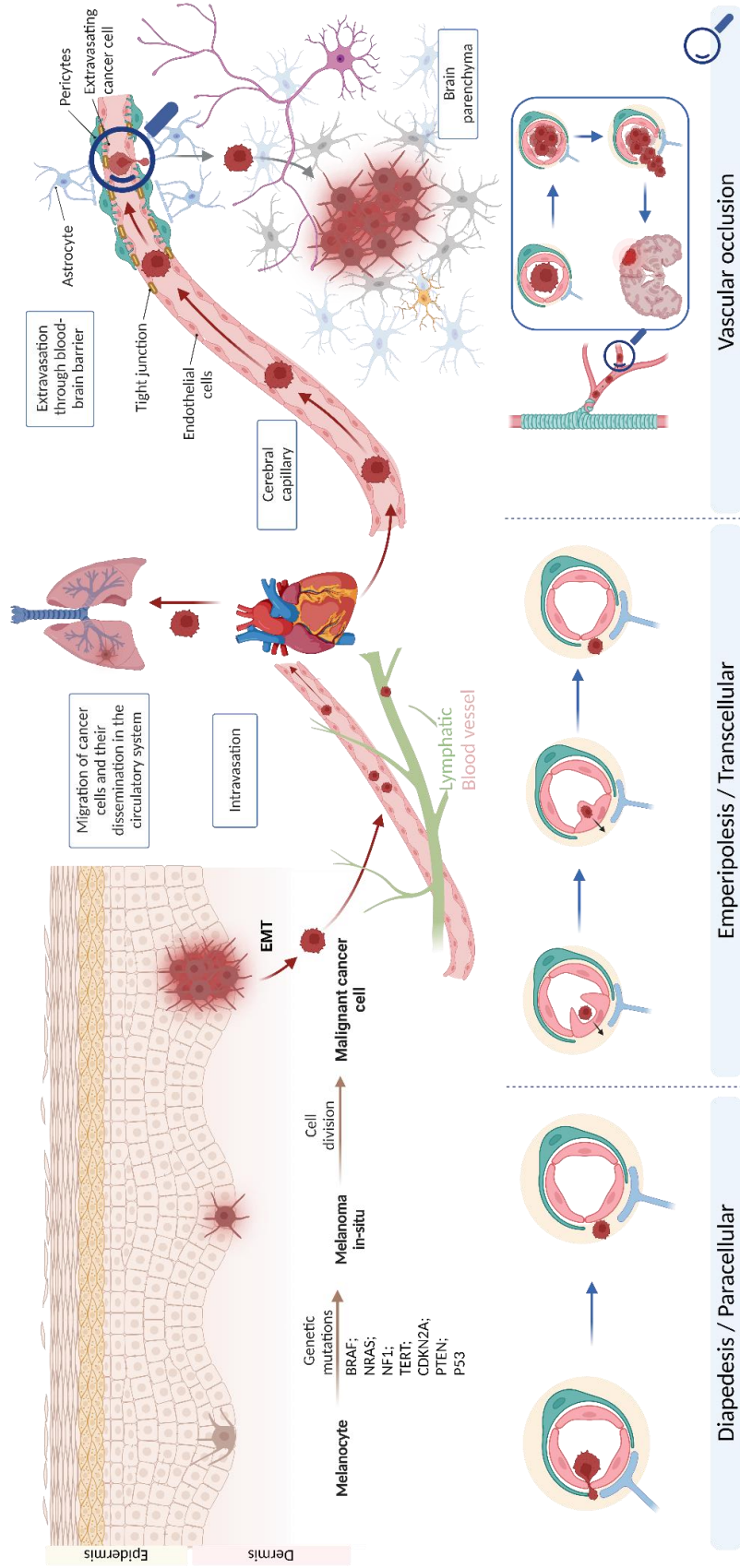


Figure 5 From melanocyte to melanoma metastasis: the pathway to the brain

Schematic illustration created using BioRender. The route of melanoma metastasis begins with a phenomenon called epithelial-mesenchymal transition (EMT) and is followed by the mechanism of intravasation into the vascular system. Once they reach the vascular system, the metastases begin to circulate within it until they reach the heart and are redirected into the small circulation. Once they have passed this stage, they can adhere to the endothelial cells of the lungs or remain blocked in the capillary network of the latter, where, after the extravasation mechanism, they can form a tumor. They may also continue their journey and return to the heart to be pumped into the systemic circulation. Upon entering the systemic circulation, metastases may reach the cerebral vascular network where they can either adhere to the endothelial cells of the brain capillaries or get stuck in them. To form a tumor in the brain parenchyma, metastases must penetrate and cross the BBB. Two transit pathways are available for metastases to cross the BBB: the transcellular and paracellular pathways. A third hypothesized route is that of vascular occlusion.

Melanoma metastases travel to the brain (**Figure 5**) starts with the epithelial-mesenchymal transition (EMT). Notch1 pathway is activated during the cell transition from an epithelial phenotype to a mesenchymal one, leading to the overexpression of N-cadherin (Murtas et al. 2017). Once the newly generated metastases reach the circulatory system via intravasation, two routes are possible: through the general blood circulatory system or through the lymphatic system. Both routes lead to the heart and to the small circulation where the metastasizing cells can eventually stop and form a tumor. Metastasizing cells that stay in the circulatory system eventually reach the brain capillaries where the blood pressure is lower compared to the rest of the artery circuit. At this point, the metastases may start to adhere to the endothelial cell layer, for example through the interaction between the vascular cell adhesion molecule VCAM-1 and VLA4 integrin (Klemke et al. 2007). Once they have adhered, three passageways have been observed and hypothesized. Recent work from Fazakas et al. (2019), showed that melanoma in their BBB *in vitro* model, is able to cross endothelial cells via the paracellular passage and that breast cancer cells cross via the transcellular pathway or emperipolesis (Fazakas et al. 2011). The vascular occlusion hypothesis needs to be yet confirmed, it may occur when metastases get stuck in brain capillary beds and start to divide, and finally manage to reach the brain parenchyma by creating an infarction.

6. AIM OF THE THESIS

One feature of these disease pathogeneses that remains to be comprehensively explored, and as such a particularly challenging field of interest, both from a biological and pharmaceutical point of view, is the passage of cancer and immune cells through the vascular endothelium. The research aim of the present study is the ideation and consequent creation of effective *in vitro* and *in vivo* models to investigate the mechanism by which tumor cells reach the brain parenchyma during the early stage of the blood-brain barrier invasion and subsequent integrity loss, which adds to disease pathogenesis.

This research comes in the wake of a preliminary recent study carried out by the LCNP group, which showed that breast cancer treatment with docetaxel seems to increase brain metastases by destabilizing the blood-brain barrier integrity (Bernatz et al. 2019). The group used an *in vitro* BBB model as well as an *in vivo* murine model of left heart ventricle injection. When examining studies of BBB invasion and integrity loss, one major matter of contention is that each study employs various BBB models and applies different criteria, such as for example cell line origin, thus making it hazardous and inaccurate to compare the dysfunction mechanisms.

Melanoma homing to the brain makes this tumor type a particularly valid candidate to investigate the BBB invasion phenomena.

In the present study, we replicated the cellular composition of the BBB to show how the NVU is affected by brain metastases. The knowledge surrounding the metastatic invasion cascade of the BBB would be substantially lacking without *in vitro* models. Along with the ease of use, the relatively low costs, and the high flexibility, *in vitro* models allow the use of human cell lines to mimic certain features of disease pathology. These advantages over traditional preclinical platforms in testing efficacy and toxicity are particularly important in future drug discovery. Here, we put in place an easily reproducible *in vitro* BBB model established coculturing immortalized human cell lines. We then tested this model integrity and suitability to brain metastasis invasion using the amelanotic melanoma A375 cell line and tried to assess the impact that the invasion of the BBB induces in this tumor cell line.

Within the BBB *in vitro* microenvironment and as a pilot study, attempted to determine whether there was a difference in the gene expression of the A375 cell line before and after

crossing the BBB *in vitro*. The potential findings, may in the long run, help develop novel therapies to maintain BBB integrity and function.

In addition, we put in place an *in vivo* murine model using A375 melanoma cells to inject the left heart ventricle in order to recreate the metastasizing process to the brain and be able to observe the early stage of melanoma invasion of the BBB to determine the time lapse between the injection and the tumors reaching the brain parenchyma. For this latter task we used correlative light imaging and electron microscopy.

PART II. MATERIALS AND METHODS

1. IN VITRO MODEL

1.1. CELL CULTURE

Immortalized human cerebral microvascular endothelial cells (hCMEC/D3) were cultured in EGM-2 bullet kit from Lonza. SV40-immortalized human brain vascular pericytes were cultured in pericytes medium (PM) from ScienCell Research Laboratories. SVGA human immortalized astrocytic cell line and A375 melanoma cell line were cultured in DMEM full from Lonza, supplemented with 10% FBS, 1% penicillin/streptomycin, 1% ultraglutamine, 1% Sodium Pyruvate from Gibco. A375_mCherry was cultured in DMEM full with 100µg of G418 (puromycin) for selection. A375 (ER) mono resistant cells were cultured with 15 nM Encorafenib (BRAFi) to maintain their resistance. Double resistant A375 (DR) cells were cultured with 200 nM Binimetinib (MEKi) to maintain their resistance. All the inhibitors were diluted in fresh DMEM 1% ultraglutamine, 1% sodium pyruvate, 10% FBS.

hCMEC/D3, SV40-HBVP, SVGA cell lines were provided by Prof. Dr. Ulrike Naumann from the Hertie-Institut für Klinische Hirnforschung at Tübingen Neuro Campus. A375 cell lines were provided by Associate Professor Dr. Stephanie Kreis from the Signal Transduction Group at the Department of Life, Science and Medicine (DLSM) at the University of Luxembourg. Further details on the media composition are provided in the Appendix.

1.2. TESTING OF CULTURE MEDIA

In order to find the culture medium able to maintain the cells in an environment that allows the formation of a sustainable coculture *in vitro*, we tested the different culture media that are used for the culture of immortalized human cells on each cell type as shown in **Figure 6**. We then tested the viability of the cells using trypan blue.

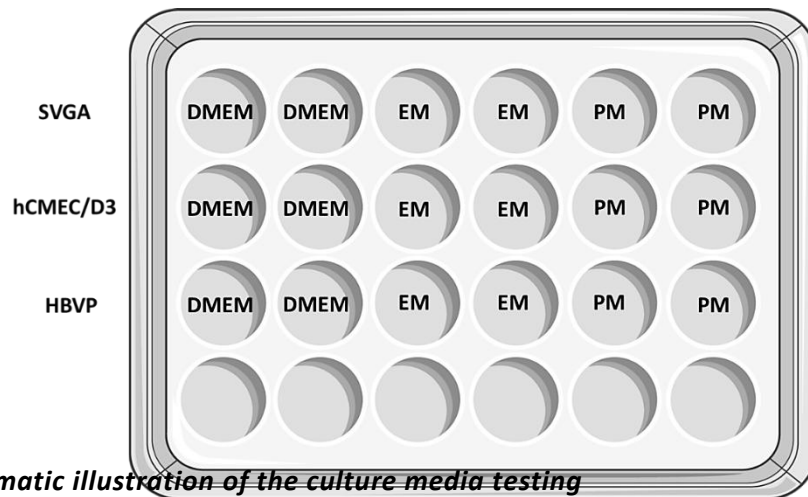


Figure 6 Schematic illustration of the culture media testing

Schematic illustration created using BioRender. Culture media testing to identify the medium that provides optimal sustainability of the hicBBB *in vitro* model.

1.3. PROLIFERATION ASSAY

To measure the proliferation of the human immortalized blood-brain barrier (hicBBB) and A375, cells were seeded on 24-well plates at a density of 5×10^4 cells per well were maintained in the cell incubator at 37 °C/5% CO₂. Plates were transferred to IncuCyte Live Cell Analysis System (Sartorius, Göttingen, Germany) where hicBBB and A375 cells were visualized for 96h at 2h intervals with a 10x magnification objective for image acquisition. Cell density was calculated for each time point from two ROIs per well by applying a phase contrast mask that allows cell/per field identification. A minimum of three biological replicates with two technical replicates were performed for statistical analysis.

1.4. MIGRATION AND INVASION ASSAY

The Boyden chamber migration assay was previously detailed by (Ilina et al. 2022). The migratory abilities of hicBBB and A375 cells were assessed using 8µm pore Boyden chambers without coating (ThinCert cell culture inserts, Greiner) or coated with FN and PLL from Sigma Aldrich. 50,000 cells were seeded in the upper part of the Boyden chambers in their original culture medium without creating chemoattractant gradient. After 24-48-72 hours, cells were

fixed in 4% PFA for 10 minutes and washed briefly twice in PBS and non-migrating cells were removed. Cell nuclei were stained with DAPI for 5 minutes and washed twice in PBS before imaging. Migrating or invasive cells were quantified by counting the number of cells on the underside of the membrane using a Nikon DS Ri2 microscope (Nikon, Tokyo, Japan) with a 10x magnification objective (5 representative fields per membrane). The experiments were conducted in three biological replicates (each with two technical replicates). Details on the invasion potential of the hicBBB cell lines are provided in the Appendix (Figure 47).

1.5. hicBBB FORMATION PROTOCOL

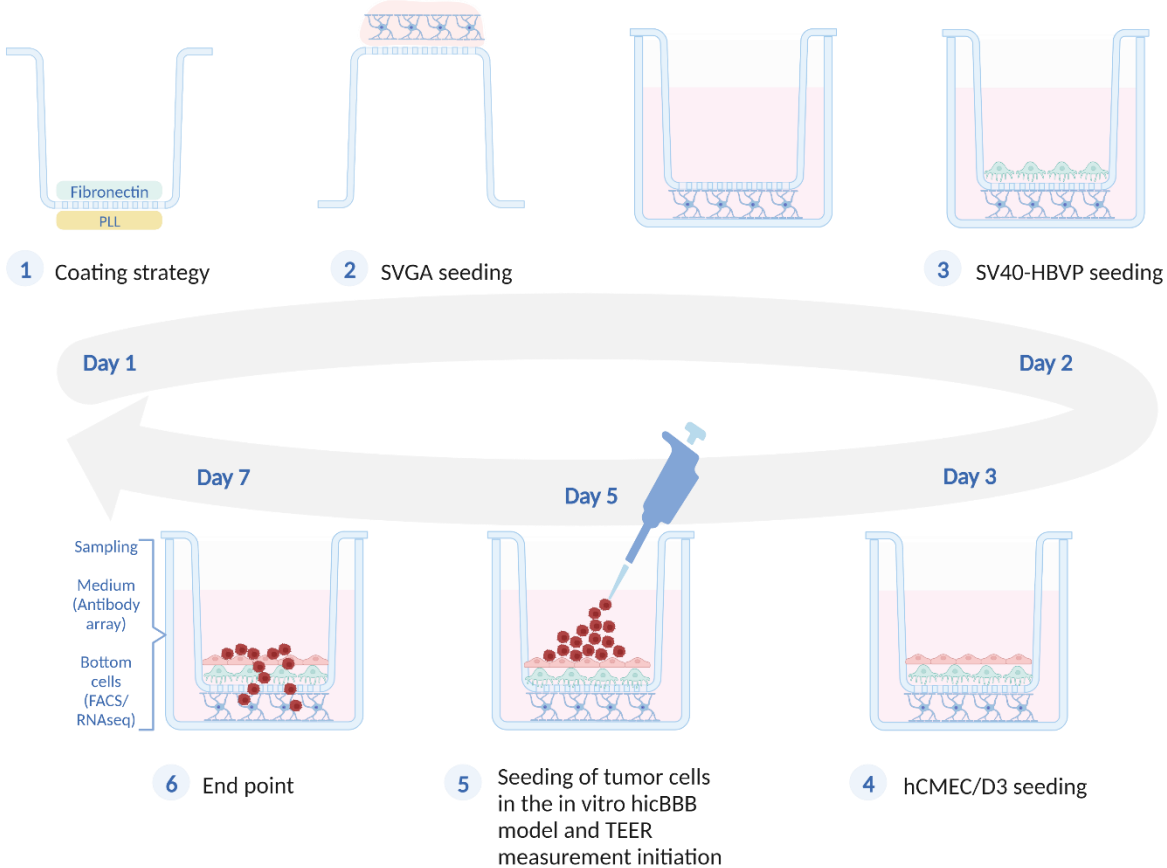


Figure 7 Schematic illustration of the hicBBB in vitro model formation protocol

Schematic created using BioRender. Description of the individual steps required for the formation of the *in vitro* hicBBB model.

The hicBBB *in vitro* model is made in Boyden chamber ThinCert translucent with 8 μm pores from Greiner. Further details of the process can be found in the schematic illustration above (Figure 7).

Day 1 Coating and SVGA seeding

The bottom side of the ThinCert is coated with Poly-L-Lysine (PLL) from Sigma Aldrich at 0.001%. The upper side is coated with human plasma-derived fibronectin (FN) at a concentration of 5 $\mu\text{g}/\text{cm}^2$ from Sigma Aldrich. $4,5 \times 10^5$ SVGA cells are seeded on the underside of the PLL-precoated ThinCert using DMEM as medium. For 45 minutes, the cells are allowed to adhere to the PLL-coated bottom surface. Then, they are turned upside down and placed in the incubator overnight.

Day 2 Pericytes seeding

Inserts already with astrocytes are transferred to a new 24-well plate with PM. $4,5 \times 10^5$ SV40-HBVP cells are seeded on the upper chamber coated with human FN using PM. They are then placed in the incubator overnight.

Day 3 hCMEC/D3 seeding

The inserts containing SVGA and SV40-HBVP are transferred to a new 24-well plate with EGM-2 medium. $7,5 \times 10^5$ hCMEC/D3 cells are seeded on the upper chamber coated with SV40-HBVP. Then they are placed in the incubator overnight.

Day 4 hicBBB formation

On the 4th day of the hicBBB experiment, we change the medium of the upper and lower compartment.

Day 5 TEER measurement and tumor cell seeding

TEER is measured using the nanoAnalytics CellZscope 2 by programming the frequency from 1 Hz to 100 kHz. During this step of the protocol, we also seed $5,0 \times 10^6$ A375 wt cells or treatment resistant.

Day 6 Tumor cell migration

On day 6 after seeding tumor cells in the *in vitro* hicBBB model, we change the medium (200 μ l) of the upper and lower compartment while constantly measuring the TEER.

Day 7 Tumor cell sorting

We finish the TEER measurement and prepare the hicBBB for tumor cell sorting by flow cytometry or for immunofluorescence, we also collect the supernatant that we will apply on the antibody array (see FACS sorting section).

1.6. TIME-LAPSE OBSERVATION OF TUMOR CELLS CROSSING THE hicBBB MODEL

We proceeded to a live-cell imaging observation using confocal microscopy to assess the average time lapse during which tumor cells pass through the hicBBB *in vitro* model. For this purpose, we followed A375 cells expressing mCherry through the hicBBB model using confocal microscopy. Before transferring the model to the microscope chamber for live imaging, we stained the bottom cell layer (SVGA cells) using Hoechst. We then transferred the coculture to a 24-well plate with glass bottom and incubated it at 37 °C and 5% CO₂ in the Zeiss LSM 880 incubator. We acquired images every 15 minutes overnight.

1.7. hicBBB IN VITRO MODEL PERMEABILITY TEST

To assess the permeability of the hicBBB model, we used dextran-coupled fluorophores. Once the hicBBB is fully formed or after seeding the A375 cells, we applied a solution that contains the usual Endothelial Cell Growth Medium-2 BulletKit (EGM-2) with a concentration of 10 μ M of Antonia RED 3kD from Sigma Aldrich (AR). Then, we sampled 100 μ l from the lower chambers of the hicBBB model every 30 minutes five times. Then we read the raw fluorescence using a CLARIOstar[®] plate reader. Finally, we used the raw fluorescence unit (RFU) to visualize the passive permeability of the hicBBB.

1.8. FACS SORTING OF FLUORESCENT TUMOR CELLS

For sorting A375 cells, we washed the insert containing hicBBB and tumor cells with PBS and immersed the lower part of the ThinCert in trypsin to harvest cells from the SVGA side of the membrane. Subsequently, we sorted the cells using the mCherry signal or the CellTracker[™] Deep Red Dye. As a control, we used all cells that comprise the hicBBB as well as the original A375 cells to isolate fluorescent cells and eliminate any auto-fluorescence.

1.9. ANTIBODY ARRAY

We used the conditioned medium of hicBBB on antibody arrays. We used human MMP antibody array, human cytokine antibody array, human angiogenesis array, human MAPK array from abcam following the protocol given by the supplier.

TARGET	REFERENCE
MMP ANTIBODY ARRAY	ab134004
HUMAN CYTOKINE ANTIBODY ARRAY	ab133998
HUMAN ANGIOGENESIS ARRAY	ab134000
HUMAN MAPK ARRAY	ab211061

Table 2 Antibody array reference table

Further details on the antibody arrays' composition are provided in the Appendix.

1.10. IMMUNOFLUORESCENCE

Immunofluorescence (IF) was performed on cell monolayers as well as hicBBB models that had been previously fixed in paraformaldehyde (PFA), permeabilized with 1.5% Triton solution, blocked with 5% donkey serum, and then incubated overnight with the primary antibody (**Table 3**).

ANTIBODY NAME	COMPANY	REFERENCE	CELL	HOST SPECIES
ANTI-PDGFR BETA	Abcam	ab32570	SV40-HBVP	Rabbit
ANTI-ZO-1	Abcam	ab190085	hCMEC/D3	Goat
ANTI-CD31/PECAM-1	Abcam	ab9498	hCMEC/D3	Mouse
ANTI-A-SMA	Abcam	ab5694	SV40-HBVP	Rabbit
ANTI-CLAUDIN 5	Abcam	ab15106	hCMEC/D3	Rabbit
ANTI GFAP	Synaptic Systems	173 004	SVGA	Guinea Pig
ANTI-OCCLUDIN ANTIBODY (TIGHT JUNCTION)	Abcam	ab235986	hCMEC/D3	Rabbit

Table 3 Antibody reference table for IF and WB

The next day, the sample was incubated with the secondary antibody for two hours (**Table 4**).

ANTIBODY TARGET	FLUOROPHORE	COMPANY	REFERENCE	HOST SPECIES
-----------------	-------------	---------	-----------	--------------

ANTI-GOAT	Alexa Fluor® 488	Jackson ImmunoResearch	705-545-003	Donkey
ANTI-RABBIT	Cy™3 550	Jackson ImmunoResearch	711-165-152	Donkey
ANTI-GUINEA PIG	Alexa Fluor® 647	Jackson ImmunoResearch	706-605-148	Donkey
ANTI-MOUSE	Alexa Fluor® 555	Life technologies	A21422	Goat

Table 4 Secondary antibody reference table

1.11. IMMUNOCYTOCHEMISTRY

All immunocytochemistry (ICC) analyses were performed at the National Health Laboratory according to the standard procedure that is followed in the pathology routine. Cell pellets were prepared and fixed with PFA, embedded in kerosene and then stained for the following marker. Each stain was accompanied by a corresponding hematoxylin and eosin stain to verify histologic features. SOX10, HMB45, MelanA, BRAFV600E.

1.12. TEER MEASUREMENT WITH THE CELLZSCOPE2

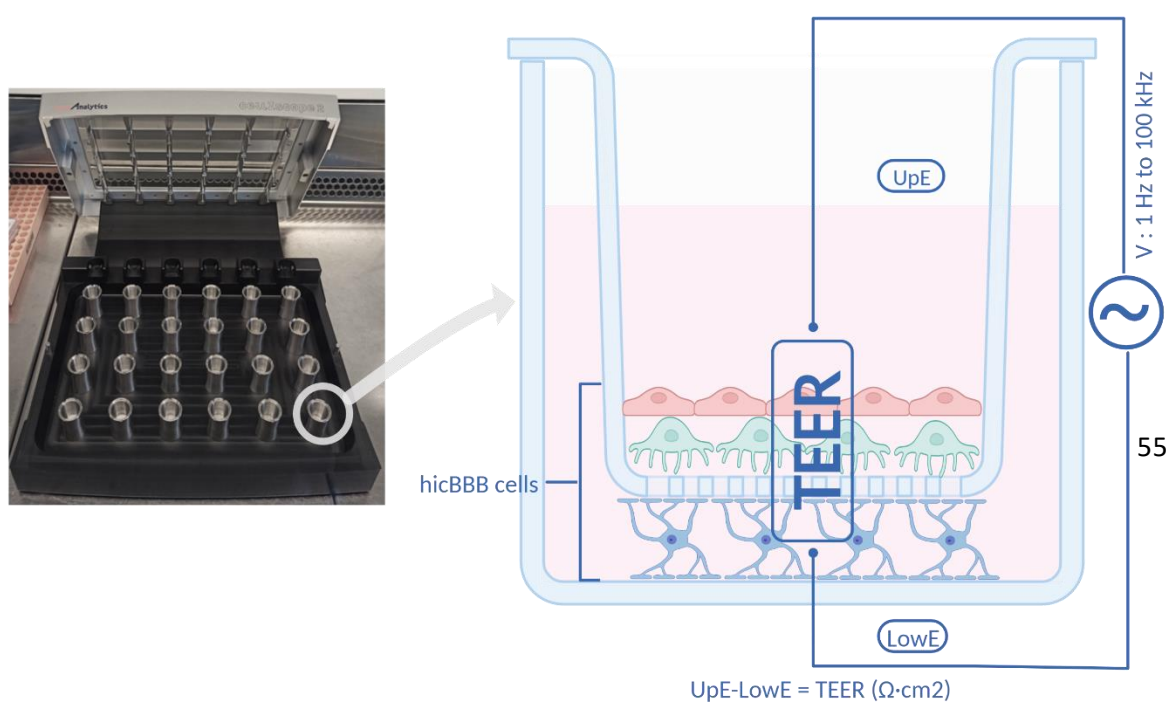


Figure 8 Schematic representation of TEER measurement using the cellZscope2

Schematic representation of TEER measurement using the cellZscope2 showing the impedance difference between the upper and lower chambers of the transwell generated by the presence of the *in vitro* hicBBB model. UpE = upper electrode; LowE = lower electrode; TEER = trans-endothelial electrical resistance.

To measure the efficiency as well as the resistance of the hicBBB model we use the cellZscope2 (NanoAnalytics, Münster, Germany) during the experiment described above according to the manufacturer's protocol (**Figure 8**). The TEER is recorded every 15 minutes for all wells. The measurement starts with the calibration of the machine to check that all electrodes are functional.

1.13. ELECTRON MICROSCOPY

The first step in the preparation of a sample for the electron microscope begins with a crucial step, which is fixation. For this we used the Karnovsky fixative which is composed of 2% Paraformaldehyde, 2.5% Glutaraldehyde in 0.1M Cacodylate buffer at pH 7.4, always prepared freshly before fixation. Then there is a post-fixation step, for this, we used a 1% osmium solution in 0.1M Cacodylate buffer. Successively, there is a dehydration step in an ethanol bath from 30% to 90% with an increase in concentration of 20% at each successive bath, to finish in a 100% ethanol bath. We then placed the dehydrated samples in 2 consecutive baths of 100% acetone. Finally, we embedded the samples in an epoxy resin according to the recipe below.

COMPOSITION /HARDNESS	SOFT	MEDIUM	HARD
AGAR100	24g	24g	24g
HARDENER DDSA	22g	16g	9g
HARDENER MNA	6g	10g	15g
ACCELERATOR BDMA	1,5g	1,5g	1,5g

Table 5 Table of alternative compositions of the EM resins

The following solution recipe was used to process our samples. We put the samples in successive baths of resin mixed with acetone as described below:

¼ resin + ¾ solvent: 1 hour

½ resin + ½ solvent: 1 night

¾ resin + ¼ solvent: 3 hours

Pure Resin: 1 hour

Pure Resin: 1 night

Pure Resin: 1 hour

Finally, we placed the samples in fresh pure resin for 72 hours at 60 °C for its polymerization. Once the polymerization step completed, we proceeded to cut the samples with an ultramicrotome to obtain 80 nm ultrathin slices that can be observed with a scanning transmission electron microscope (STEM).

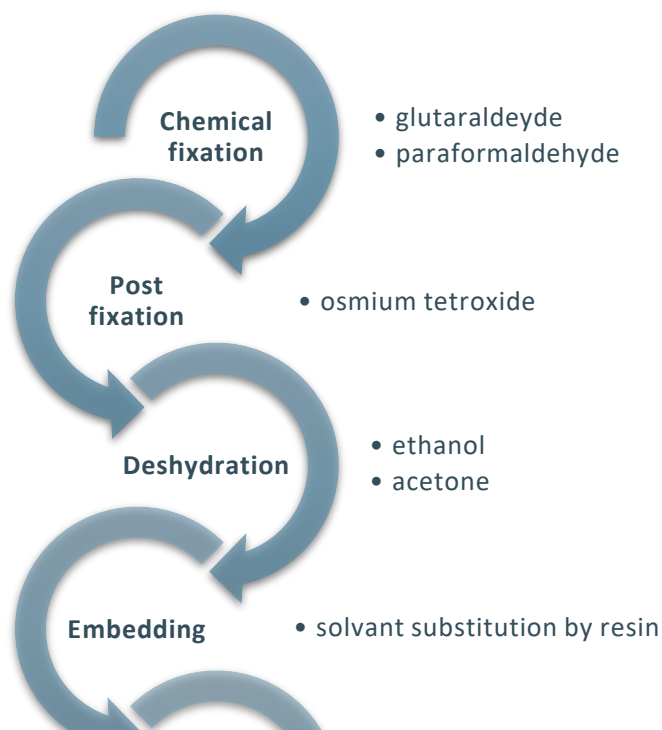


Figure 9 Schematic representation of sample processing for electron microscopy

STEM observation requires that samples be cut into extremely thin cross-sections. This thickness allows the electrons to either pass through the sample or not. Following fixation and dehydration, the samples are embedded in a rigid resin to facilitate cutting. Then, using a device called an ultramicrotome, the samples are cut into ultrathin 50-100 nm-thick slices. In order to enhance the contrast of the final image, STEM samples are additionally treated with uranyl acetate or coated with carbon.

1.14. 3'-END RNA-Seq



Figure 10 Schematic representation of the library preparation for the 3' mRNA-Seq from Lexogen

Schematic overview of QuantSeq FWD library preparation. The first step is the generation of the library by reverse transcription targeting the polyA tails as binding points, this step is followed by PCR amplification and purification and then sequencing. Schematic from Lexogens QuantSeq 3' mRNA-Seq Library Prep Kit for Illumina (FWD) manual.

Following snap freezing after cell sorting, the cell pellets were transferred to the LuxGen sequencing platform. RNA extraction was performed using Trizol. Then, the library was prepared (Lexogen schematic) for the Lexogen QuantSeq™ 3' mRNA-Seq kit with a capacity of 20M reads per sample, this following the protocol provided by the supplier. After this alignment, the count for each gene was generated and the data analysis was then performed by the LIH bioinformatics platform using the DESeq2 pipeline.

1.15. STATISTICAL ANALYSIS

Differences between two groups were analyzed by unpaired Student's t-test or ANOVA using GraphPad Prism 6.0 software (Graphpad software, La Jolla, CA, USA). Unless otherwise specified, error bars indicate standard deviation and experiments were performed at least three times in biological and technical replicates. Asterisks indicate significant differences (* $p < 0.05$, ** $p < 0.01$, and *** $p < 0.001$). Blinding during data analysis was not performed.

2. IN VIVO MODEL

2.1. LEFT HEART VENTRICLE INJECTION ASSISTED BY ULTRASOUND DEVICE

In order to recreate the process of brain metastasis, adult immunodeficient Nude (Nu/Nu) female mice were chosen, and they were purchased from Charles River Laboratories in France. The first strain of immuno-compromised mice to be employed in cancer research were the nude mice. They were developed by the National Institutes of Health (NIH). Nude mice exhibit spontaneous FOXP1 gene deletion. As a result, the animal does not possess a fully developed thymus and is therefore unable to produce T cells, which renders it immunodeficient. As they do not reject tumor cells, nude mice are the most suitable choice in the field of cancer studies.

Our *in vivo* model consists in injecting 5×10^5 A375 cells expressing mCherry into the left ventricle of a mouse heart. The injection of cells was performed in 0.1 ml of PBS using an insulin syringe. Prior to tumor cell injection, the position of the heart and the possibility of injection were assessed by ultrasound. The animals were anesthetized intraperitoneally with buprenorphine (0.1 mg / kg) in 0.1 ml injectable solution and kept in a sleep state with isoflurane breathing during the procedure. After the procedure, the mice were closely monitored and evaluated using score sheets. From the procedure until sacrifice, each mouse was weighed and assessed for pain or behavioral change daily. The animals were maintained under specific pathogen-free conditions and housed in a 12-hour light/dark cycle with *ad libitum* access to water and food.

All the procedures involving animal handling were performed in accordance with the Luxembourgish law (based on the European Directive 2010/63/EU) and were approved by the national authorities and the Animal Welfare Structure (AWS) at LIH (protocol number LCNP-2018-01).

2.2. IMMUNOFLUORESCENCE BRAIN SLICES SCREENING

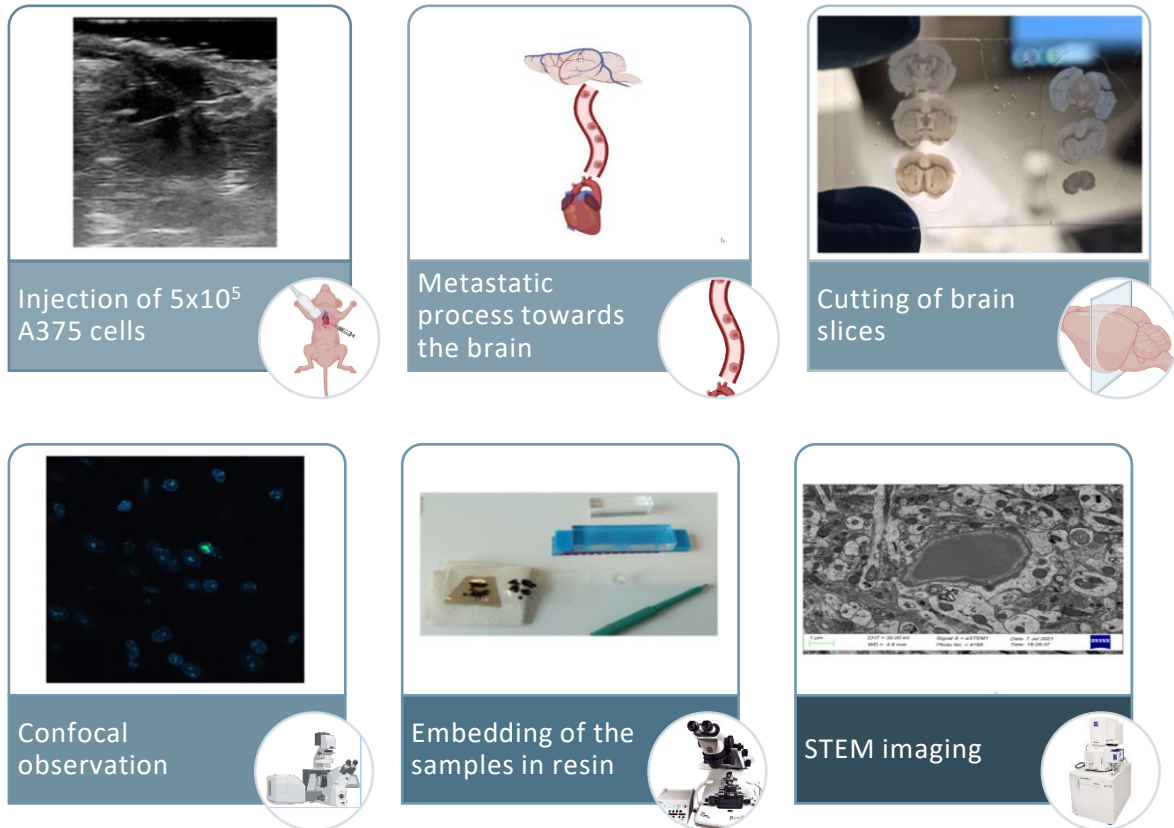


Figure 11 Schematic representation of the *in vivo* model of the metastatic process to the brain

Injection of 5×10^5 A375 cells into the left ventricle of the mouse heart with ultrasound guidance. Brain metastasis process from day 2 to day 10. Sacrifice of two mice every 24 hours for 10 days. Removal of the mouse brains. Cutting of the murine brains using a vibratome. Search for mCherry signal using a confocal microscope. Embedding of the murine brain slices in resin and cutting of the obtained samples using an ultramicrotome. Observation of the samples using a STEM.

To localize mCherry-expressing A375 cells adhering or blocked in a brain capillary, we first extracted the brain and any other organs that may be a potential site for tumor cells flowing freely through the vasculature. Then we immersed the organ in Karnovsky's solution for fixation, after which we cut the brains of the mice into sections of $100 \mu\text{m}$ thickness using a vibratome. Subsequently, we examined the brain using confocal microscopy looking for mCherry signal expression. In order to validate the observation of correct mCherry expression, we employed several markers, such as ZO-1, GFAP (**Table 2**) that help to reduce

the background and improve the contrast. We also used an antibody against the mCherry protein that is expressed by A375 cells (mCherry antibody Rabbit mAb, Bioké, Ref. 43590). Once the spots were selected, we embedded the brain slice as described in the electron microscopy section mentioned earlier. Once the samples were placed in the resin, we used the coordinates of the confocal observation and reduced the observation area by cutting the edge of the sample. We then cut the sample with an ultramicrotome generating 80 nm thick slices. The sample was analyzed using a STEM from Zeiss (**Figure 11**).

PART III. RESULTS

1. hicBBB CELLS IDENTIFICATION AND DESCRIPTION

1.1. hicBBB CELLS IDENTIFICATION BY IF

The blood-brain barrier plays an important role when it comes to maintaining a finely regulated microenvironment, necessary for the homeostasis of the central nervous system. The BBB is composed of endothelial cells that line the brain capillaries and interact closely with the surrounding astrocytes and pericytes. Compared to ECs in other parts of the body, ECs in the CNS have special properties that give them the faculty to finely regulate the transit of cells, molecules and ions between the blood and the brain. One of these faculties is the formation of tight junctions, thanks to which the ECs are held tightly together and a diffusion barrier is created.

Before a study model can be set up to recreate a BBB *in vitro* composed of these three cell types, the respective cell types have to be selected in such a way that they are able to grow in culture together and establish the structural organisation of a BBB, including TJs. Either primary cells, i.e. cells isolated from *in vivo* tissue, or established cultures with mitotically active, immortalized cells can be used for such endeavours. While primary cells most closely resemble the *in vivo* situation and such lend themselves to an accurate analysis of the BBB itself, immortalized cultures can be scaled and repeated in a reliable fashion. Since the analysis of the interaction of cells with the BBB in large numbers requires a high degree of reproducibility, we opted for immortalized cells. This further allows for the use of human cells, something not easily possible with primary cell culture. The first of the cell lines we use is hCMEC/D3. This cell line is derived from human temporal lobe microvessel. Its immortalization was done by lentiviral vector transduction (Weksler et al. 2013). We confirmed the endothelial differentiation of our culture by IF, using endothelium-specific markers such as CD31, Claudin-5, Occludin, ZO-1 and concluded hCMEC/D3 is suitable for the establishment of our hicBBB model (**Figure 12**).

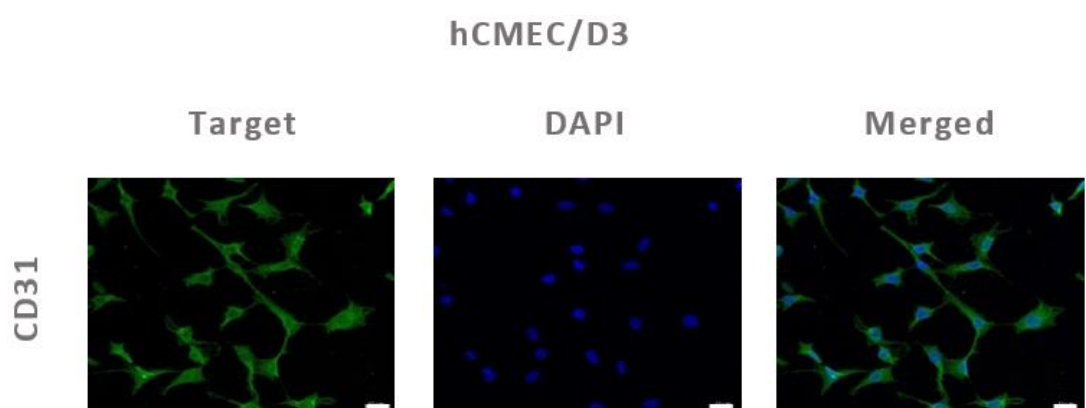


Figure 12 Immunofluorescence identification of hCMEC/D3 cells in the in vitro hicBBB model
Immunofluorescence micrograph performed using a confocal microscope to observe the expression of the following hCMEC/D3 endothelial cell markers: CD31, claudin 5, occludin, ZO-1. Magnification 20 x. Scale bar 20 μ m. Nuclear staining using DAPI is shown in blue.

For the pericytes, our choice fell on the immortalized pericytes cell line SV40-HBVP derived from human brain vessels, which was provided to us by the laboratory of Ulrike Naumann in Tübingen. The expression of markers that can be used to identify pericytes was previously established by the laboratory that provided us with the SV40-HBVP cell line. However, we also proceeded with an IF verification of the expression of PDFR β and α SMA, which are specific markers for pericytes (**Figure 13**).

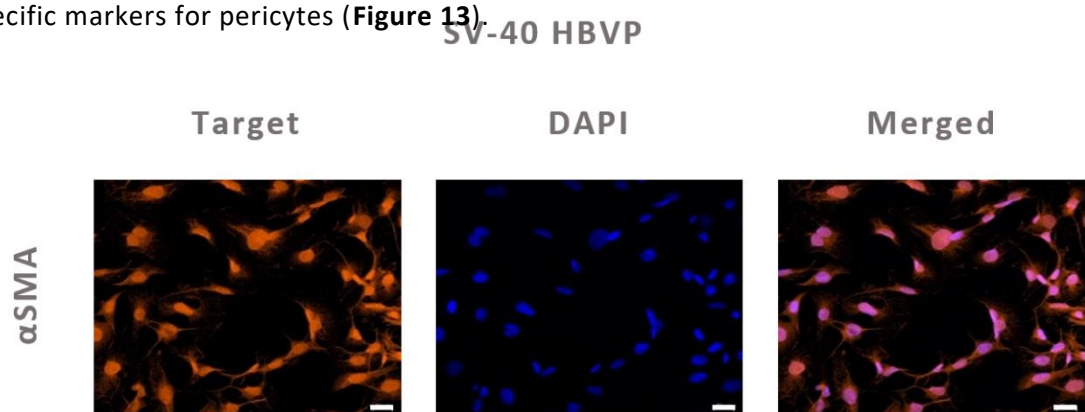


Figure 13 Immunofluorescence identification of SV40-HBVP cells in the *in vitro* hicBBB model
Immunofluorescence micrograph performed using a confocal microscope to observe the expression of the following SV40-HBVP pericytes markers: α SMA and PDGFR β . Magnification 20 x. Scale bar 20 μ m. Nuclear staining using DAPI is shown in blue.

To implement our model, the last cell type needed is astrocytes. The selected SVGA, an immortalized human astrocytes cell line. We proceeded with the verification of the glial fibrillary acidic protein GFAP expression, a marker in the identification of astrocytes (**Figure 14**).

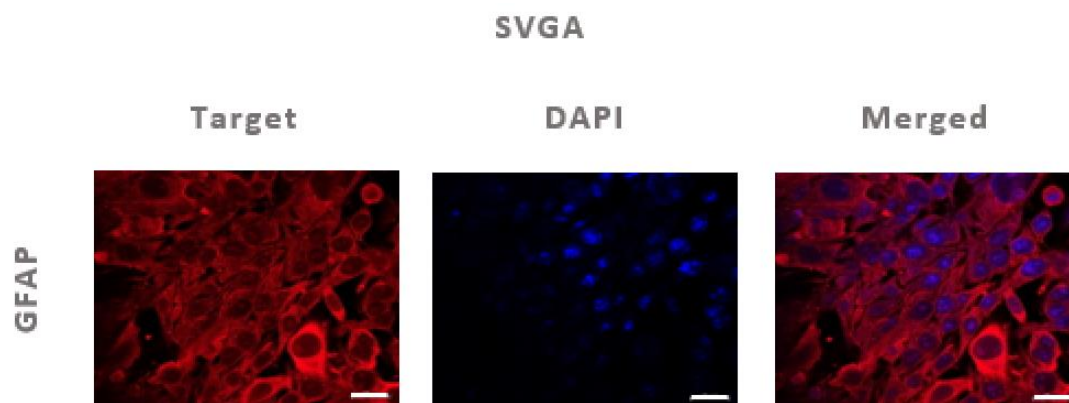


Figure 14 Immunofluorescence identification of SVGA cells in the *in vitro* hicBBB model
Observation of the astrocyte marker GFAP applied to SVGA cells by performing an immunofluorescence micrograph using a confocal microscope. Magnification 40 x. Scale bar 20 μ m. Nuclear staining using DAPI is shown in blue.

In summary, the specific positive immunofluorescent staining of endothelial cells, pericytes and astrocytes permits the selection of these cell lines to create the human immortalized cell *in vitro* model of the BBB. As a next phase, we sought a way to identify and track the A375 melanoma cell line through the BBB.

2. TUMOR MODEL IDENTIFICATION

2.1. IDENTIFICATION OF THE A375 CELL LINE BY ICC

As a tumor invasion model in interaction with the *in vitro* model of the BBB, we used A375 cells kindly provided to us by the lab of Stephanie Kreis. A375 cells are a line of human melanoma cells derived from a solid tumor of a 54-year old female patient with malignant melanoma (Giard et al. 1973).

ICC examination confirmed that A375 cells were not stained with the MelanA marker (**Figure 15 h**). This result is consistent with the fact that Microphthalmia-associated transcription factor (MITF) protein is known to be down-regulated in amelanotic melanoma.

To confirm the differentiation of the cell line and its identity, we further did ICC for BRAF V600E, Sox10 and S100.

Figure 15 shows multiple immunocytochemistry (ICC) stainings performed on the A375 cell line after formalin fixation and paraffin embedding (FFPE). The ICC was conducted to identify a potential marker that can be used to track tumor cells that invade the BBB and enter the brain parenchyma.

Figure 15 a shows ICC staining performed on the A375 cell line with hematoxylin and eosin. This allowed us to acquire information about the shape and structure of the cells. The purple color represents the nuclei of the cells.

Figure 15 b shows positive antibody staining by anti-BRAF V600E, which is a specific marker to the mutation that occurs in melanoma when a valine (V) is substituted by a glutamic acid (E) at position 600 of the BRAF protein. This mutation leads to continuous activation of BRAF, which is known to be oncogenic.

Next, we focused on SOX10 (**Figure 15 d**), the nuclear transcription factor known for its role in regulating neural crest and peripheral nervous system development. Melanocytes are derived from the neural crest and are generally positive for SOX10, this marker is used within pathology laboratories as a marker for melanoma. ICC examination showed that the pellet of

A375 cells showed positive nuclear staining for anti-SOX10 antibody, which may mean that SOX10 may be a potential marker for our screening.

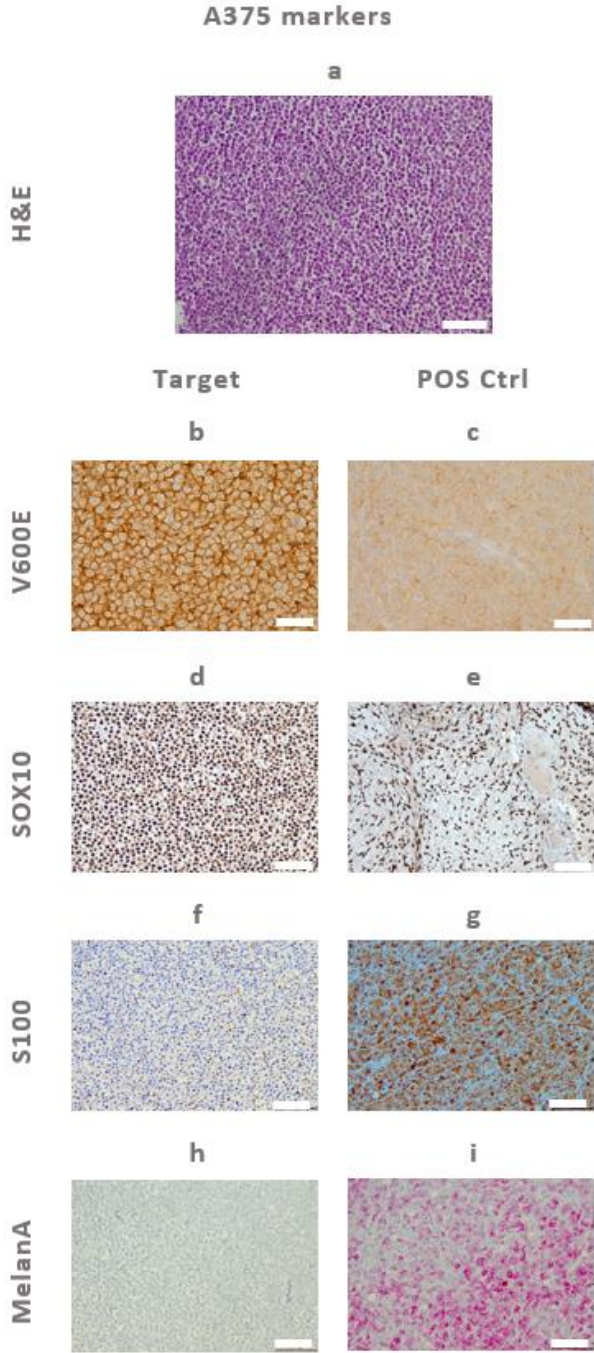


Figure 15 Search for a specific A375 cell line marker

a ICC staining of A375 cell pellets with hematoxylin and eosin after formalin fixation and paraffin embedding (FFPE); **b, d, f, h** ICC staining of A375 cell pellets by anti-BRAF V600E, anti-SOX10, anti-S100, anti-MelanA ; **c, e, g, i** IHC staining of melanoma skin cancer tissue as a positive control. Magnification 10 x. Scale bar 100 μm. Cells were stained with DAB in brown and with hematoxylin in blue.

When dimeric, S100 is similar to calmodulin, and like SOX10, it is usually expressed in neural crest-derived cells (**Figure 15 f**). ICC examination showed that the pellet of A375 cells showed positive cytoplasmic staining for anti-S100 antibody, which may mean that S100 may be a potential marker for our screening. Although the A375 cell line results positive for S100 and SOX10, these markers cannot be used to properly track cells in a system where other cells express the same ones. A375 cell line results positive for BRAF mutation, however the anti-BRAF V600E antibody is unusable as it was produced in murine hosts, this makes a positive label to BRAF V600E indistinguishable from the background generated by the reaction of murine antibodies to murine epitopes. We concluded that anti-BRAF V600E is not suitable for detection of melanoma in murine brain tissue. Therefore, we decided to use EM to determine whether melanosomes were sufficiently present in the cells to allow identification of melanomas in the *in vivo* model.

2.2. hicBBB CELLS AND A375 MELANOSOME OBSERVATION BY ELECTRON MICROSCOPY

After identifying the cells using specific markers, the next step was to find a feature that could be identified by electron microscopy and without prior staining, which could help us discriminate A375 cells from the cells of the hicBBB model *in vitro* as well as from the cells of the mice brains of the *in vivo* model. For this purpose, we had to perform electron microscopy imaging of hicBBB cells (**Figure 16, Figure 17 a**) and of A375 cells with melanosomes. In **Figure 17 b**, indicated by the number 3, we can observe the melanosomes (Walts et al. 1988).

Taken together, the results of the IHC staining in conjunction with the EM observation provide two possible ways to identify and track tumor cells across both the *in vitro* and *in vivo* models. Namely, the specific anti-V600E staining against the BRAF mutation and the presence of potential melanosomes imaged by EM. In the next chapter, we will investigate whether the tumor model possesses the ability to migrate and invade the Boyden chambers and the rate at which A375 cells and hicBBB cells grow.

hCMEC/D3 & SV-40 HBVP

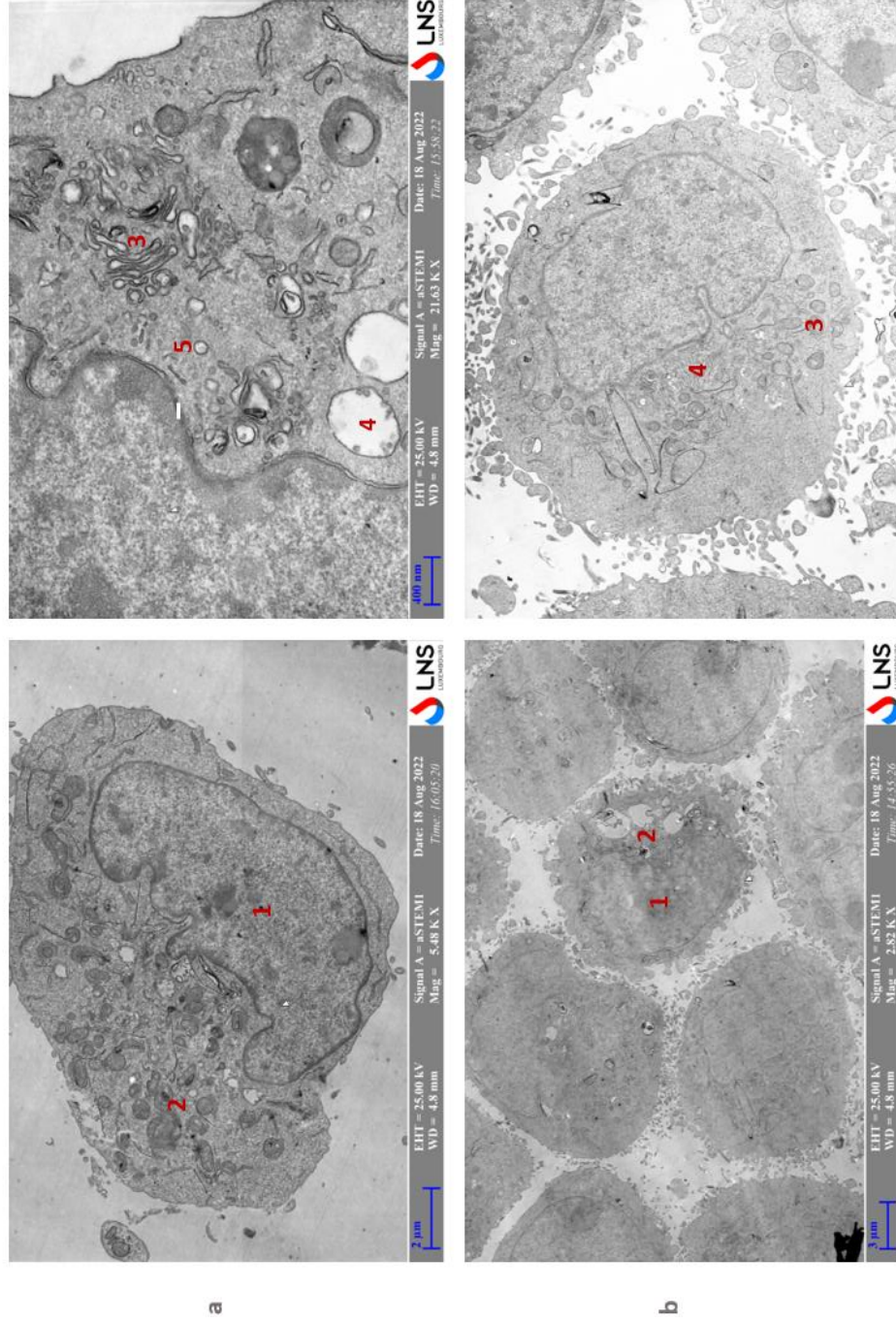


Figure 16 Scanning transmission electron microscope (STEM) observation of hCMEC/D3 cells and SV-40 HBVP cells

a STEM micrograph observation of hCMEC/D3 cell line. **1** Nucleus **2** Mitochondria **3** Endoplasmic reticulum **4** Vacuolae **5** Transport vesicles. Left image magnification 5480 x. Scale bar 2 μm. Right image magnification 21630 x. Scale bar 400 nm. **b** STEM micrograph observation of SV-40 HBVP cell line. **1** Nucleus **2** Vacuolae **3** Mitochondria **4** Endoplasmic reticulum.

SVGA & A375

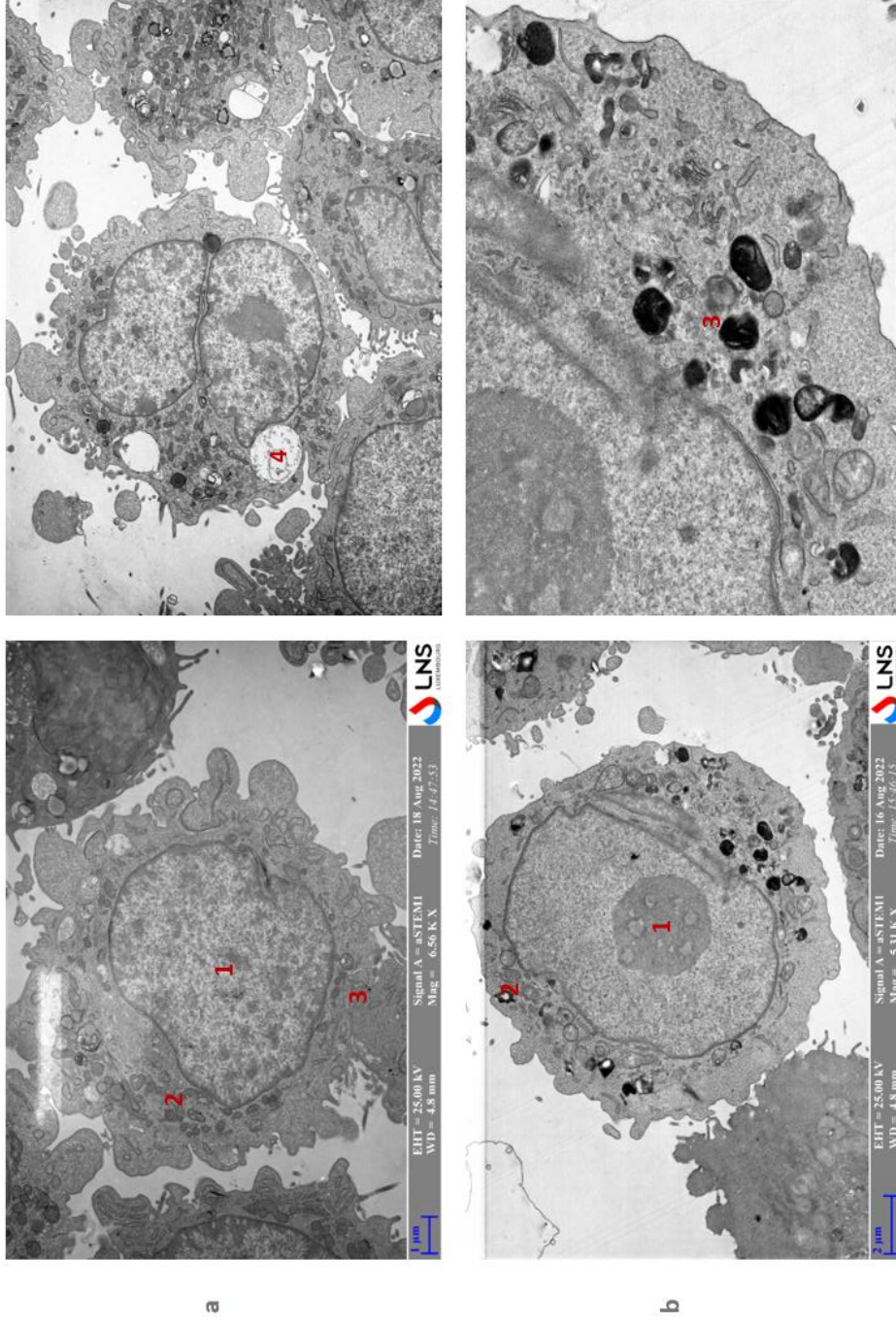


Figure 17 Scanning transmission electron microscope (STEM) observation of SVGA and A375 cells

a STEM micrograph observation of SVGA cell line **1** Nucleus **2** Mitochondria **3** Endoplasmic reticulum **4** Vacuolae. Magnification 6560 x. Scale bar 1 μm . **b** STEM micrograph observation of A375 cell line **1** Nucleus **2** Mitochondria **3** Melanosome. Magnification 5310 x. Scale bar 2 μm .

3. MIGRATORY AND INVASIVE POTENTIAL OF THE A375 CELL LINE AND PROLIFERATION POTENTIAL OF THE CELLS FROM THE IN VITRO hicBBB MODEL AND FROM THE A375 CELL LINE

Following the analysis of hicBBB model cells and A375 cells by IF or ICC to determine the presence of specific markers, we next turned our attention to the migratory and invasive potential of the A375 cell line.

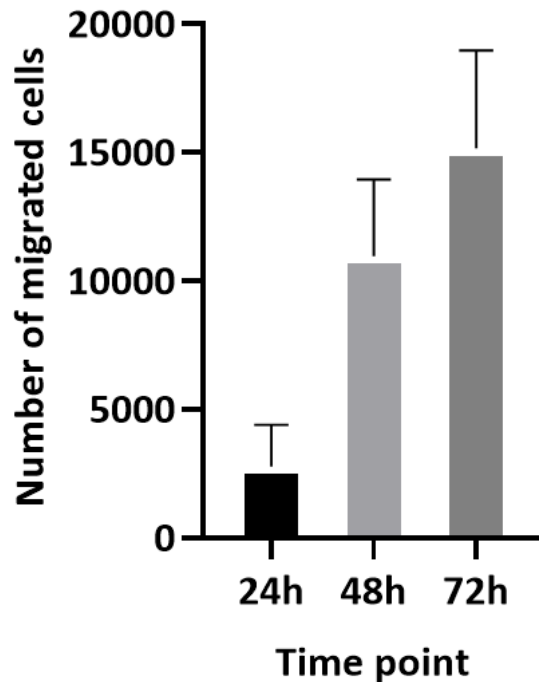


Figure 18 Migration potential of the A375 cell line

Migration potential of the A375 melanoma cell line over 72 hours. Error bars represent SD (n=3).

Therefore, we proceeded to examine the migration and invasion potential of A375 cells at 24 hours, 48 hours and 72 hours (**Figures 18, 19**). We were able to observe that when the migration potential is compared to the invasion potential, it seems that both PLL and FN coatings tend to reduce the number of cells present on the membrane at each time point. This led us to believe that the coating provides additional anchorage to the tumor cells and does not prevent them from continuing their transit across the membrane. Taken together, the information gathered, leads us to believe that the coating could trigger the invasion phenomenon we were looking for in our model. This could indicate that A375 cells produce

proteolytic enzymes such as MMPs, which help them to degrade the coating present on the membrane. It has been shown previously (Banerji et al. 2008) that the A375 cell line expresses MMP2 and MMP9 when in the presence of FN.

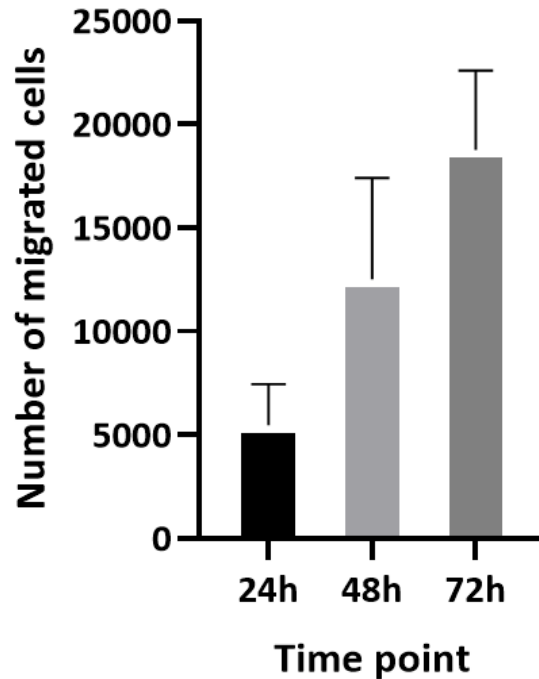


Figure 19 Invasion potential of the A375 cell line

Invasion potential of the A375 melanoma cell line on a PLL+FN coated membrane over 72 hours. Error bars represent SD (n=3).

Next, we proceeded to determine the proliferation potential of all the different cell lines that we used to build our *in vitro* hicBBB model (Figure 20). On the y-axis, we can see the percentage of confluence of the cells in culture while on the x-axis, we can see the time period during which confluence of the cells in culture was observed. We can see that after 24 hours in culture, the confluence seems to remain unchanged for the four cell lines. However, after 40 hours of culture, we can see that the A375 cell line reaches a confluence of 50% compared to the other three cell lines which only reach 20% confluence. We can also see that after 60h of culture, the A375 cell line reaches 100% confluence, while the endothelial cell line, the pericyte line and the astrocyte line only reach 50% confluence.

It is important to highlight this information because the rate of cell growth had to be taken into consideration when developing our *in vitro* hicBBB model to ensure that the cells that formed it did not start to die due to the lack of nutrients that are limited in a well.

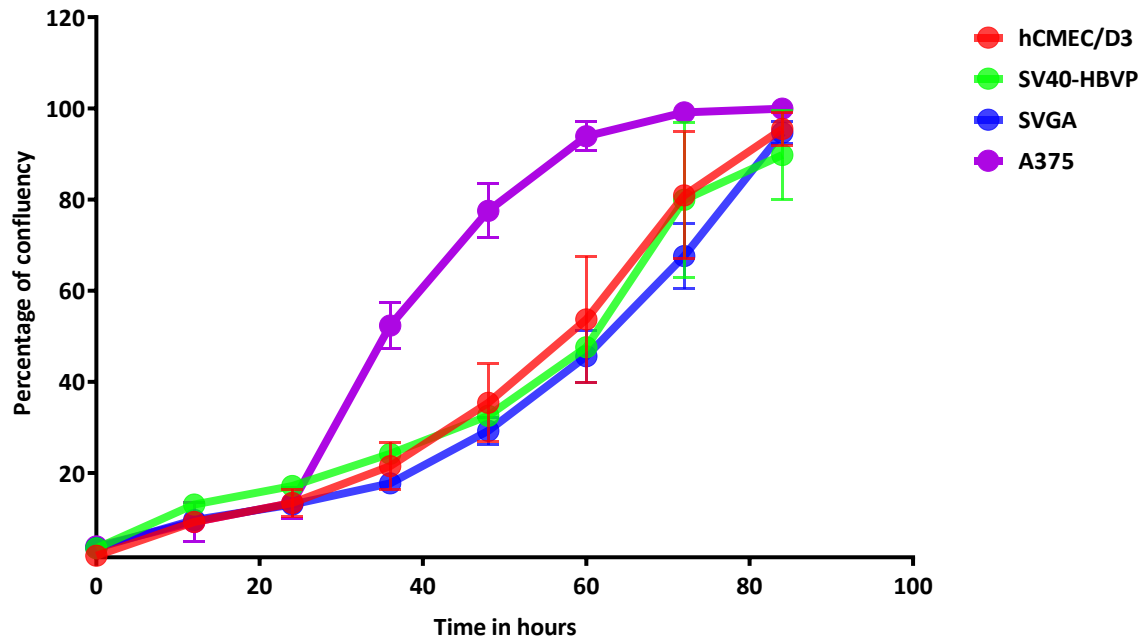


Figure 20 Cell proliferation assessment of the *in vitro* hicBBB model and the A375 cell line
Proliferation potential determined by the cellular confluency of the hicBBB *in vitro* model cells and of the A375 cell line over time. Cell confluency is given as percentage. Error bars represent SD (n=3).

In the first part of this chapter, we confirmed that the A375 cell line that we use as a tumor model has invasive and migratory potential. In addition, we have shown a confluency analysis of the tumor cells as well as the cells that make up the hicBBB model. All of this information will help us to maintain our *in vitro* model stable once the cells are in coculture. The next chapter will focus on the type of medium needed to maintain the cells in coculture.

4. MEDIUM DETERMINATION FOR THE hicBBB MODEL

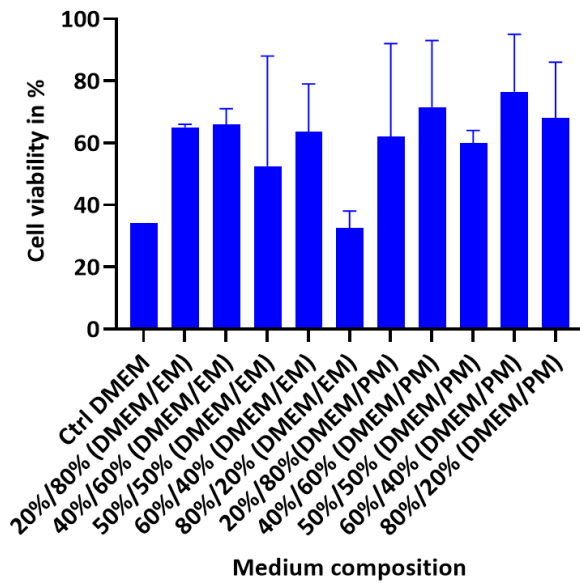


Figure 21 SVGA viability in a gradient of mixed media

Viability of SVGA cells exposed to the mixed medium. Error bar represents SD (n=1).

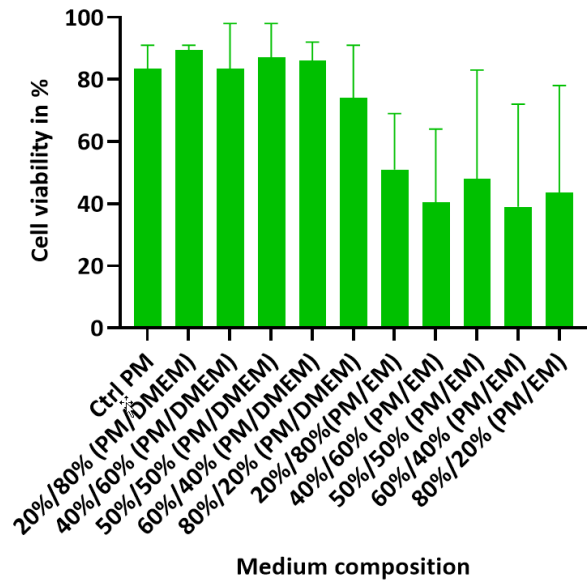


Figure 22 SV40-HBVP viability in a gradient of mixed media

Viability of SV40-HBVP cells exposed to the mixed medium. Error bar represents SD (n=1).

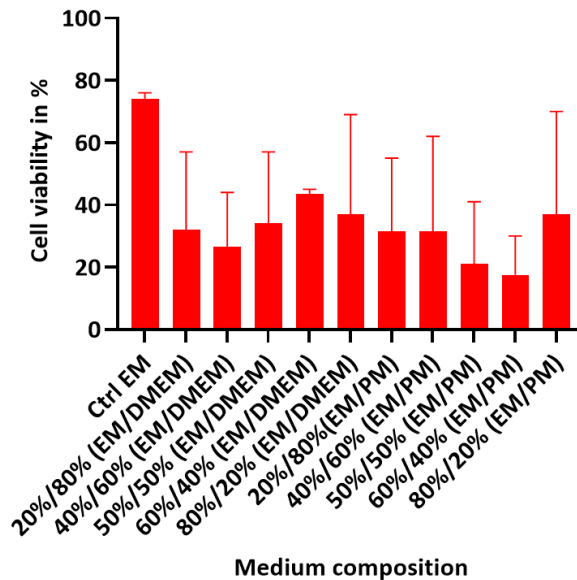


Figure 23 hCMEC/D3 viability in a gradient of mixed media

Viability of hCMEC/D3 cells exposed to the mixed medium. Error bar represents SD (n=1).

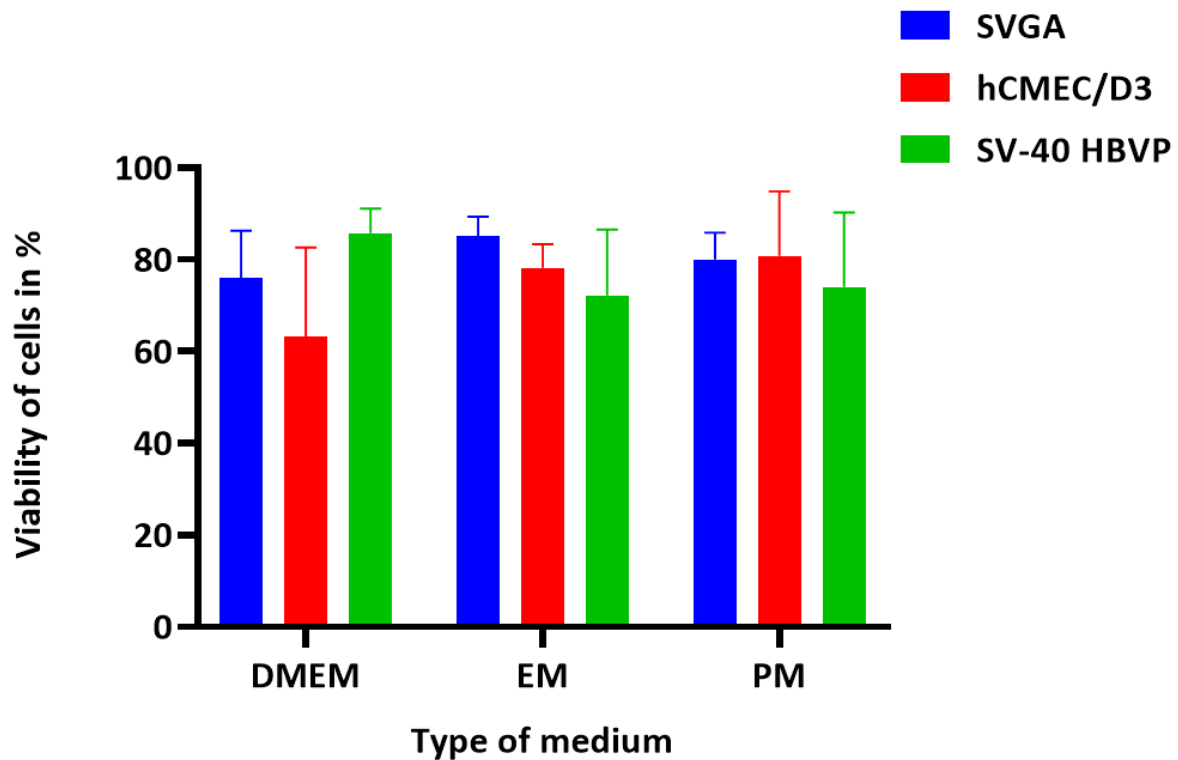


Figure 24 hicBBB cells viability in different media

Viability of the different cell types when exposed to the respective original media. Error bar represents SD (n=3).

Each culture medium is different, for instance the endothelial cell medium contains growth factors that are not present in DMEM or PM, but also molecules such as hydrocortisone and heparin that are known to promote the formation of tight junctions between EC. In order to determine the optimal culture medium to maintain the cells in triple coculture, we performed two experiments: in one we cultured each of the cell lines that compose the model in a mixed medium derived from the mixture of the different original culture media of these cell lines; in another we cultured each of these cell lines in the unchanged medium of the other cell lines of the model.

After performing confluence analysis on each cell line of the hicBBB *in vitro* model, we started looking for the type of medium that could maintain the cells in a state where they could form a model. The three cell lines we used to develop our hicBBB *in vitro* model each require a different culture medium. We first tested whether the mixture of media we routinely use for monoculture would be suitable for each of these three cell lines.

Figure 22 shows the SV40-HBVP cell line in different mixed culture media and at different concentrations. These media were obtained by mixing PM medium, used for the culture of pericytes, DMEM medium, used for the culture of astrocytes, and EM medium, used for the culture of endothelial cells. On the y-axis we can see the cell viability in percentage and on the x-axis we can see the different mixtures of culture media that were tested. The mixture between PM and DMEM does not seem to have an impact on the viability of pericytes, but when we look at the mixture between PM and EM, we see a decrease in their viability. This decrease in viability may be explained by the presence of some constituents of the EM medium.

When we examine the viability of SVGA, we can observe that the cellular viability of the DMEM control and of the 80% DMEM/20% EM condition is about 30%. Whereas when DMEM is mixed with larger amounts of other media, cell viability is about 70% (**Figure 21**). These results for SVGA are therefore not usable given the cell viability of the control.

In a next step, we took a closer look at the effect that the composition of the media has on hCMEC/D3. When we look at the graph, we see that none of the media that were tested seems to be suitable for endothelial cell culture (**Figure 23**). Therefore, we decided to test the viability of the cell lines only using the respective culture media of each actor in the hicBBB *in vitro* model (**Figure 24**).

We can observe that after 24 hours of culture spent in different cell media, the cell viability of all human immortalized cells does not seem to be affected by the change of culture medium. The results presented in **Figures 21, 22** and **23** are contradicted by the results presented in **Figure 24**. We therefore decided to repeat the experiment whose results are shown in **Figure 24**, to determine the accuracy of the results. It turned out that the results shown in **Figure 24** are reproducible. These results led us to use only the endothelial cell-specific medium EBM-2 for the development of our hicBBB model in the presence of all three cell types. In addition, EBM-2 medium contains certain components such as hydrocortisone and ascorbic acid that help maintain endothelial cell function. Hydrocortisone tends to reduce permeability to macromolecules by preserving the membrane glycocalyx and by reducing physical and chemical stresses such as the presence of TNF α (**Supplementary Figures 49** and **50**). We tested the impact of TNF α on hCMEC/D3 and SVGA coculture as well as on our hicBBB model *in vitro*, and it appeared that after treatment there is a decrease in TEER. Ascorbic acid is an antioxidant that acts as a cell protector. Other growth factors such

as human fibroblast growth factor (hFGF), vascular endothelial growth factor (VEGF), insulin growth factor (IGF), and human epithelial growth factor (hEGF) are present to support endothelial cell growth, but they may also have a significant impact on the maintenance and growth of SVGA and SV40-HBVP.

Testing of different culture media on the hicBBB model cell lines has shown that the optimal medium to maintain the functionality of the latter is the endothelial cell medium. In the next chapter, we will observe and monitor the formation of our *in vitro* model by confocal microscopy, transendothelial electrical resistance and permeability assay.

5. FORMATION OF THE hicBBB MODEL

5.1. OBSERVATION OF THE hicBBB BY CONFOCAL MICROSCOPY

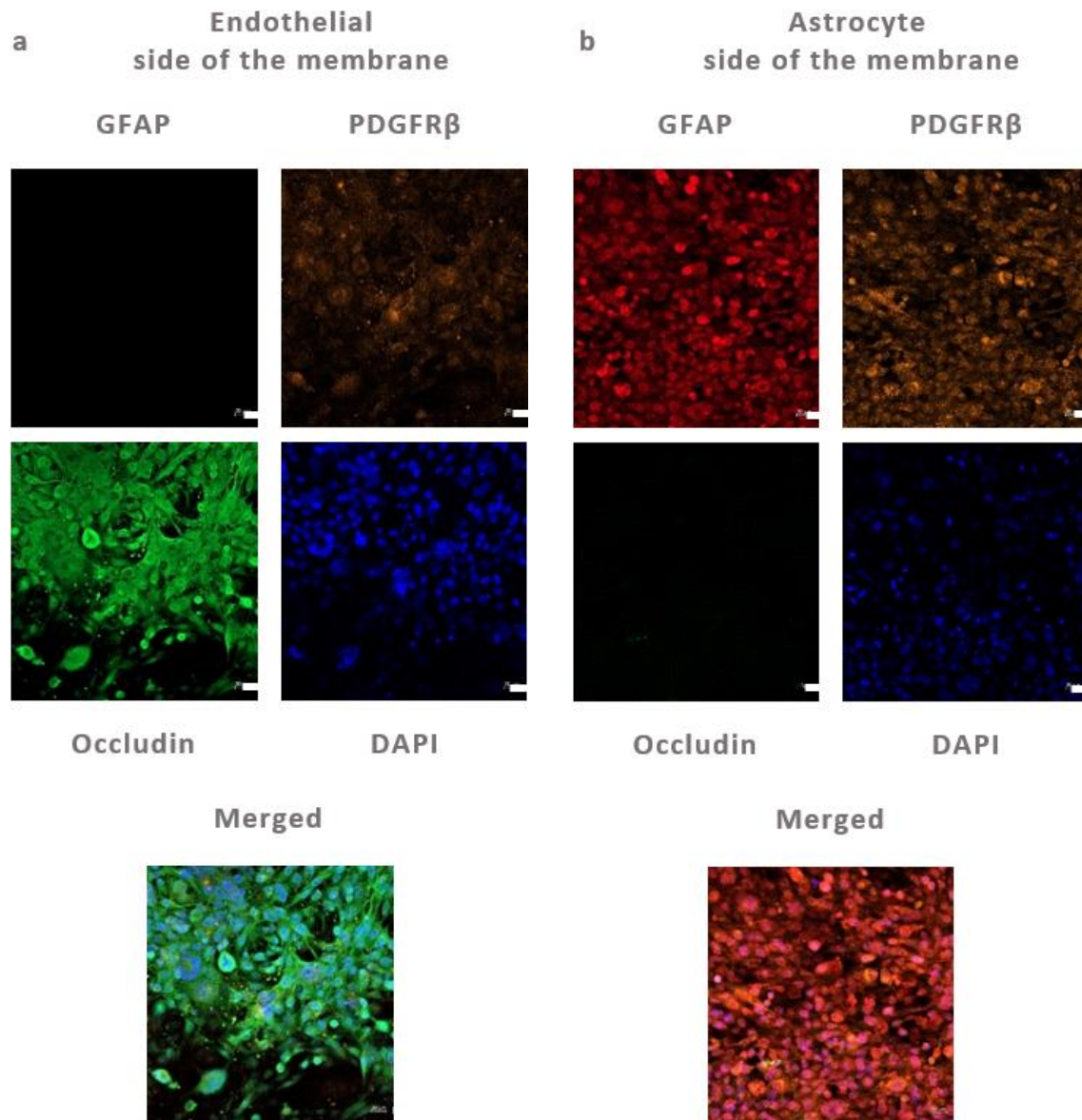


Figure 25 Microscopic observation of the hicBBB Z-stack by IF

a shows the upper part of the transwell where a triple immunofluorescence staining was performed using the following antibodies: GFAP, PDGFR β and occludin. Magnification 20 x.

Scale bar 20 μm . Nuclear staining using DAPI is shown in blue. **b** displays the lower part of the transwell where a triple immunofluorescence staining was performed using the following antibodies: GFAP, PDGFR β and occludin. Magnification 20 x. Scale bar 20 μm . Nuclear staining using DAPI is shown in blue.

Following their identification, we combined the three cell lines to form our hicBBB model *in vitro*. In the next section, we will explain how we confirmed the formation of the hicBBB model *in vitro* and how it reacted when confronted with the presence of melanoma tumor cells. To ensure that all the hicBBB cells were in place during model development, we performed IF to verify their location as well as the expression of specific markers that characterize them (**Figures 25 a and b**). **Figure 25 a** shows the upper compartment of the Boyden chamber 48 hours after the formation of the hicBBB model. We used IF staining of GFAP as a marker for astrocytes, occludin as a marker for endothelial cells, PDGFR β as a marker for pericytes, and DAPI for nuclear staining. We then imaged the model using a confocal microscope to obtain a Z-stack on both sides of the membrane (**Figure 25 b**). Overall, the triple staining showed us that the cells are in the correct order, namely hCMEC/D3, SV40-HBVP, SVGA.

5.2. TEER MEASUREMENT OF THE NEWLY FORMED hicBBB

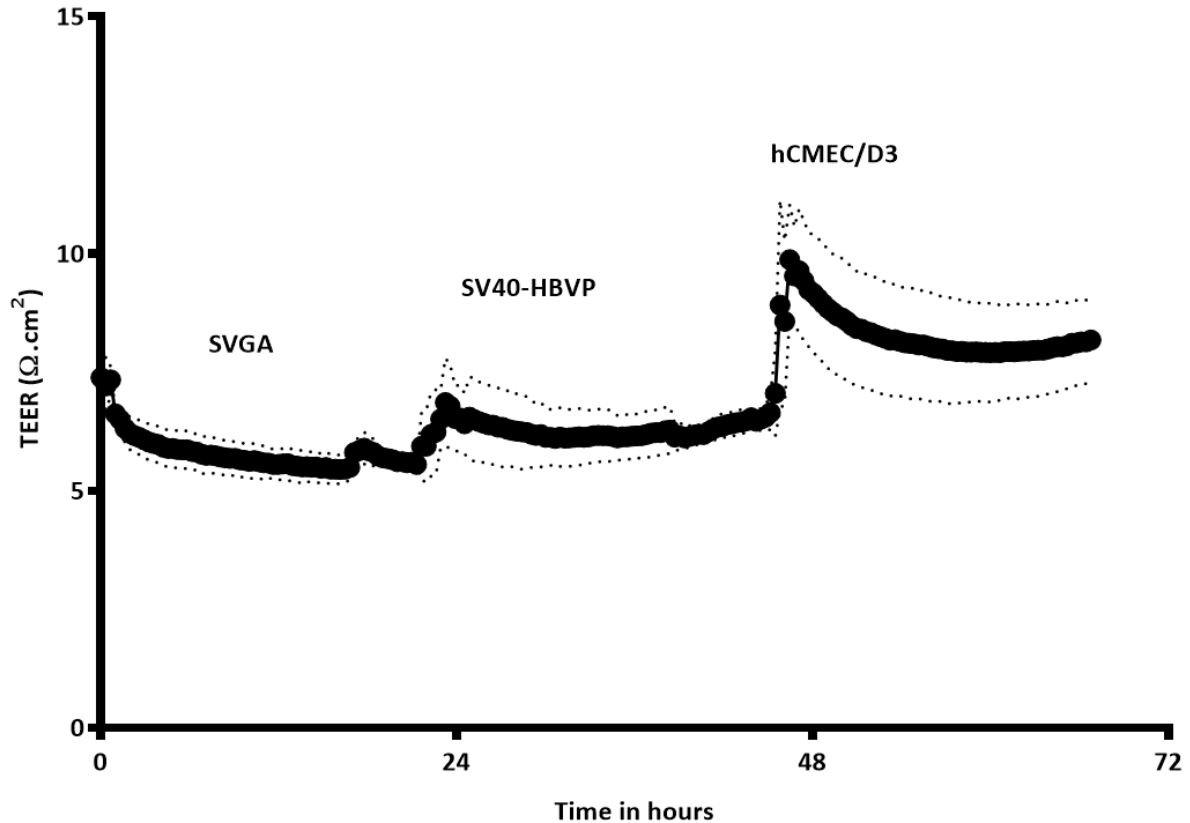
Next, we tested and measured the TEER of our model during BBB formation (**Figure 26**). The y-axis of the graph represents the TEER value ($\Omega\cdot\text{cm}^2$), this is the strength and tightness of the endothelial cell tight junction network over time, the latter is represented in hours on the x-axis. TEER is proportional to the number of tight junctions that are between the endothelial formations, in other words, the higher the TEER, the higher the number of tight junctions.

We can see that the addition of SVGA and SV40-HBVP to the model does not increase the TEER but HCMEC/D3 does. Immortalized human microvascular brain endothelial HCMEC/D3 cells are known and sold as BBB endothelial cells. They are known to have an overall low TEER amounting to $8\Omega\cdot\text{cm}^2$. The murine brain endothelium bEND5, for example, expresses a somewhat higher TEER amounting to $12\Omega\cdot\text{cm}^2$ (Czupalla et al. 2014), and the porcine

cerebral microvascular endothelial cells (PBMVEC) express an even higher TEER reaching $200\Omega\cdot\text{cm}^2$. However, our model was conceptualized so that all the cells we used were from a human donor.

Figure 26 Assessment of hicBBB formation using TEER measurement

Assessment of hicBBB model formation by means of TEER. Dash line represents SD (n=3).



Further details on the values of the TEER measurements are provided in the Appendix (Figure 48).

5.3. PERMEABILITY OF THE hicBBB USING A FLUORESCENT TRACER

We assessed the passive chemical resistance of the BBB using a dextran compound coupled to a fluorophore called Antonia Red, which has a molecular weight of 3kD (Figure 27). On the y-axis in Figure 27, we can see the raw fluorescence unit, while on the x-axis we can see its progression over time. We observe that the model reaches its optimal permeability after 48 hours of triple coculture. The information collected so far, leads us to conclude that our

hicBBB model has all the necessary characteristics to be used in the study of the BBB invasion process by tumor cells.

It is worth noting that the permeability of the model alone was tested without changing its medium for 72 hours after formation, in order to determine whether the model would require a change of medium every 24 hours. Furthermore, in a parallel experiment using TEER, once formed, we tested the integrity of the model when changing its medium every 24 hours, and it was determined that it can be maintained for more than 72 hours.

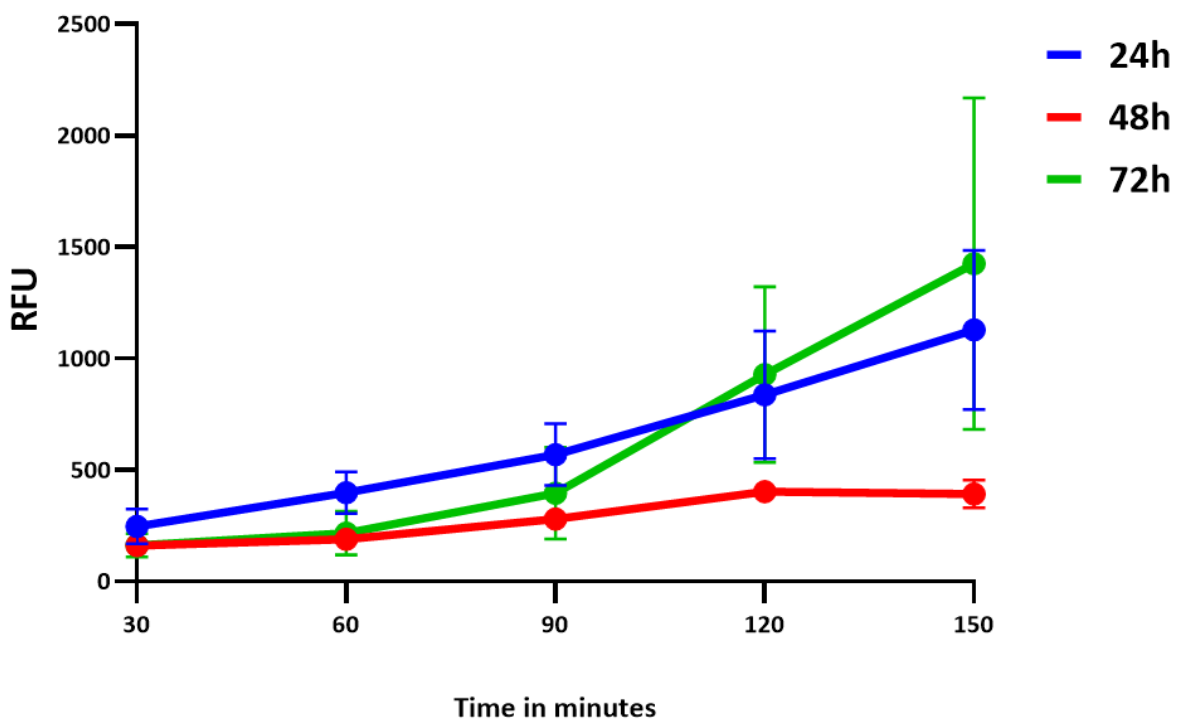


Figure 27 Changes in the permeability of the hicBBB model at different time points

Tracer-based permeability measurement at 24 hours, 48 hours and 72 hours. Error bar represents SD (n=3).

In this chapter, we begin by showing that the cell lines that compose the hicBBB are layered in the intended manner. Next, we assess the integrity and resistance of the *in vitro* model using TEER and observe by means of a fluorescent tracer that the optimal permeability of the hicBBB model is reached after 72 hours of coculture. Following this, we will investigate the effects of the presence of the A375 cell line on the *in vitro* model and whether tumor cells are able to initiate or even complete the crossing of the different cell layers.

6. EXPOSURE OF THE hicBBB MODEL TO TUMOR CELLS

6.1. TEER MEASUREMENT OF THE hicBBB WHEN EXPOSED TO A375 CELLS

Once the hicBBB model had been validated, the experimental part of our study could be initiated. This involved the use of A375 tumor cells to destabilize the hicBBB model. This new step has consisted in the appreciation of the impact that the presence of A375 melanoma cells can generate on the hicBBB model. First, we exposed our hicBBB *in vitro* to different concentrations of A375 melanoma cells (1×10^5 , 5×10^5 , 1×10^6) and we kept a control as a reference for comparison with the conditions where tumor cells are present, but also to make sure that the model is well formed. On the graph (Figure 28), we can see that the control reached $10 \Omega \cdot \text{cm}^2$. When we compared the first two lowest concentrations to the control, we observed a decrease of $3 \Omega \cdot \text{cm}^2$. In the same time frame, the purple curve representing a concentration of 1 million A375 tumor cells, decreases by $5 \Omega \cdot \text{cm}^2$. These results led us to believe that A375 cells are able to disrupt and cross the hicBBB model after 48 hours of coculture, although there is no statistical significance.

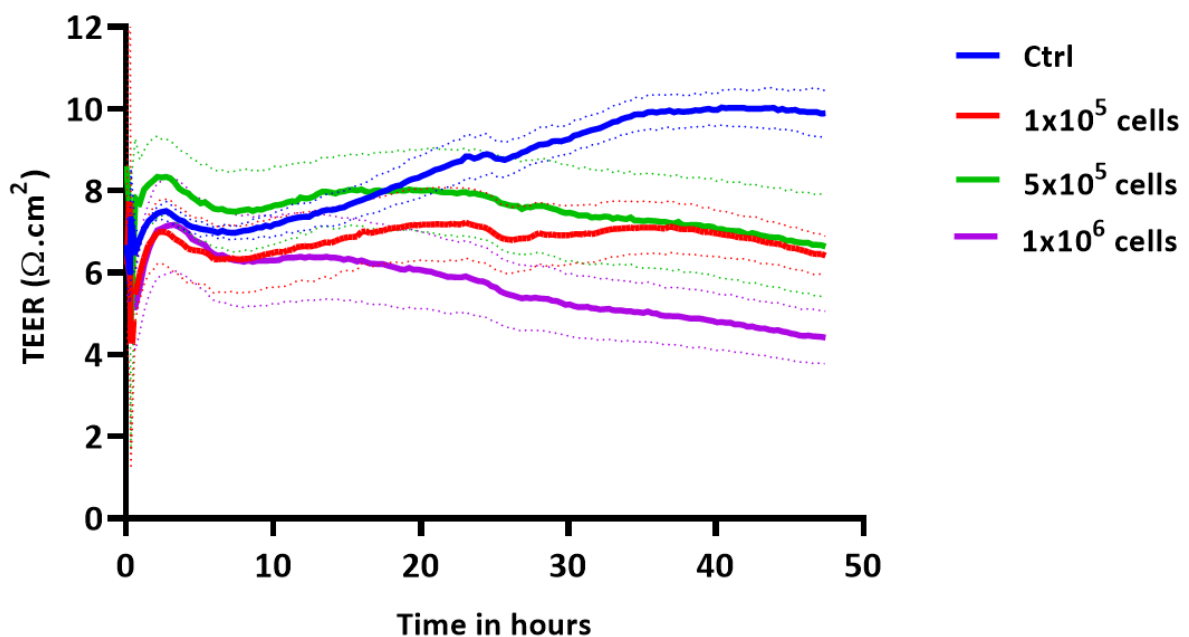


Figure 28 Impact of the presence of A375 melanoma cells on the in vitro hicBBB model assessed by TEER

Impact of the presence of different cell concentrations of A375 on the hicBBB measured over a 50-hour period using TEER. Dash line represents SD (n=3).

6.2. MEASUREMENT OF THE hicBBB PERMEABILITY WHEN EXPOSED TO A375 CELLS

Thereafter, we wanted to validate whether the A375 tumor cell line was also able to disrupt the passive permeability of the hicBBB. For this, we used a dextran coupled to a fluorophore with a molecular weight of 3kD (**Figure 29**). It is important to note that after seeding the tumor cells, in order to prevent nutrient deficiency and acidification of the medium as well as to ensure the integrity and functioning of the model, the medium was changed every 24 hours.

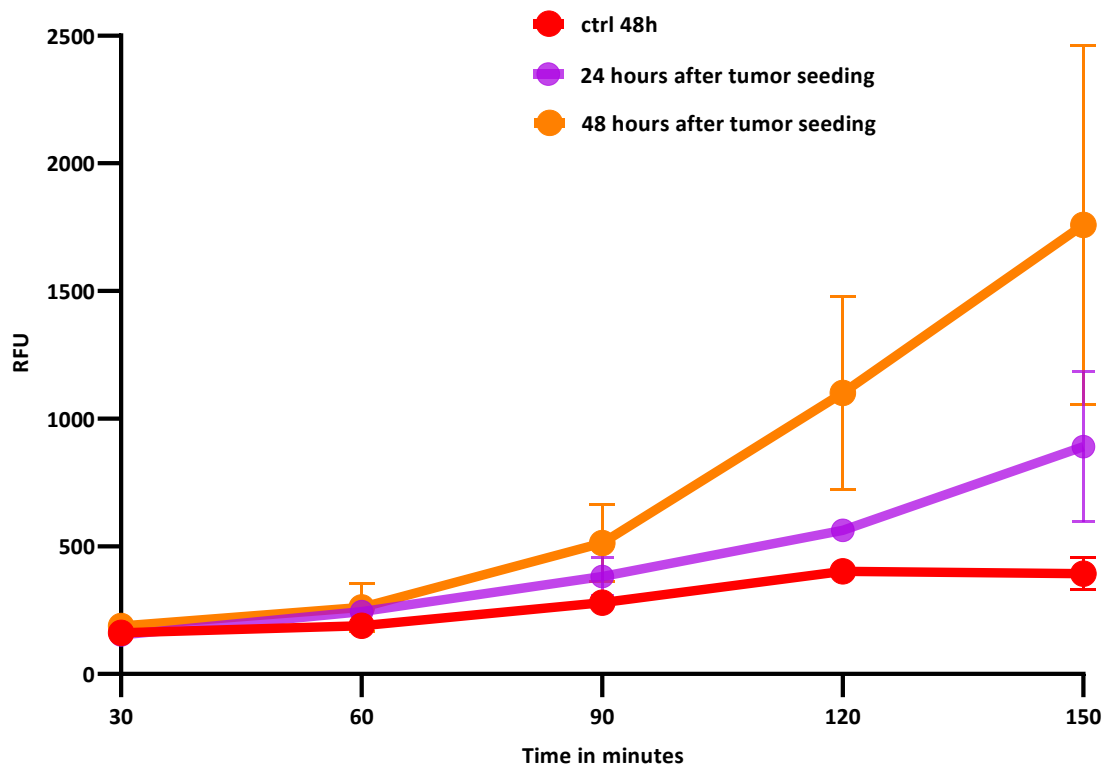


Figure 29 Impact of the presence of A375 melanoma cells on the in vitro hicBBB model assessed by permeability assay

Impact of the presence of the A375 cell line on the permeability of the hicBBB measured at 24 and 48 hours with a fluorescent tracer. Error bar represents SD (n=3).

In **Figure 29**, the red line on the graph represents the hicBBB control. We were able to observe that after a 48 hours incubation in the presence of A375 cells, the hicBBB model showed an increase in its permeability compared to the control and the condition after a 24 hours incubation in the presence of A375 cells. We established previously that the A375 cells have an impact on the permeability of the hicBBB model. At this point, we can hypothesize that this impact is time dependent. Overall, the data suggest that A375 cells begin to migrate 24 hours after the start of coculture and that the longer the tumor cell remain in culture with the model, the greater their impact. At present, we have established a temporal starting point for tumor migration through the *in vitro* model.

6.3. IN VITRO TRACKING OF A375 CELLS CROSSING THE hicBBB MODEL

In order to validate the previously formulated hypothesis, as well as to study the period during which A375 tumor cells pass through the hicBBB model, we carried out a live *in vivo* imaging strategy. After assembling the hicBBB and waiting 48 hours for the model to form, we seeded its upper chamber with the A375 melanoma cell line expressing mCherry. Meanwhile, we stained the lower layer of SVGA using Hoechst (**Figure 30**).

The reason we chose Hoechst is that it stains the nuclei of the cells without altering the cellular physiological process. Then, we placed the model in a 24-well plate with a glass bottom in order to image it using a live confocal microscope overnight. The confocal micrography performed during the incubation of the model, allowed us to observe a red fluorescent signal from an A375 cell, implying that the cells started to invade the hicBBB model during the incubation period. In addition, the red and blue signals do not appear to be at the same depth, which likely means that A375 cells still need time to cross the model to be fully visible.

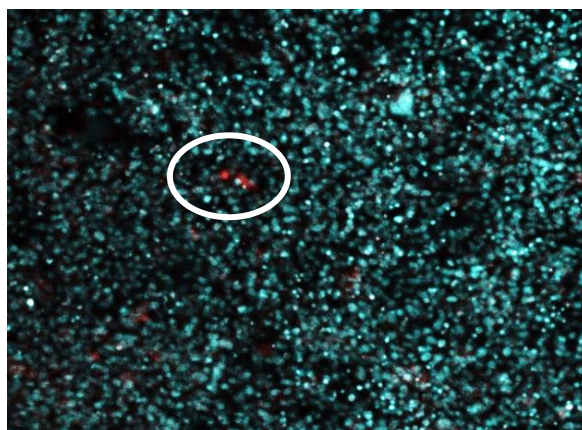


Figure 30 Live in vitro tracking by confocal microscopy of A375 mCherry cells crossing the in vitro hicBBB model

Photograph taken with a confocal microscope of the lower part of the transwell containing SVGA cells in blue and A375 mCherry cells in red after 24 hours of coculture. Scale 100 μm .

To assess the exact time at which we can observe the first cell crossing the model, we implemented a multiple endpoint fixation strategy (**Figure 31**). **Figure 31** shows the 48 hours time point after seeding A375 mCherry into the fixed hicBBB model. There are two areas where a red fluorescent signal can be seen, on the upper side of the membrane and in the middle of the blue fluorescent layer of the astrocytes. This leads us to believe that there are two populations of cells: one that remains on the top layer and another that crosses the model. We can thus conclude that A375 mCherry melanoma cells take 48 hours to cross the hicBBB model *in vitro*. We therefore wondered what changes the presence of tumor cells would produce in the model.

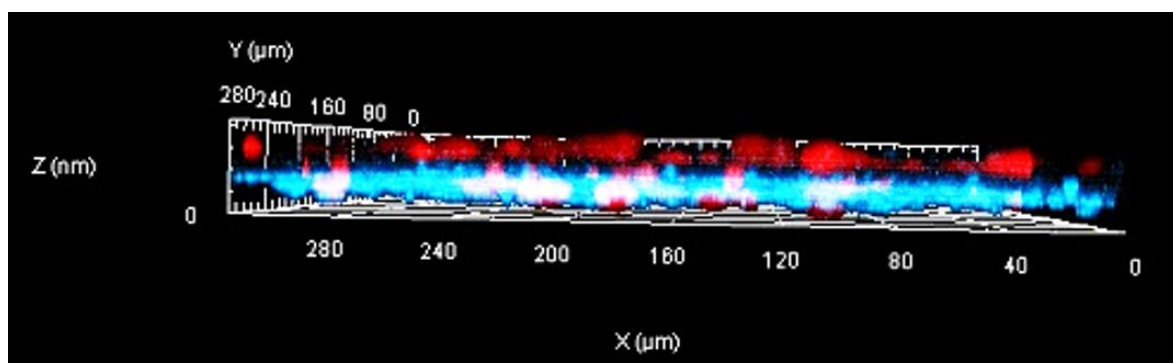


Figure 31 3D fluorescent microscopic reconstruction of the hiBBB in the presence of A375 mCherry cells

Image of the 3D reconstruction of the hiBBB model *in vitro* after 48 hours of coculture with A375 mCherry cells.

In this chapter, we first established that the presence of A375 cells tends to disrupt the hiBBB model and that this disruption is correlated with the concentration of tumor cells. We also observed that A375 cells' seeding seems to increase the permeability of the model *in vitro* and that the more tumor cells are in contact with the hiBBB model, the more permeable the latter becomes. Finally, we also determined using confocal and fluorescent microscopy that A375 cells take approximately 48 hours to cross the *in vitro* model. In the next chapter, we will screen for growth factors, cytokines, and enzymes that may be indicators of BBB invasion or rupture.

7. OBSERVATION BY ANTIBODY ARRAY OF THE hicBBB REACTION TO THE PRESENCE OR ABSENCE OF TUMOR CELLS

7.1. MMP ARRAY EXPOSED TO CONDITIONED MEDIUM

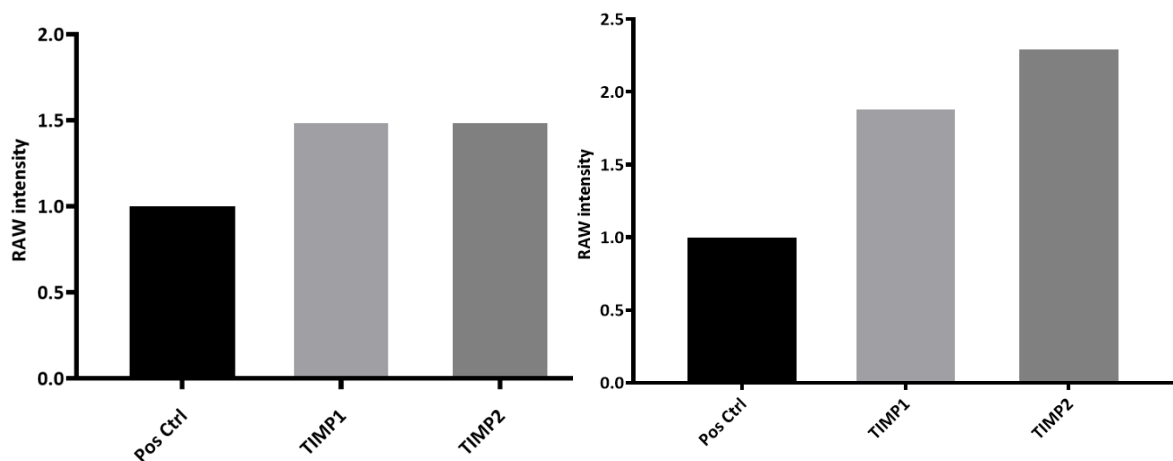


Figure 32 Summary analysis of the MMP array exposed to hicBBB-conditioned medium in the presence or absence of A375 melanoma cells

The diagram on the left displays the MMP array exposed to hicBBB-conditioned medium. The diagram on the right displays the MMP array exposed to hicBBB-conditioned medium in the presence of A375 melanoma cells. y = raw intensity normalized to positive control, x = target names (n=1).

We decided to study what changes occur in the hicBBB-conditioned culture medium in the presence or absence of A375 tumor cells. For this purpose, we used an antibody array that screens for the presence of different cytokines that may have been released into the medium. We first looked at the MMP arrays to determine if we could identify a specific agent that could be observed (**Figure 32**). When looking at **Figure 32** where the medium is solely conditioned by the hicBBB model, we can observe that out of the ten targets that are located on the MMP array, only TIMP1 and TIMP2 appear to be present in quantities above the threshold set by the internal positive control. We observed the same phenomenon when

A375 cells were added to the model. When comparing these two conditions, we see that the presence of tumor cells seems to have increased the level of detectable MMP inhibitors.

Banerji observed the same results. A (Banerji et al. 2008) in a study on the A375 cell line where they found that the presence of fibronectin, a natural component of the ECM present on the BBB, induced the production of MMP-2 and MMP-9. These MMPs are known to be enzymes that are used by tumor cells to degrade the ECM during extravasation (Voura et al. 2013). This led us to believe that the *in vitro* hicBBB model is indeed effective in faithfully reproducing an invasion of the BBB in the human body. Hence, this may imply that the model has the potential to produce TIMP to inhibit the action of MMP produced by melanoma tumor cells.

7.2. ANGIOGENESIS ARRAY EXPOSED TO CONDITIONED MEDIUM

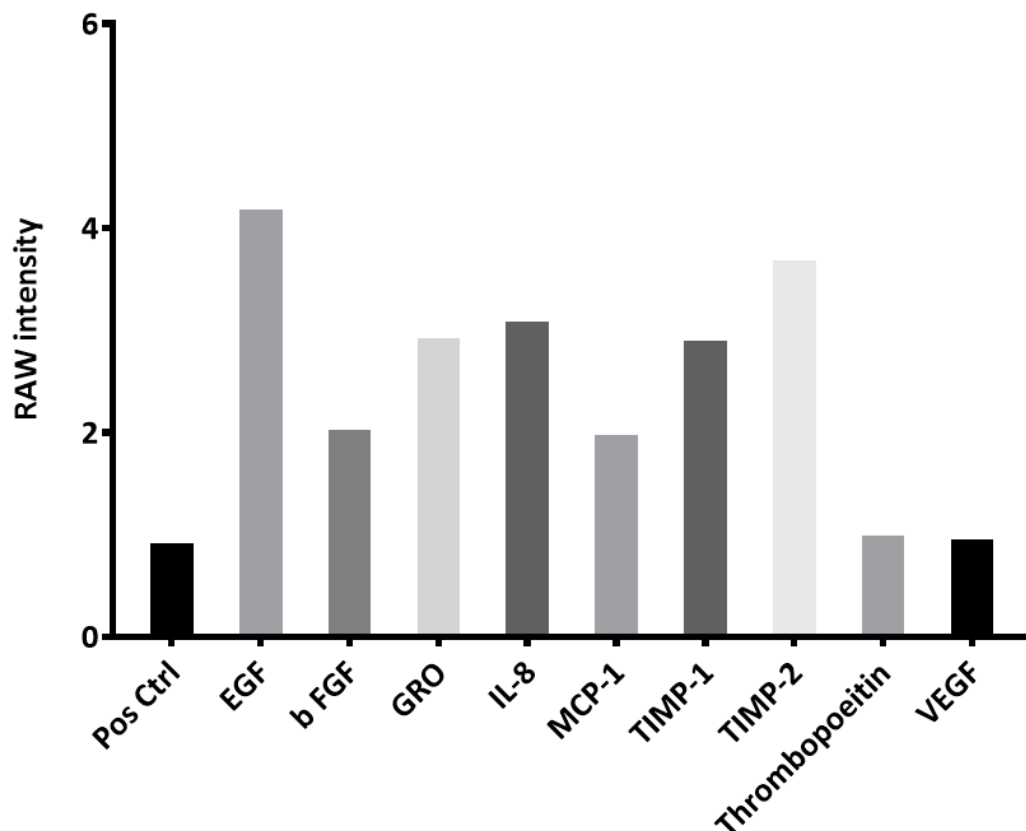


Figure 33 Summary analysis of the angiogenesis array exposed to hicBBB-conditioned medium

The diagram displays the angiogenesis array exposed to hicBBB-conditioned medium. y = raw intensity normalized to positive control, x = target names (n=1).

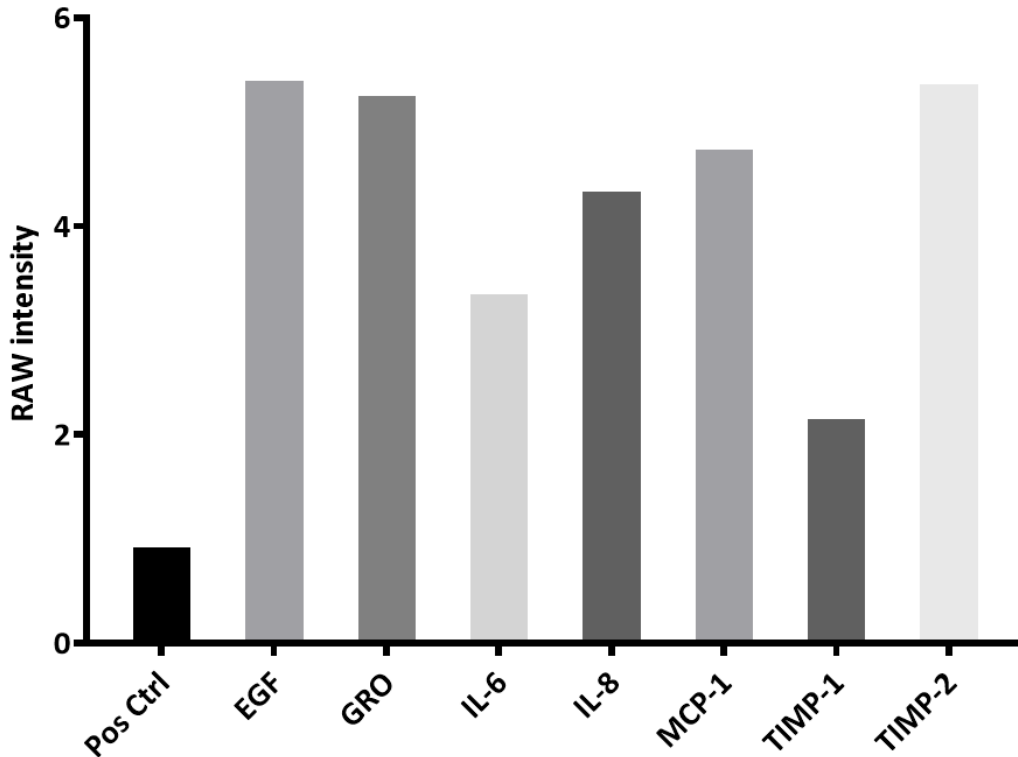


Figure 34 Summary analysis of the angiogenesis array exposed to hicBBB-conditioned medium in the presence of A375 melanoma cells

The diagram displays the angiogenesis array exposed to hicBBB-conditioned medium in the presence of A375 melanoma cells. y = raw intensity normalized to positive control, x = target names (n=1).

In a next phase, we verified whether there were other notable targets in the angiogenesis array other than those previously observed.

Growth factors displayed in Figure 33 and 34 are those that have stronger signals than the positive controls.

We were thus able to observe that the EGF initially present in the culture medium seemed to remain stable in the two conditions displayed in **Figures 33** and **34**. Other targets such as IL-6, GRO, are present in the medium.

Another noteworthy information that we were able to retrieve from the angiogenesis array is that the presence of tumor cells seems to induce FGF consumption. The latter is thought to play a role in cell adhesion to the endothelial cell layer and in the tumor cell EMT process by promoting their migration through the different tissues (Korc and Friesel 2009).

It is important to mention the presence of IL-6 in the hicBBB-conditioned medium in the presence of A375 melanoma cells because as stated in a patient-based study presented at the 2006 American Society of Clinical Oncology annual meeting, IL-6 production in patients with metastatic cancer appears to be theoretically correlated with a greater risk of developing depression and anxiety.

The production of IL-6 by a tumor when it metastasizes can be considered as a mechanism supporting the “seed and soil” cancer metastasis theory (Fidler et al. 2002). The seed and soil theory is a hypothesis suggesting that tumor cells metastasize where the local microenvironment is favorable, much like a seed that grows only if it is planted in fertile soil.

By producing IL-6, which is known to destabilize the brain microenvironment and to be correlated with pathologies of the cerebral nervous system such as Alzheimer’s (Escrig et al. 2019), the primary tumor prepares the soil for the seeding, i.e., IL-6 helps tumor cells that undergo EMT as well as intravasation to adhere to and invade their destination (Abaurrea et al. 2021; Farahani et al. 2014).

GRO is a chemokine worth highlighting in our work as it has been shown to play a role as a chemoattractant for several immune cells (Moser et al. 1990), but also as an arrest chemokine that helps monocytes to adhere to the membrane of endothelial cells by interacting with the cell adhesion molecule VCAM1 (Smith et al. 2005; Arvanitis et al. 2020).

7.3. CYTOKINE ARRAY EXPOSED TO CONDITIONED MEDIUM

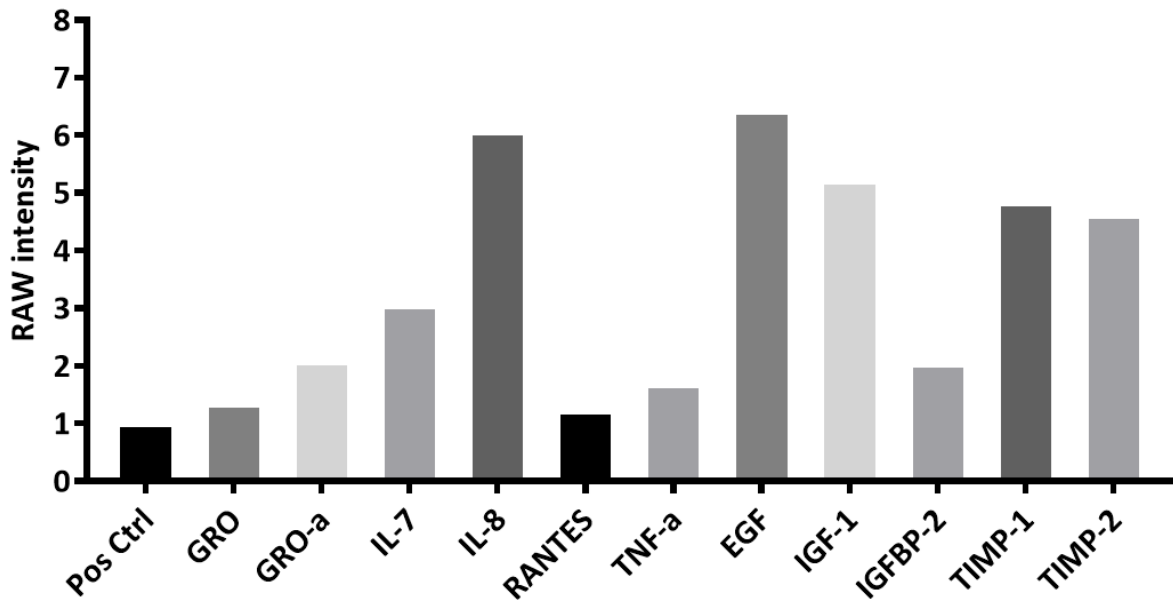


Figure 35 Summary analysis of the cytokines array exposed to hicBBB-conditioned medium
 The diagram displays the cytokines array exposed to hicBBB-conditioned medium. y = raw intensity normalized to positive control, x = target names (n=1).

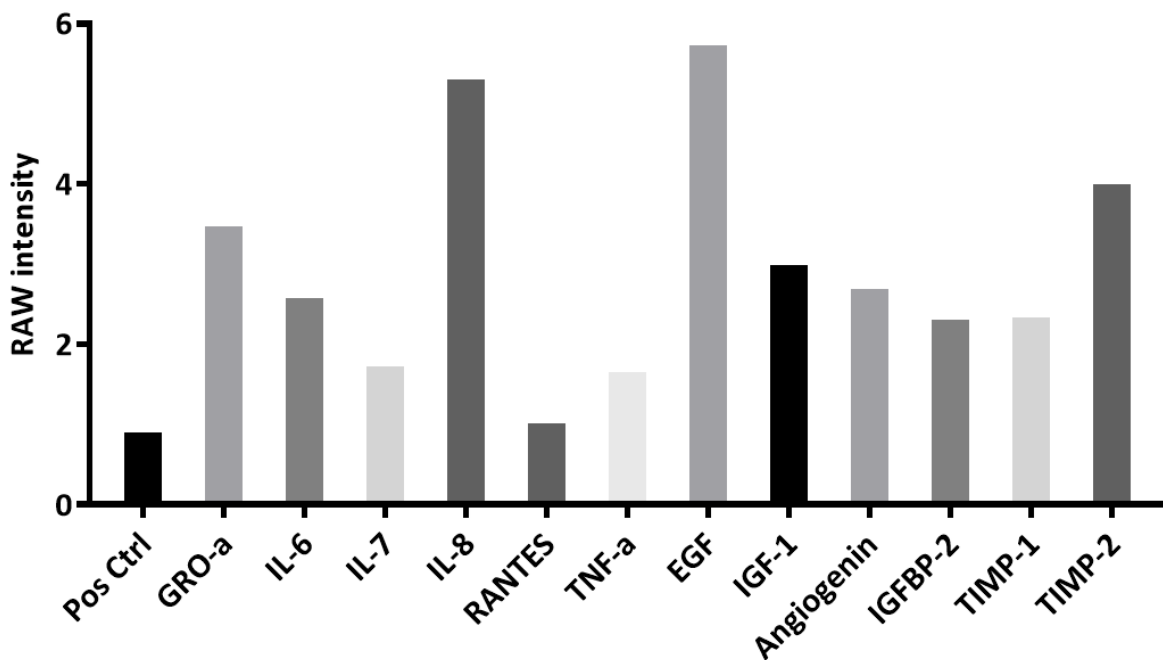


Figure 36 Summary analysis of the cytokines array exposed to hicBBB-conditioned medium in the presence of A375 melanoma cells

The diagram displays the cytokines array exposed to hicBBB-conditioned medium in the presence of A375 melanoma cells. y = raw intensity normalized to positive control, x = target names ($n=1$).

An additional array that has been used in our research to verify the presence of other targets in the conditioned media is the cytokine array (**Figures 35 and 36**), which includes 74 different targets. When reviewing the results obtained for the different conditions in the cytokine arrays, we found that, as with the MMP and angiogenesis arrays, TIMP and IL6 were present, with the addition of the interleukins IL-7 and IL-8, angiogenin, IGFBP-2, IGF-1, TNF α and RANTES.

Through the use of the different arrays, it was possible to detect cytokines, chemokines, interleukins and growth factors that are produced by the hicBBB model in the presence or absence of A375 tumor cells.

Angiogenin is known to be an essential cell growth factor that promotes the development and maintenance of melanomas, and in particular of the A375 melanoma cell line (Song et al. 2006).

Insulin growth factors such as IGFBP-2 and IGF-1 are known to be pro-tumor factors due to their influence on the PI3k/Akt pathway (Brahmkhatri et al. 2015).

Recent research has shown that miR-7, an IGF inhibitor in melanoma, can reduce tumor cell growth and even reverse to some extent, resistance to BRAFi treatment such as vemurafenib (Sun et al. 2016). In another study by Liu. P et al. 2015, miR-425 was tested in Boyden chambers on the A375 cell line to inhibit its migration and invasion (Liu et al. 2015).

Altogether, the information and data collected led us to conclude that the IGF present in the hicBBB-conditioned medium in the presence or absence of tumor cells, act in favor of the latter's survival and tissue invasion.

Our results showed that there is production of TNF α in the hicBBB-conditioned medium in the presence or absence of A375 melanoma cells, which is a disruptor of the endothelial cell layer capable of facilitating the passage not only of monocytes across the BBB during inflammation, but also that of tumor cells (Pan et al. 2011; Qiu et al. 2021).

RANTES, also known as CCL5, is a chemokine that may have an important role in the survival and migration of tumor cells across the BBB, as when coupled with its GPCR CCR5 receptor,

it activates the pro-tumor PI3K/Akt pathway and induces the production of MMP to remodel the extracellular matrix of endothelial cells in melanoma metastasis (Liu et al. 2019).

Taken together, the information gathered along with our results, has led us to the conclusion that our hicBBB *in vitro* model composed of immortalized human cell lines, can be a valid model to investigate the early invasion of the BBB by tumor cells and to possibly observe any potential change in the tumor cell line gene expression.

In the following chapter, we will introduce two A375 cell lines resistant to BRAFi and MEKi and then isolate the fluorescent tumor cells, both resistant and non-resistant, after they pass through the *in vitro* model to observe if there is a difference in gene expression.

8. RESISTANT CELLS AND FLOW CYTOMETRY SORTING

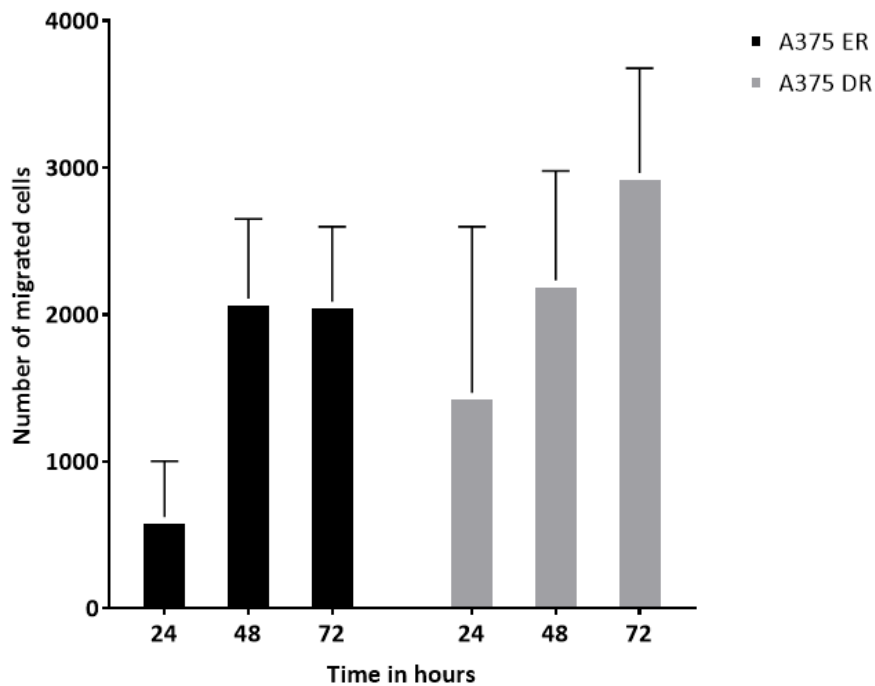


Figure 37 Migration potential of A375 mono and double treatment-resistant cell lines

The black bars on the diagram show the number of mono treatment-resistant A375 ER cells that were counted on the transwell membrane post migration at different time points. Transwell membranes were fixed after 24, 48, and 72 hours. Error bar represents SD. The gray bars on the diagram show the number of double treatment-resistant A375 DR cells that were counted on the transwell membrane post migration at different time points. Transwell membranes were fixed after 24, 48, and 72 hours. Error bar represents SD (n=3).

MEKi and BRAFi are among the standard treatments for patients with stage 4 melanoma. BRAFi is also known for having been used alone on patients and inducing a high response. However, after a period of time, the melanoma develops resistance to the treatment and the patient relapses. In order to determine if the treatment has an influence on the metastasizing potential across the BBB, we will include in our experiment both BRAFi and BRAFi combined with MEKi resistant A375 cells.

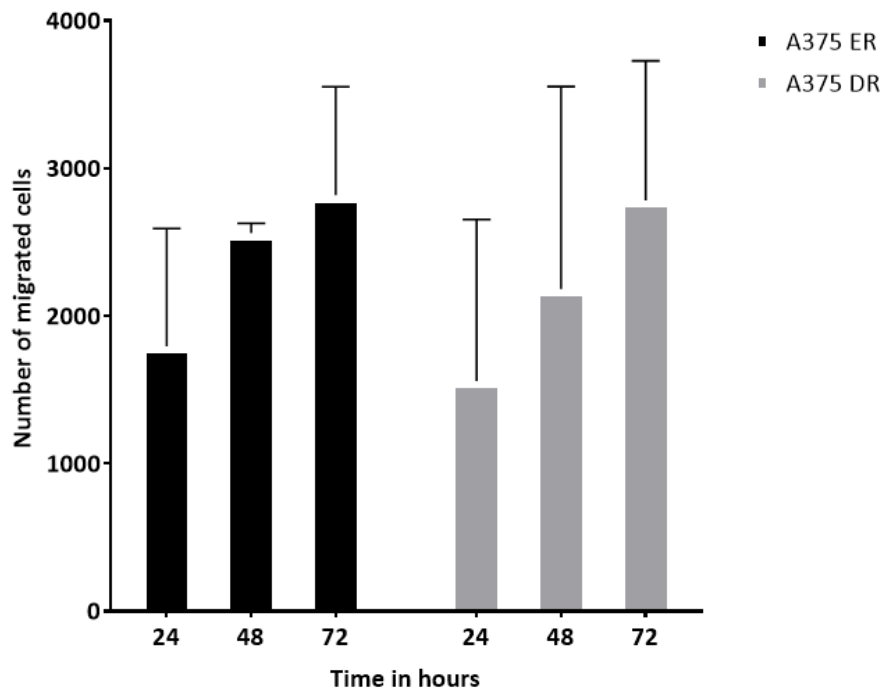


Figure 38 Invasion potential of A375 mono and double treatment-resistant cell lines

The black bars on the diagram show the number of mono treatment-resistant A375 ER cells that were counted on the transwell membrane post invasion at different time points. Transwell membranes were fixed after 24, 48, and 72 hours. Error bar represents SD. The grey bars on the diagram show the number of double treatment-resistant A375 DR cells that were counted on the transwell membrane post invasion at different time points. Transwell membranes were fixed after 24, 48, and 72 hours. Error bar represents SD (n=3).

Our next objective was to establish whether there is a difference in the migratory/invasive potential as well as a difference in the genetics between A375 wt cells, A375 double resistant cells (A375 DR) and A375 single resistant cells (A375 ER). Before adding the two resistant cell lines to our experiment *in vitro*, we must first assess whether they possess migratory and invasive potential. When we look at the 24 hours time point, we can observe that the A375 resistant cells seem to have a tendency to be more invasive than simply migratory. This might be due to the presence of fibronectin which can be an anchor point for the cells, but also a trigger in the production of MMPs in melanoma.

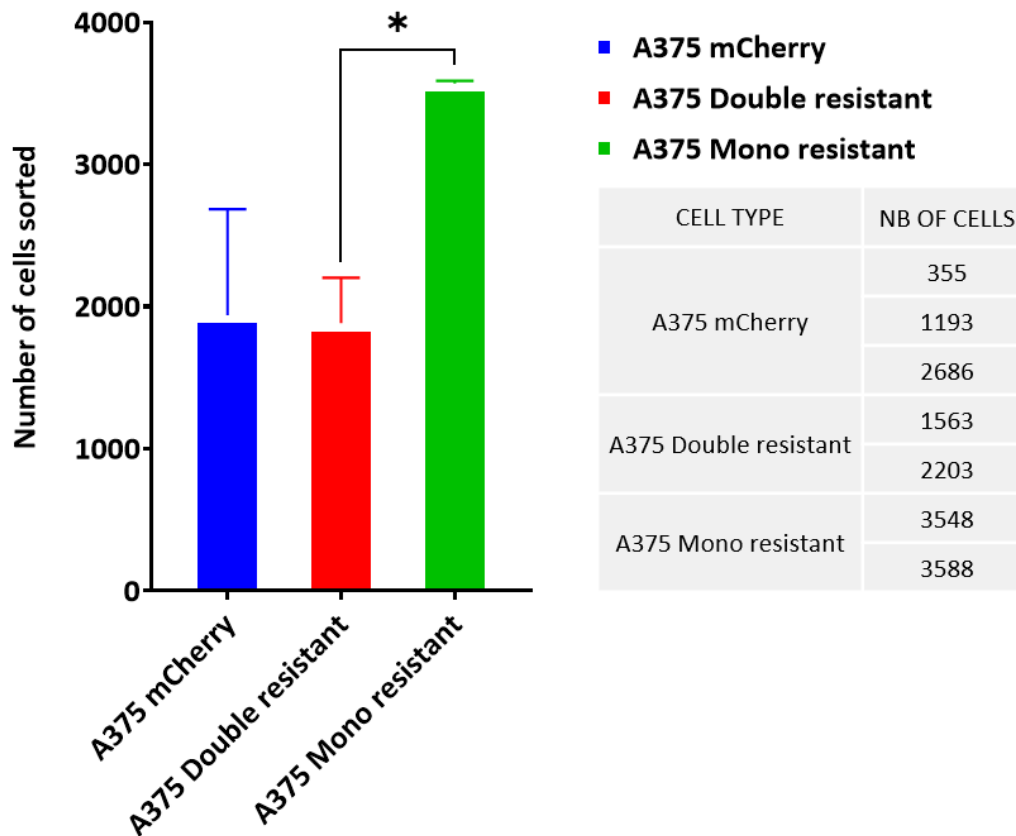


Figure 39 FACS sorting of treatment-resistant and non-treatment-resistant A375 melanoma cells that have crossed the *in vitro* hicBBB model

This diagram displays the number of cells that have crossed the hicBBB *in vitro* model. The blue bar on the diagram represents the A375 mCherry cell line, the red bar represents the A375 double treatment-resistant cell line, the green bar represents the A375 mono treatment-resistant cell line. Error bar represents SD. $0.05 > p\text{-value}^*$ obtained by t-test ($n=3$).

To investigate the genetic difference between the A375 tumor cell types that migrate through the hicBBB model, we separated them from the model by enzymatic and mechanical dissociation followed by flow cytometry sorting using either the mCherry fluorescent signal or the deep red tracer signal for resistant cells (**Figure 39**). The graph represents the average number of cells that were sorted for each A375 type. In order to collect sufficient genetic material to perform RNA-Seq, it was necessary to pool several inserts per biological replicate. Each biological replicate is composed of 18 technical replicates for each condition, each of which contains a hicBBB model. We were able to observe that compared to the control and to the A375 DR, the single resistant cells seem to invade the *in vitro* model in greater numbers. We will in a next steps try to observe a possible difference in genetic expression for the different A375 cells.

9. 3' RNA-Seq OF A375 CELLS THAT CROSS THE hicBBB MODEL

9.1. PCA CLUSTERING OF SAMPLES

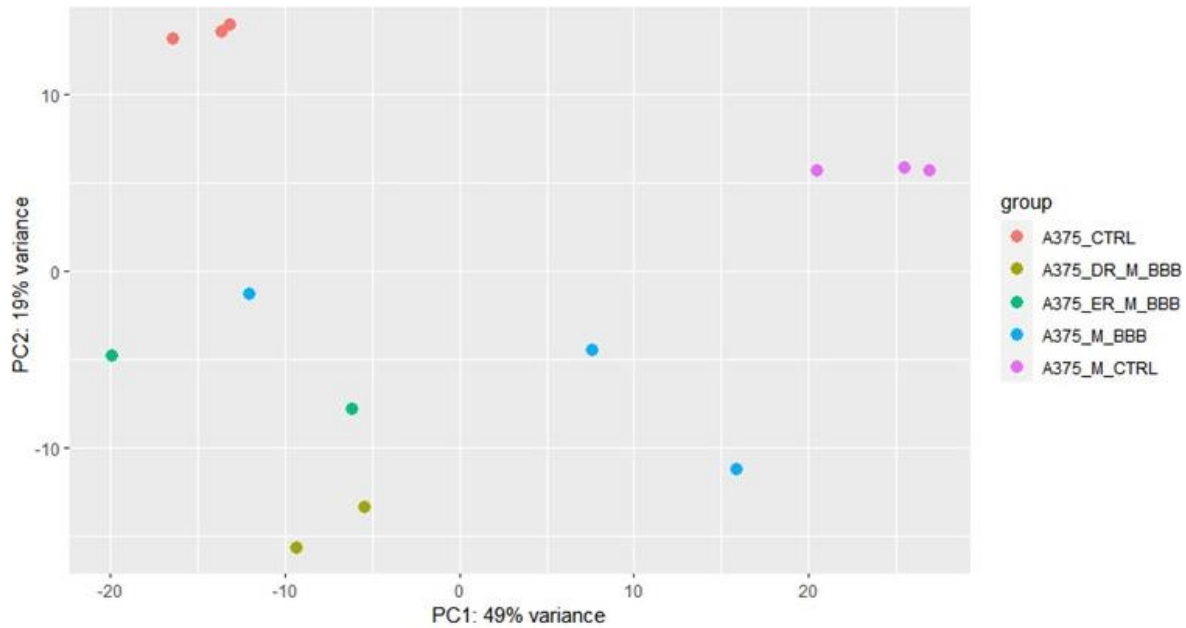


Figure 40 PCA of FACS-sorted A375 cell samples after 3' RNA-Seq

The A375_ctrl group is composed of A375 ctrl cells from a wt culture; the A375_M_CTRL group is composed of A375 ctrl cells that migrated through a transwell; the A375_M_BBB group is composed of A375 ctrl cells that crossed the hicBBB model and were sorted using FACS; the A375_M_ER group is composed of A375 mono treatment-resistant cells that have crossed the hicBBB model and have been sorted using FACS; the A375_M_DR group is composed of A375 double treatment-resistant cells that have crossed the hicBBB model and have been sorted using FACS.

Following the results showing that the mono-resistant A375 cell line seems to migrate more than the double-resistant A375 cell line in a significant way, the question that arises is whether the treatments modify the gene expression of the cells that cross the hicBBB *in vitro*. To try to find an answer to this question, we decided to perform a 3'RNA-Seq which allows us to perform gene expression analyses on small samples like ours and decreases the impact of RNA degradation on the experiment.

Figure 40 shows the clustering of the different conditions that compose the sequencing samples.

The A375 Ctrl group consists of cells in normal culture while the A375 M Ctrl group consists of A375 cells capable of migrating only through the plastic membrane of the transwell and not through the hicBBB *in vitro*. The remaining samples are treatment-resistant and non-treatment-resistant A375 cells capable of crossing the hicBBB that are harvested and then sorted by FACS.

We can observe that the two control groups do not cluster with each other or with the samples, this may be due to the fact that they were not sorted by FACS. Furthermore, we can also observe that the samples do not cluster with each other either.

From this, we deduced that further analysis of the data would show that it is not possible to distinguish the gene expression from the 3 types of A375. Further details on the 3' RNA-Seq summary report from LuxGen are provided in the Appendix.

10. IN VIVO MODEL OF THE METASTASIS PROCESS TO THE BRAIN

10.1. ULTRASOUND IMAGING OF AN INJECTION INTO THE LEFT VENTRICLE OF THE HEART

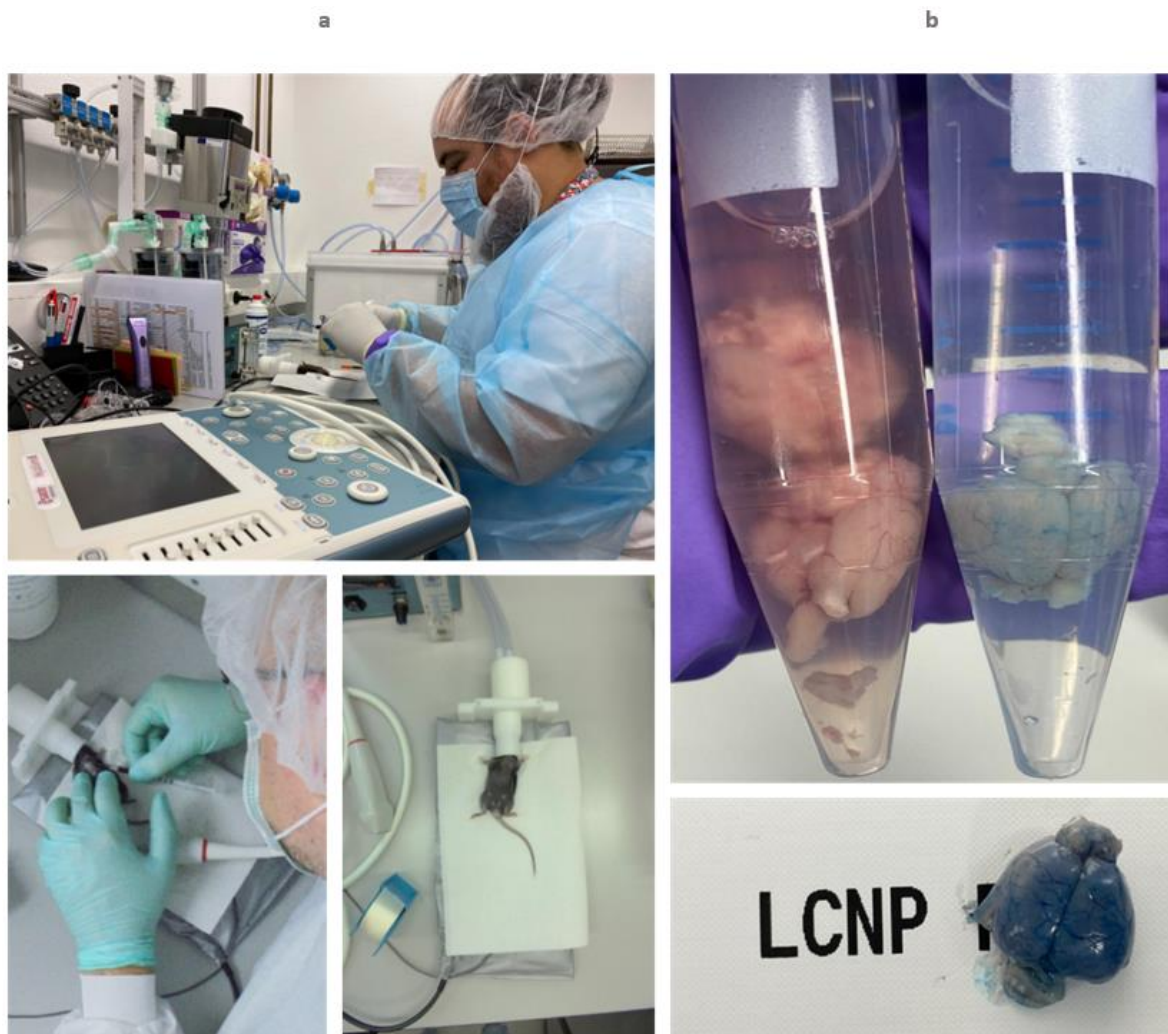


Figure 41 Description of the performing of an injection into the left ventricle of a mouse heart and verification of the needle placement using trypan blue

a Photographic images of the experimental setup of the anesthesia machine, the ultrasound machine, the heating pad to maintain the body temperature of the mouse, the positioning of the mouse to perform the injection. **b** Photographic images of the successful injection

identified by the presence of the injected trypan blue dye in the vasculature of the brain. Left tube containing a control murine brain not stained with trypan blue, right tube containing a murine brain that was successfully stained with trypan blue.

As part of our work on the early mechanisms of brain metastasis of melanoma, in addition to an *in vitro* model, we have also recreated an *in vivo* model. To this end, we injected a suspension of A375 mCherry tumor cells into the left ventricle of the heart of nude mice thus recreating the process of brain metastasis.

Figure 41 a, shows in images the set-up for the injection into the left ventricle of the heart. A critical point during the injection is the respect and the well-being of the animal, for this reason it is necessary to constantly monitor its health status during and after the experimental surgical procedure. First, the animal must be adequately sedated and anesthetized. When the mouse is asleep and under the influence of anesthesia, its body temperature tends to decrease, which can lead to the death of the animal or to a perturbation of the hemodynamic system. Since the intention is to use the vascular system to convey tumor cells to the brain capillaries, it is important to mitigate the effect of anesthesia by maintaining the body temperature of the mouse in a physiological state. Once the mouse is properly anesthetized and placed in a safe position, we can now begin to locate the heart using an ultrasound machine (**Figure 42**). A subsequent step is to locate the left ventricle of the heart. If no physical abnormalities are detected, we proceed to prepare the syringe. Finally, we inject the suspension containing $5 \cdot 10^5$ A375 tumor cells.

In order to successfully inject the tumor cells, it was necessary to train ourselves. For our training, we used trypan blue to ensure the precision of our injections. Indeed, when these are performed correctly, we obtain a brain presenting a blue vasculature (**Figure 41 b**). The photograph in **Figure 41 b**, shows two tubes, one containing the brain of an animal where the injection failed and the other containing a blue brain where the injection was successful.

Figure 42, is a picture of an injection in the left ventricle of a mouse heart being monitored by ultrasound. Once the mouse has been injected, we let it recover under close monitoring until the date of its sacrifice, when we finally harvest the brain following cervical dislocation.

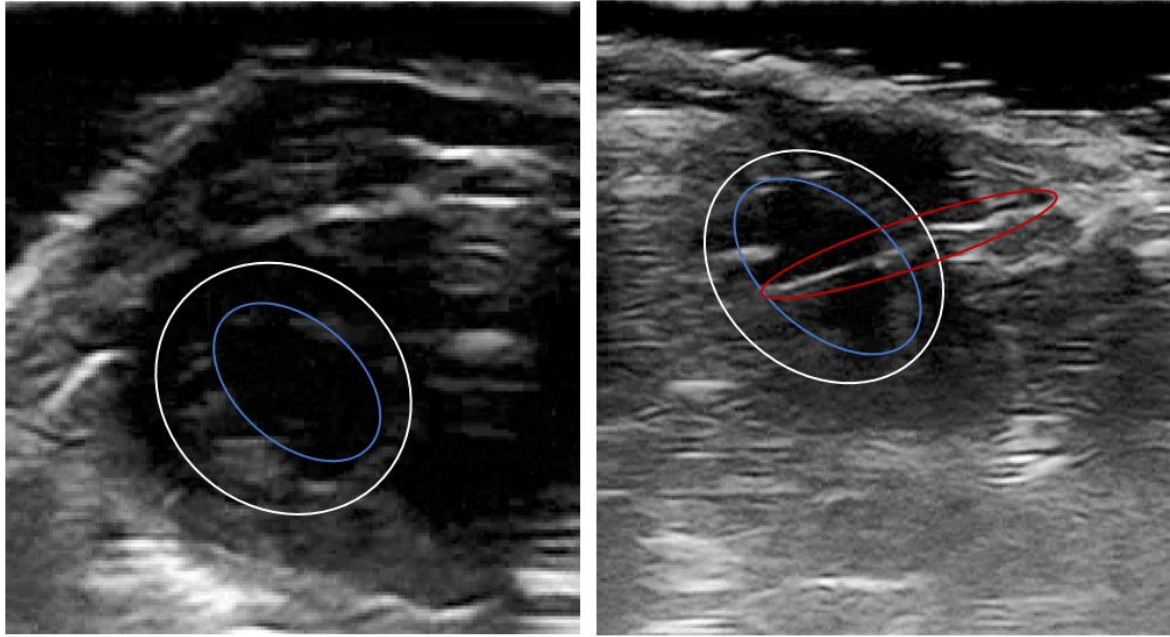


Figure 42 *Ecographic images of the left ventricular area of a mouse heart before (left) and during (right) injection*

The two-dimensional image on the left depicts the left ventricular area of a mouse heart before injection observed by ultrasound. The area outlined by the white circle indicates the outer wall of the left ventricle of the heart; the area outlined by the blue circle indicates the inner wall of the left ventricle of the heart. The two-dimensional image on the right depicts the left ventricular area of a mouse heart during injection observed by ultrasound. The area outlined by the white circle indicates the outer wall of the left ventricle of the heart; the area outlined by the blue circle indicates the inner wall of the left ventricle of the heart; the area outlined by the red circle indicates the needle.

10.2. BRAIN SCREENING STRATEGY USING CONFOCAL MICROSCOPY

Our research protocol was developed so as to harvest two brains each day for 10 days from the second day after injection. After they are harvested, we fix the brains using Karnovsky's ME fixative solution. Following harvesting and fixation, the brains are sliced into 100 μm thick slices. After these steps are completed, we examine the brain for mCherry signal using a confocal microscope. To ensure that the cells we are observing are indeed A375 mCherry cells, we verify the expression of the mCherry protein within the cell using a specific anti-mCherry protein antibody (**Figures 43 and 44**).

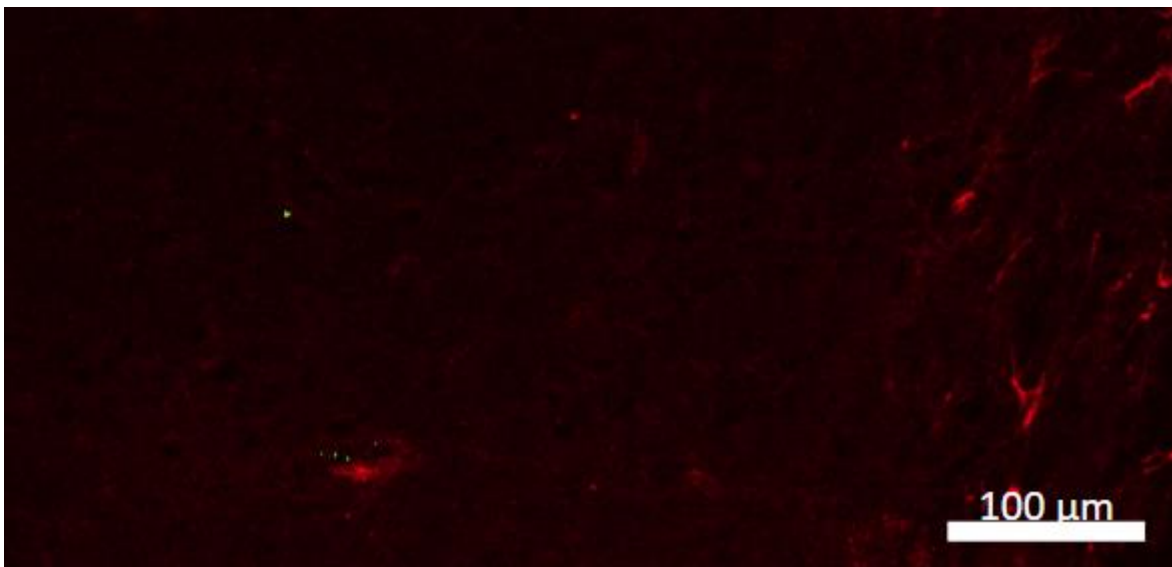
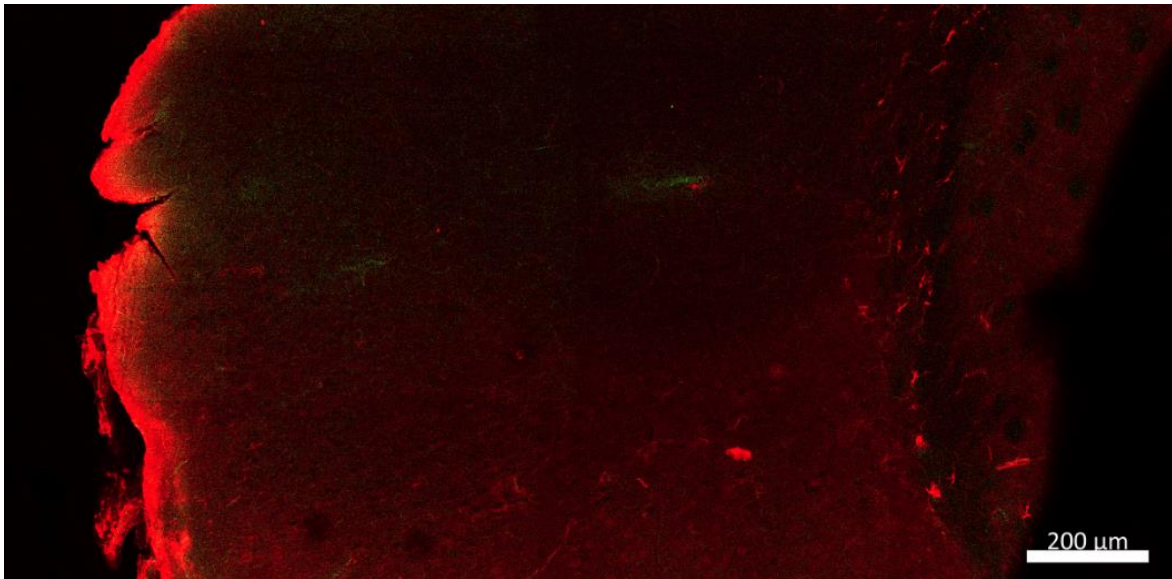


Figure 43 Images captured by fluorescence confocal microscopy of a potential A375 mCherry cell identified in the brain parenchyma of a mouse 10 days after injection

Images captured by fluorescence confocal microscopy (top) of an area within the brain parenchyma that seems to contain a potential A375 mCherry cell identified using an anti-mCherry antibody coupled to an AF 488 secondary antibody. Red fluorescent staining represents brain cells that are positive to GFAP, the latter was used to increase the contrast between brain tissue and what seem to be potential metastases. Scale bar 200 μm. Magnified x10. Zoom of the same fluorescence confocal microscopy image (bottom). Scale bar 100 μm. Magnified x10.

Once an mCherry signal is detected, we image a sequence of Z images to establish the depth of the cell as well as its position in the tissue. The imaging of these cells is an important part of identifying morphological features that would contribute to a better orientation in the tissue during EM imaging (**Figure 43-44**).

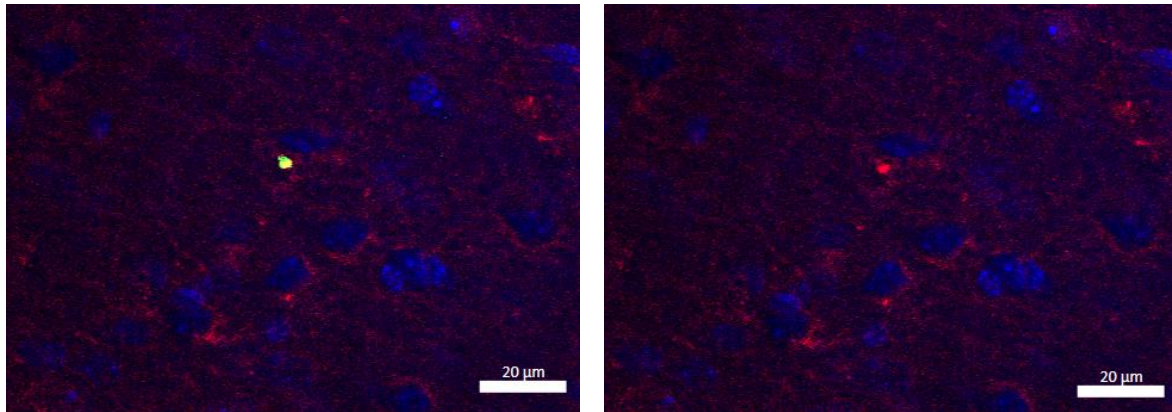


Figure 44 Images captured by fluorescence confocal microscopy of a potential A375 mCherry cell identified in the brain parenchyma of a mouse 10 days after injection

Images captured by fluorescence confocal microscopy of an area within the brain parenchyma that seems to contain a potential A375 mCherry cell identified using an anti-mCherry antibody coupled to an AF 488 secondary antibody (left). Red fluorescent staining represents brain cells that are positive to GFAP and mCherry positive cells (right). Scale bar 20 μm . Magnified x20.

10.3. SAMPLE PREPARATION FOR EM IMAGING

Upon determining the location of an mCherry signal in the brain parenchyma, we post-fix the tissue with osmium and then dehydrate it with an ethanol gradient. We then proceed to embed the tissue samples in epon resin. Once the resin is fully polymerized, we proceed to cut 80 nm thick slices using an ultramicrotome. This delicate task was performed by Anaïs Carpentier, EM technician at LNS. With these steps completed, we image our freshly cut brain samples that may contain tumor cells.

10.4. EM OBSERVATION OF A MOUSE CONTROL SAMPLE

After preparing the samples for electron microscopy, we imaged control tissue samples from murine brains to become familiar with the ultrastructure of the brain tissue and in particular with the capillaries in order to be able to recognize melanoma cells.

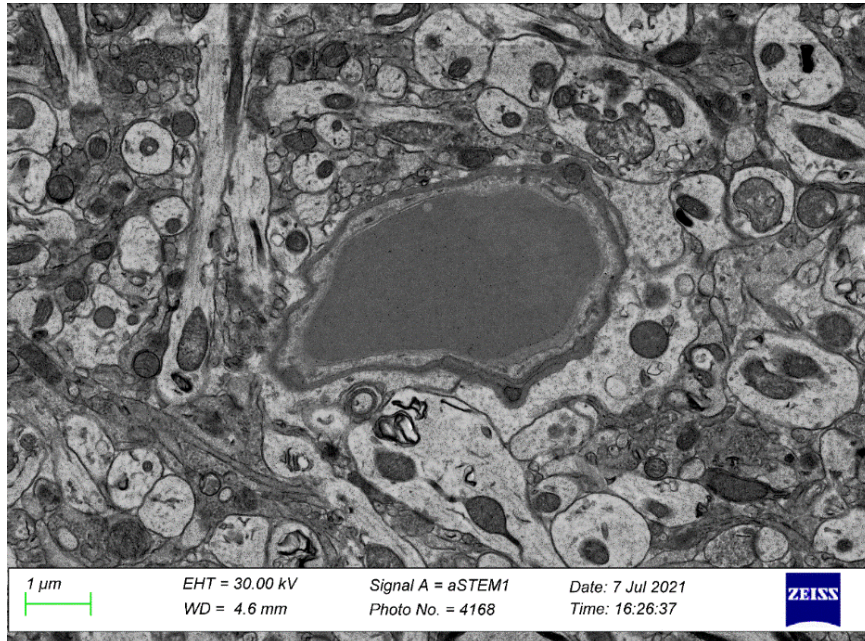


Figure 45 STEM observation of a brain capillary in a control sample

STEM micrograph of a brain capillary in a control tissue sample. The micrograph shows the lumen of the capillary containing a red blood cell; an endothelial cell lining the capillary and forming tight junctions visible in the upper right area of the capillary; pericytes surrounding the capillary. The image also shows the end feet of an astrocyte in the lower right area of the capillary. Scale bar 1 μm.

10.5. STEM OBSERVATION OF MOUSE BRAIN TISSUE INJECTED WITH A375 CELLS

Following the screening of the murine brains with a confocal microscope, we believe we have succeeded in visualizing potential A375 melanoma cells. For the identification of these cells, we relied on the ultrastructural characteristics of their melanosomes (2). Indeed, **Figure 46** is a low magnification sequence of images obtained by STEM, upon epon resin embedding

and ultrathin sectioning of 80 nm thick slices, which seem to show stage IV mature melanosomes.

Melanosomes within melanocytes undergo four stages of maturation, which can be distinguished by their ultrastructure (SEIJI et al. 1963). In the early stages (I and II), melanocytes are devoid of pigment but contain irregular amyloid fibrils that gather and form evenly spaced sheets. The gradual deposition of melanin on the sheets indicates stage III, and their covering is an indication of stage IV. Nevertheless, further investigations are needed to establish with certainty that the cells observed are indeed A375 cells. Having already performed immunolabeling followed by confocal fluorescence microscopy and conventional EM analysis, an additional possibility could be immunolabeling followed by electron microscopy analysis using melanin-specific antibodies coupled to gold particles.

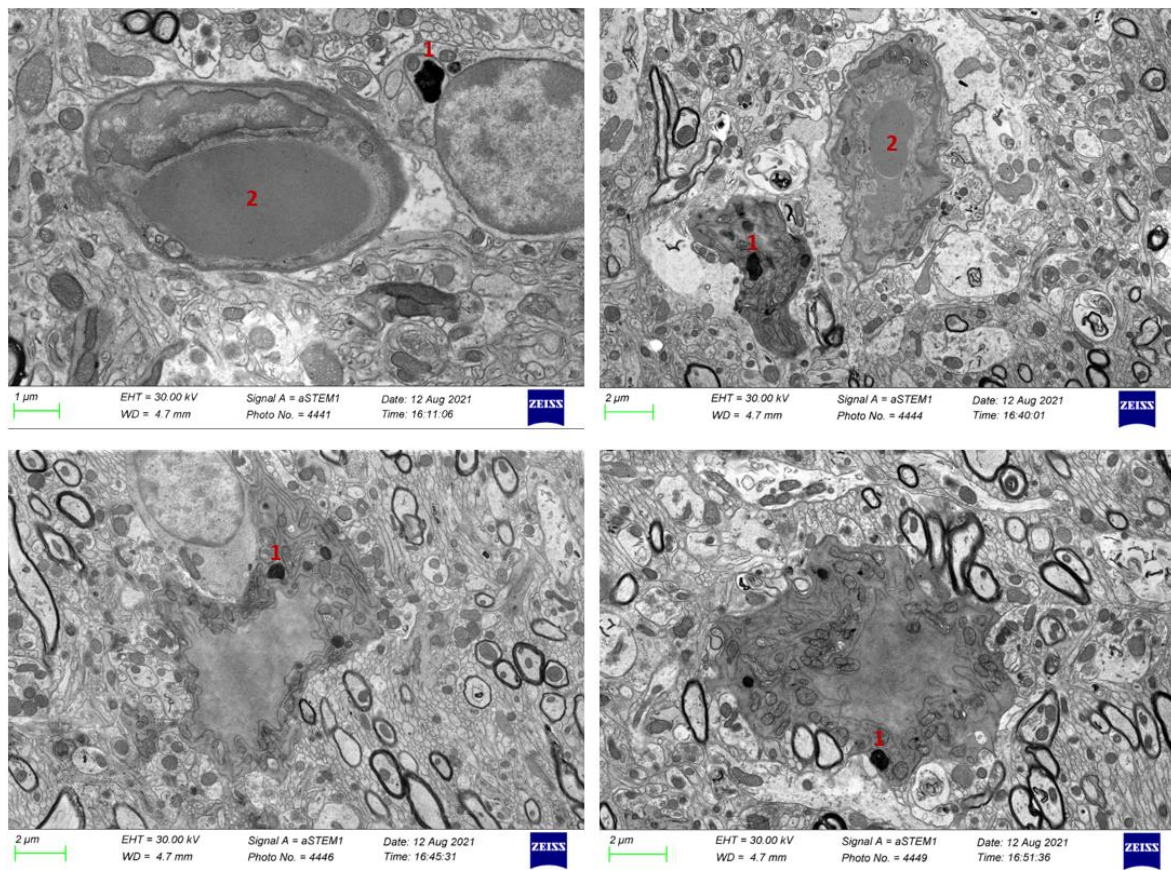


Figure 46 STEM observation of potential melanoma cells after invasion of the capillaries in a mouse brain 10 days post injection

STEM micrograph of brain capillaries from a mouse 10 days after injection. The micrographs show 4 potential spots of invasion of brain capillaries by melanoma metastases. 1.

melanosomes 2. Capillaries. Top left image scale bar 1 μm ; top right, bottom left and right images scale bar 2 μm .

Overall, confocal and EM observations allowed us to identify potential invasion points in murine brain samples that were left with circulating A375 cells for ten days.

PART IV. DISCUSSION AND OUTLOOK

1. IN VITRO hicBBB MODEL DISCUSSION

1.1. hicBBB MODEL FORMATION

To investigate the early stages of BBB invasion by melanoma tumor cells, we first set up a 3D model of three immortalized human cell lines, namely hCMEC/D3, SV40-HBVP and SVGA. We then assessed the expression of specific markers in these cell lines to ensure that they were adequate for the formation of our *in vitro* model. For instance, we made use of occludin and ZO-1 to identify the endothelial cell line (Weksler et al. 2013; Czupalla et al. 2014; Zhang et al. 2019), PDGFR β and α SMA to identify the SV40-HBVP line (Sweeney et al. 2016; Brown et al. 2019; Dore-Duffy and Cleary 2011), and GFAP to identify the SVGA cell line (Petzold and Murthy 2011; Verkhatsky et al. 2016; Lin et al. 2010). We then proceeded to test the stability and integrity of our model by means of TEER followed by a permeability test, which uses a tracer that crosses the BBB by passive diffusion (Sandoval and Witt 2008; Czupalla et al. 2014; Bernatz et al. 2019).

Established cell culture models such as the ones used in this approach usually rely on a combination of nutrients and growth factors to ensure adequate culturing conditions. While these conditions are well established for the individual cell lines, coculture requires additional optimization, which was systematically done in this study.

All the cell lines tested positive for the respective markers listed above. Both the TEER test and the permeability test have allowed us to confirm the integrity and stability of the *in vitro* model (Czupalla et al. 2014; Erickson et al. 2020). Eventually, these two inferences allowed us to conclude that we have successfully developed an *in vitro* model of BBB and that this one reaches its full potential after 48 hours of culture.

After 24 hours, we observe that the A375 resistant cells seem to have a tendency to be more invasive than simply migratory. This might be due to the presence of fibronectin which can be an anchor point for the cells, but also a trigger in the production of MMPs in melanoma.

Nevertheless, the human immortalized endothelial cell line that composes our model has certain limitations, namely : its TEER is relatively low when compared to cell lines of porcine or even murine origin (Srinivasan et al. 2015); as aforementioned hCMEC/D3 presents a reduced expression of claudin-5 (Weksler et al. 2013), the latter being a major component of tight junctions, its low expression leads us to conclude that other endothelial cell lines or primary cells could be potential candidates to replace the immortalized cell line hCMEC/D3 used in our project.

A similar observation can be drawn with regard to the SV40-HBVP and SVGA cell lines, indeed in order to obtain a BBB model that is as close as possible to human physiology and therefore exhibiting a higher TEER and a lower permeability, the use of better-characterized cell lines or primary cells can be favored.

Once these changes are made to the composition of the model, a variation in the transit times of the A375 cells through the new model could be observed. Furthermore, these modifications could have a substantial impact on the formation of cell-cell contacts between tumor cells and BBB cells, as well as between the cells the constituent cells of the BBB.

Additionally, in order to optimize the model, the use of a more physiological medium could also be considered. Indeed, the mediums used to maintain the cell lines and the model itself in culture contain a higher concentration of nutrients and growth factors compared to a physiological environment, which has the effect of boosting cell metabolism. Conversely, it can be hypothesized that a physiological medium would have an impact on the invasion potential of the tumor cells and on the formation of the model.

1.2. IDENTIFICATION OF POTENTIAL A375 MARKERS AND DETECTION OF MELANOSOMES BY ELECTRON MICROSCOPY

In this section, we describe how we proceeded to the identification of potential markers of A375 and to the detection of melanosomes by electron microscopy.

We started with the immunocytochemical labeling of A375 cells using the V600E marker, which is a BRAF mutation-specific marker, the SOX10 and S100 markers, which are neural crest derived cell specific markers, and the MelanA marker, which is specific to melanocytes. As a result of these markings, we were able to determine that the A375 melanoma cell line was positive for the V600E (Capper et al. 2011), SOX10 and S100 markers and negative for the MelanA marker (Redmer 2018; Shain and Bastian 2016; Herwig et al. 2016; Kashani-Sabet 2014; Banerji et al. 2008).

However, the three markers found in the A375 cell line could not be exploited for the following reasons: the anti-V600E antibody derives from a murine host, which disqualifies it as an eventual candidate for use in the screening of the mouse brains to detect early

melanoma invasion events in our *in vivo* model; the SOX10 and S100 markers are commonly used for the detection of melanomas outside the central nervous system, the reason being that the cell types that constitute the brain and melanoma cells, both derive from the neural crest, and thus both the astrocytic cells in our *in vitro* model as well as the cells that constitute the mouse brain would test positive for both markers making differentiation between the two impossible (Pytlak et al. 2019; Karamchandani et al. 2012). Based on these premises, we have undertaken to look for an alternative approach to identify melanomas. For this purpose, we attempted to find melanoma-specific structures. We have consequently chosen to use the presence of melanosomes, which we detected by electron microscopy, as a marker of differentiation. We were successful in detecting melanosomes in the amelanotic cell line A375, which eventually enabled us to recognize melanomas among other cells (Bracalente et al. 2016; Skoniecka et al. 2021).

1.3. hicBBB MODEL SUITABILITY ASSESSMENT

Once the reliability of the hicBBB model was ascertained, we exposed it to the A375 melanoma cell line that expresses the mCherry protein. We began by monitoring the impact that tumor cells have on both the TEER and the permeability of our model *in vitro* (Ludwig et al. 2002). We have found that the presence of tumor cells reduces the TEER and the permeability after 48 hours of coculture. The drop in TEER that occurs with the increase in A375 cell concentration can also be greatly influenced by the lack of nutrients in the environment. This lack puts all the cells present in the coculture in competition and the ones that are more sensitive to the variation in glucose availability eventually die. This may have been the case in our experiment where hCMEC/D3 and SV-40 HBVP were cocultured with A375 cells in a confined upper compartment of a Boyden chamber. This shortage of nutrients could be avoided if the model was supplied with a constant flow of nutrients, as is the case in the brain vasculature. From a technical point of view, the addition of a peristaltic pump to allow the constant flow of fresh medium would allow to obtain an *in vitro* model closer to the physiological reality. In a second phase, we tracked A375 mCherry across the model using live confocal imaging. This has allowed us to determine that A375 mCherry employs 48 hours to pass from one side to the other of the model.

We have also been looking for potential molecular factors that may provide information on the mechanism of BBB invasion by tumor cells. We noticed that molecules such as IGF, GRO (Moser et al. 1990), or angiogenin were present in the model environment during its invasion by A375 mCherry. In addition, interleukins such as IL-6, IL-7, and IL-8 were also detected by antibody array (Moser et al. 1990; Smith et al. 2005; Song et al. 2006; Sun et al. 2016; Liu et al. 2019; Liu et al. 2015). It is important to mention the presence of IL-6 in the hicBBB-conditioned medium in the presence of A375 melanoma cells because as stated in a patient-based study presented at the 2006 American Society of Clinical Oncology annual meeting, IL-6 production in patients with metastatic cancer appears to be theoretically correlated with a greater risk of developing depression and anxiety.

The production of IL-6 by a tumor when it metastasizes can be considered as a mechanism supporting the “seed and soil” cancer metastasis theory (Fidler et al. 2002). The seed and soil theory is a hypothesis suggesting that tumor cells metastasize where the local microenvironment is favorable, much like a seed that grows only if it is planted in fertile soil. By producing IL-6, which is known to destabilize the brain microenvironment and to be correlated with pathologies of the cerebral nervous system such as Alzheimer’s (Escrig et al. 2019), the primary tumor prepares the soil for the seeding, i.e., IL-6 helps tumor cells that undergo EMT as well as intravasation to adhere to and invade their destination (Abaurrea et al. 2021; Farahani et al. 2014).

The IGF present in the hicBBB-conditioned medium in the presence or absence of tumor cells act in favor of the latter’s survival and tissue invasion.

Our results showed that there is production of TNF α in the hicBBB-conditioned medium in the presence or absence of A375 melanoma cells, which is a disruptor of the endothelial cell layer capable of facilitating the passage not only of monocytes across the BBB during inflammation, but also that of tumor cells (Pan et al. 2011; Qiu et al. 2021).

RANTES, also known as CCL5, is a chemokine that may have an important role in the survival and migration of tumor cells across the BBB, as when coupled with its GPCR CCR5 receptor, it activates the pro-tumor PI3K/Akt pathway and induces the production of MMP to remodel the extracellular matrix of endothelial cells in melanoma metastasis (Liu et al. 2019).

This led us to conclude that the hicBBB seems to be an appropriate model to study the early stages of BBB invasion *in vitro*. Accurate titration of the different growth factors, enzymes

and cytokines would certainly help in gaining insight into the microenvironment of a metastatic invasion event.

1.4. STUDY OF EARLY STAGE INVASION OF THE hicBBB BY TUMOR CELLS

Following the validation of the suitability of the hicBBB *in vitro* model to the study of the early stages of the BBB invasion, the next step involved a pilot project that investigated the invasion at a genetic level, of the model by BRAFi and BRAFi-coupled MEKi resistant and non-resistant A375 melanoma cells (In et al. 2020). For this purpose, we sorted the cells of the hicBBB model astrocyte layer to isolate melanoma cells that were positive for mCherry or deep red tracer. In order to keep the genetic materials of the cells that crossed, a sorting using a *RNAlater*[™] has a sorting solution will maybe greatly improves the quality of the genetic material collected during the RNA extraction steps (Loontjens et al. 2019).

We then analyzed the sorted cells by 3' RNA-Seq, in an attempt to avoid degradation of the genetic material artefacts. When we then examined the clustering using PCA, we found that the hicBBB appears to induce a specific change in tumor cell expression (Luebker and Koepsell 2019; Kakadia et al. 2018).

1.5. hicBBB MODEL – CONCLUSION AND OUTLOOK

Altogether, the results presented in this chapter have led us to conclude that we have succeeded in creating an *in vitro* model suitable for the study of the early invasion of the BBB by tumor cells. We have succeeded, to a certain extent, in the endeavor to replicate the mechanism of invasion of the brain by melanoma metastases, which we have witnessed crossing the BBB.

We created an *in vitro* model using an immortalized human cell line, which we successively tested for stability by measuring its TEER using CellZscope 2 and by measuring its permeability using a tracer consisting of a fluorochrome coupled to a dextran molecule with a weight of 3kD in total. Upon completion of these steps and validation of the stability of the hicBBB model, we exposed it to the A375 mCherry melanoma cell line. At this stage, our main objective was to establish whether or not A375 cells were able to cross the hicBBB model, for this purpose we imaged the model membrane using confocal microscopy and were able to observe that the melanoma cells took an average of 48 hours to cross the cell barrier in the absence of a chemoattractant gradient. This could mean that the cells were prone to invade the model. We may therefore conjecture that the presence of fibronectin and growth factors is the cause (Banerji et al. 2008) . Indeed, the latter play a role in facilitating the transport and anchoring of tumor cells during their transit through the BBB *in vitro*. In addition, during this phase of the experiment, we collected the conditioned medium to which we exposed different ELISA-based antibody arrays in order to detect potential growth factors, cytokines and enzymes. This experiment must be repeated several times to confirm the presence of specific molecules and followed by the subsequent exact titration of the latter; we have nevertheless observed the presence of TIMP, GRO and IL-8, all molecules known to play a role in the metastasis process.

Subsequently, we implemented a pilot study using the hicBBB model to establish whether it can be used to observe possible differences in gene expression between the cells that cross the hicBBB and the control cells. Hence, we isolated three types of fluorescent A375 BRAFi and MEKi-coupled BRAFi resistant and non-resistant melanoma cells lines that crossed the hicBBB using enzymatic dissociation coupled with gentle mechanical dissociation and FACS sorting. During FACS sorting, we observed that the amount of A375 BRAFi cells was significantly higher than the amount of A375 MEKi-coupled BRAFi cells. Finally, we sent the collected cells to LuxGen and performed a 3' RNA-Seq to determine if we could process the genetic material acquired using our dissociation protocol and distinguish between migrating and non-migrating A375 cells. The 3' RNA-Seq did not allow us to discriminate between resistant and non-resistant A375 cells, however, we were able to discriminate between cells that migrated through the hicBBB model and cells that did not migrate through it. The cluster of migrated cells we observe in the PCA could be induced by FACS sorting, therefore no

definitive conclusion can be drawn on the overall results obtained using 3' RNA-Seq. In order to address this concern, it may be envisaged to sort control cells by FACs.

A next step in the exploitation of this model could be the analysis of the gene expression of the different BBB actors in order to elucidate whether the presence and passage of resistant and non-resistant A375 cell lines can induce alterations.

To take the study further, the following additions are envisageable: analyze proteins from the cell-cell contact between tumor cells and hicBBB cells; use either iPSC-derived cells or primary cells to form the BBB to circumvent the limitations of the endothelial cell line; investigate what the presence of tumor cells generates on the cells constituting the BBB; use of alternative tumor cell types known to metastasize to the brain, such as breast cancer and lung cancer, could also be envisaged to investigate early BBB invasion.

2. IN VIVO MODEL OF EARLY BRAIN INVASION OF BLOOD-BRAIN BARRIER

2.1. TRAINING FOR MODEL EXPLOITATION

To create an *in vivo* model of the hematogenous spread process of metastases into the brain, we had to organize our work into different steps (Chambers et al. 2001; Miarka and Valiente 2021; Daphu et al. 2013).

First, we had to find a way to inject the tumor cells into the cerebral vasculature of a mouse, preventing them from getting stuck in other organs and never reaching the brain. For this specific reason, it was necessary to identify the injection site that was most proximal to the cerebral vasculature. Two alternatives were possible: an intracarotid injection or an intracardiac injection of the left heart ventricle. Both of these alternatives involve advantages as well as disadvantages.

With an intracarotid injection, the entire volume of the injection reaches the brain. Nevertheless, this is a high-risk procedure, as it requires the animal to be cut open. During this surgical intervention, a lesion of the carotid artery could quickly lead to the loss of the animal, in addition, the post-operative period is cumbersome and requires additional precautions in the care of the rodents (Zhang et al. 2017) .

Unlike intracarotid injection, intracardiac injection of the left ventricle does not require open surgery, which makes it much less invasive and less burdensome from a postoperative point of view. The major disadvantage of this type of injection, which also makes it technically difficult, is that it is performed without a direct view of the heart. This has a considerable impact on the chances of success when the injections are administered by an inexperienced technician. During the intracardiac injection of the left ventricle, part of the injected volume gets lost because when the left ventricle ejects blood, the latter goes into the different branches of the aortic arch, namely the brachiocephalic trunk, the left common carotid artery and the left subclavian artery (Prendiville et al. 2014; Poggioli et al. 2014) .

After taking into consideration the respective limitations of the two injection techniques, we opted for the use of the intracardiac injection. We had to practice in order to acquire the necessary technical skills to puncture the small left ventricle of a mouse heart and thus be able to replicate the experiment conducted by Edwin Goldmann.

2.2. INJECTION OF A375 CELLS AND DETECTION OF THEIR FLUORESCENT SIGNAL IN THE BRAIN

Following the achievement of our training, we injected nude mice with 5×10^5 A375 mCherry cells (Zhou and Zhao 2014) . Then, we harvested the brain tissue every day for 10 days and subsequently fixed it. Once this step was completed, we sliced the brain into 100 μm thick coronal sections with a vibratome, all in order to localize the mCherry protein signal with the help of an antibody directed against it. A double staining, which allowed us to rely on two fluorescent signals to localize potential sites of early BBB invasion. The latter sites were difficult to locate as we encountered a number of limitations related to the mCherry protein signal after fixation. These may have been due to the fixative that combines formaldehyde and glutaraldehyde, which is used in electron microscopy to ensure optimal preservation of tissue structures. In the images where we suspect the presence of A375 fluorescent cells, the observed signal seems to be an artifact because we are not able to discern a nucleus and its size is too small to originate from a whole cell. Nevertheless, it may be possible that due to the serial cutting, we are not able to see the whole cell. Indeed, the image that we observe is in 2D whereas the sample is a 3D structure, it is therefore possible that the information has been lost or not seized because fragmented.

Furthermore, the markers used to identify A375 cells seem to be an additional parameter that deserves consideration. Indeed, we encountered difficulties because the only markers that were available to us were either nonspecific when used to label brain tissue or incompatible with the tissue itself. One potential solution to the screening method issue might be to conduct the experiment again using a melanoma cell line that expresses melanin. This alternative approach would allow the use of melanoma-specific markers such as HMB45 or MelanA (Weinstein et al. 2014) .

Another way to circumvent the limitations of the fixation process on the screening method would be to slice the brain using a cutting matrix, immediately after harvesting and before fixation. Ideally, this modification in the protocol would make it possible to observe the fluorescent signal of the mCherry protein expressed by A375 cells.

Additionally, the barcoding of A375 cells for single cell tracking across the BBB and into the brain parenchyma could be considered to overcome the limitations of fluorescent cell tracking.

2.3. IN VIVO MODEL – CONCLUSION AND OUTLOOK

In fine, our objective was to establish an *in vivo* model in order to identify potential sites of early BBB invasion and thus take the first step towards understanding the mechanisms at play when tumor cells succeed in breaching the blood-brain barrier to reach the brain parenchyma.

Ten days after the injection of A375 cells, under EM we were able to observe multiple spots in the brain parenchyma containing artifacts that have the same appearance as melanosomes. The results obtained and presented in this work are indeed primitive and preliminary to what is required for a sustainable and evolutionary implementation of protocols, but we hope that they can lead to additional advances in the future (Herman et al. 2019; Fazakas et al. 2011).

To take our experiment a step further, a future phase could be to study the early invasion mechanism of the BBB using laser microdissection coupled with mass spectrometry. Using laser microdissection, it would be possible to isolate the cell-cell contact between the tumor cells and the different actors of the BBB. The mass spectrometer would then be used to analyze the content of the harvested sample for anchoring proteins, such as integrins, selectins and cadherins (Schey et al. 2013; Ogiso et al. 2022) .

To go even further, the combined use of focused ion beams coupled to a scanning electron microscope (FIB-SEM) after having isolated the cell-cell contact could be considered in order to remove unwanted artifacts. Nanoscale secondary ion mass spectrometry (NanoSIMS)

could then be used as a means of analyzing the elements that make up the cell-cell contact (Nuñez et al. 2017; Carpenter et al. 2013).

PART V. APPENDIX

1. DETAILS OF THE MEDIA COMPOSITION

Dulbecco's Modified Eagle's Medium (DMEM)

Description	CAS #	Chemical Formula	Concentration		Molarity	
			g/L	mg/L	mM	uM
Calcium Chloride Anhydrous	10043-52-4	CaCl ₂	0.200	200.000	1.802	1.802E+03
Dextrose	50-99-7	C ₆ H ₁₂ O ₆	4.500	4.500E+03	24.978	2.498E+04
Ferric Nitrate Nonahydrate	7782-61-8	Fe(NO ₃) ₃ • 9H ₂ O	1.000E-04	0.100	2.475E-04	0.248
Magnesium Sulfate Anhydrous	7487-88-9	MgSO ₄	0.098	97.670	0.811	811.415
Potassium Chloride	7447-40-7	KCl	0.400	400.000	5.366	5.366E+03
Sodium Bicarbonate	144-55-8	NaHCO ₃	3.700	3.700E+03	44.042	4.404E+04
Sodium Chloride	7647-14-5	NaCl	6.400	6.400E+03	109.514	1.095E+05
L-Arginine Monohydrochloride	1119-34-2	C ₆ H ₁₄ N ₄ O ₂ • HCl	0.084	84.000	0.399	398.747
L-Glutamine	56-85-9	C ₅ H ₁₀ N ₂ O ₃	0.584	584.000	3.996	3.996E+03
Glycine	56-40-6	HO ₂ CCH ₂ NH ₂	0.030	30.000	0.400	399.627
L-Histidine Monohydrochloride Monohydrate	5934-29-2	C ₆ H ₉ N ₃ O ₂ • HCl • H ₂ O	0.042	42.000	0.200	200.382
L-Isoleucine	73-32-5	HO ₂ CCH(NH ₂)CH(CH ₃)CH ₂ CH ₃	0.105	104.800	0.799	798.963
L-Leucine	61-90-5	HO ₂ CCH(NH ₂)CH ₂ CH(CH ₃) ₂	0.105	104.800	0.799	798.963
L-Lysine Monohydrochloride	657-27-2	C ₆ H ₁₄ N ₂ O ₂ • HCl	0.146	146.200	0.800	800.438
L-Methionine	63-68-3	HO ₂ CCH(NH ₂)CH ₂ CH ₂ SCH ₃	0.030	30.000	0.201	201.072
L-Phenylalanine	63-91-2	HO ₂ CCH(NH ₂)CH ₂ C ₆ H ₅	0.066	66.000	0.400	399.540
L-Serine	56-45-1	HO ₂ CCH(NH ₂)CH ₂ OH	0.042	42.000	0.400	399.657
L-Threonine	72-19-5	HO ₂ CCH(NH ₂)CH(OH)CH ₃	0.095	95.200	0.799	799.194
L-Tryptophan	73-22-3	C ₁₁ H ₁₂ N ₂ O ₂	0.016	16.000	0.078	78.343
L-Valine	72-18-4	HO ₂ CCH(NH ₂)CH(CH ₃) ₂	0.094	93.600	0.799	799.317
D-Calcium Pantothenate (Vitamin B5)	137-08-6	C ₁₈ H ₃₂ CaN ₂ O ₁₀	4.000E-03	4.000	8.394E-03	8.394
Choline Chloride	67-48-1	HOCH ₂ CH ₂ N(CH ₃) ₃ Cl	4.000E-03	4.000	0.029	28.647
Folic Acid	59-30-3	C ₁₉ H ₁₉ N ₇ O ₆	4.000E-03	4.000	9.062E-03	9.062
D-Inositol	87-89-8	C ₆ H ₁₂ O ₆	7.000E-03	7.000	0.039	38.846
Niacinamide (Nicotinamide)	98-92-0	C ₆ H ₆ N ₂ O	4.000E-03	4.000	0.033	32.757
Pyridoxine Monohydrochloride	58-56-0	C ₈ H ₁₁ N ₃ O	4.000E-03	4.000	0.019	19.455
Riboflavin (Vitamin B2)	83-88-5	C ₁₇ H ₂₀ N ₄ O ₆	4.000E-04	0.400	1.063E-03	1.063
Thiamine Monohydrochloride (Vitamin B1)	67-03-8	C ₁₂ H ₁₈ N ₄ O ₄ S	4.000E-03	4.000	0.012	11.859
Phenol Red	34487-61-1	C ₁₉ H ₁₄ O ₅ S	0.015	15.000	0.040	39.851
Pyruvic Acid Sodium Salt	113-24-6	CH ₃ COCO ₂ Na	0.110	110.000	1.000	999.636
L-Tyrosine Disodium Salt, Dihydrate	122666-78-9	C ₉ H ₉ NO ₃ Na ₂ • 2H ₂ O	0.104	103.790	0.397	397.374
L-Cystine Dihydrochloride	30925-07-6	C ₆ H ₁₂ N ₂ O ₄ S ₂ •2HCl	0.063	62.580	0.200	199.808
Sodium Phosphate Monobasic, Anhydrous	7558-80-7	NaH ₂ PO ₄	0.109	108.690	0.906	905.750

Endothelial Cell Medium

EGM™-2 BulletKit™ Medium (CC-3162), No BBE (Bovine Brain Extract), hEGF, Hydrocortisone, GA-1000 (Gentamicin, Amphotericin-B), FBS (Fetal Bovine Serum) 10 ml, VEGF, hFGF-B, R3-IGF-1, Ascorbic Acid, Heparin

Pericytes Medium

PM consists of 500 ml of basal medium, 10 ml of FBS (Cat. #0010), 5 ml of Pericyte Growth Supplement (PGS, Cat. #1252) and 5 ml of penicillin/streptomycin solution (P/S, Cat. #0503).

2. ANTIBODY ARRAY DETAILS

	A	B	C	D	E	F	G	H
1	Pos	Pos	Neg	Neg	MMP-1	MMP-2	MMP-3	MMP-8
2	Pos	Pos	Neg	Neg	MMP-1	MMP-2	MMP-3	MMP-8
3	MMP-9	MMP-10	MMP-13	TIMP-1	TIMP-2	TIMP-4	Neg	Pos
4	MMP-9	MMP-10	MMP-13	TIMP-1	TIMP-2	TIMP-4	Neg	Pos

Table 6 ab134004 Human MMP Antibody Array - Membrane (10 targets)

	A	B	C	D	E
1	Pos	Pos	Pos	Pos	Neg
2	I-309	IL-1 α	IL-1 β	IL-2	IL-3
3	IL-12 p40/p70	IL-13	IL-15	IFN- γ	MCP-1
4	MIP-1 δ	RANTES	SCF	SDF-1	TARC
5	Oncostatin M	Thrombopoietin	VEGF	PDGF-BB	Leptin
6	FGF-4	FGF-6	FGF-7	FGF-9	Flt-3 Ligand
7	IGFBP-3	IGFBP-4	IL-16	IP-10	LIF
8	NT-4	Osteopontin	Osteoprotegerin	PARC	PIGF

	F	G	H	I	J	K
1	Neg	ENA-78	GCSF	GM-CSF	GRO	GRO- α
2	IL-4	IL-5	IL-6	IL-7	IL-8	IL-10
3	MCP-2	MCP-3	MCSF	MDC	MIG	MIP-1b
4	TGF- β 1	TNF- α	TNF- β	EGF	IGF-I	Angiogenin
5	BDNF	BLC	Ck β 8-1	Eotaxin	Eotaxin-2	Eotaxin-3
6	Fractalkine	GCP-2	GDNF	HGF	IGFBP-1	IGFBP-2
7	LIGHT	MCP-4	MIF	MIP-3 α	NAP-2	NT-3
8	TGF- β 2	TGF- β 3	TIMP-1	TIMP-2	Pos	Pos

Table 7 ab133998 Human Cytokine Antibody Array Membrane (80 targets)

A	B	C	D	E	F	G	H
POS	POS	NEG	NEG	Angiogenin	EGF	ENA-78	b FGF

POS	POS	NEG	NEG	Angiogenin	EGF	ENA-78	b FGF
GRO	IFN- γ	IGF-I	IL-6	IL-8	LEPTIN	MCP-1	PDGF-BB
GRO	IFN- γ	IGF-I	IL-6	IL-8	LEPTIN	MCP-1	PDGF-BB
PIGF	RANTES	TGF- β 1	TIMP-1	TIMP-2	Thrombopoietin	VEGF	VEGF-D
PIGF	RANTES	TGF- β 1	TIMP-1	TIMP-2	Thrombopoietin	VEGF	VEGF-D
BLANK	BLANK	BLANK	BLANK	BLANK	BLANK	NEG	POS
BLANK	BLANK	BLANK	BLANK	BLANK	BLANK	NEG	POS

Table 8 ab134000 Human Angiogenesis Antibody Array - Membrane (20 targets)

	A	B	C	D	E	F	G	H
1	Pos	Pos	Neg	Neg	Akt (pS473)	CREB (pS133)	ERK1 (pT202/Y204)	GSK3a (pS21)
2								
3	GSK3b (pS9)	HSP27 (pS82)	JNK (pT183)	MEK (pS217/221)	MKK3 (pS189)	MKK6 (pS207)	MSK2 (pS360)	mTOR (pS2448)
4								
5	P38 (pT180/Y182)	p53 (pS15)	P70S6K (pT421/S424)	RSK1 (pS380)	RSK2 (pS386)	Neg	Neg	Pos
6								

Table 9 ab211061 Human MAPK Phosphorylation Antibody Array (Membrane 17 Targets)

*Each antibody is spotted in duplicate vertically

3. INVASION POTENTIAL OF THE hicBBB CELL LINES

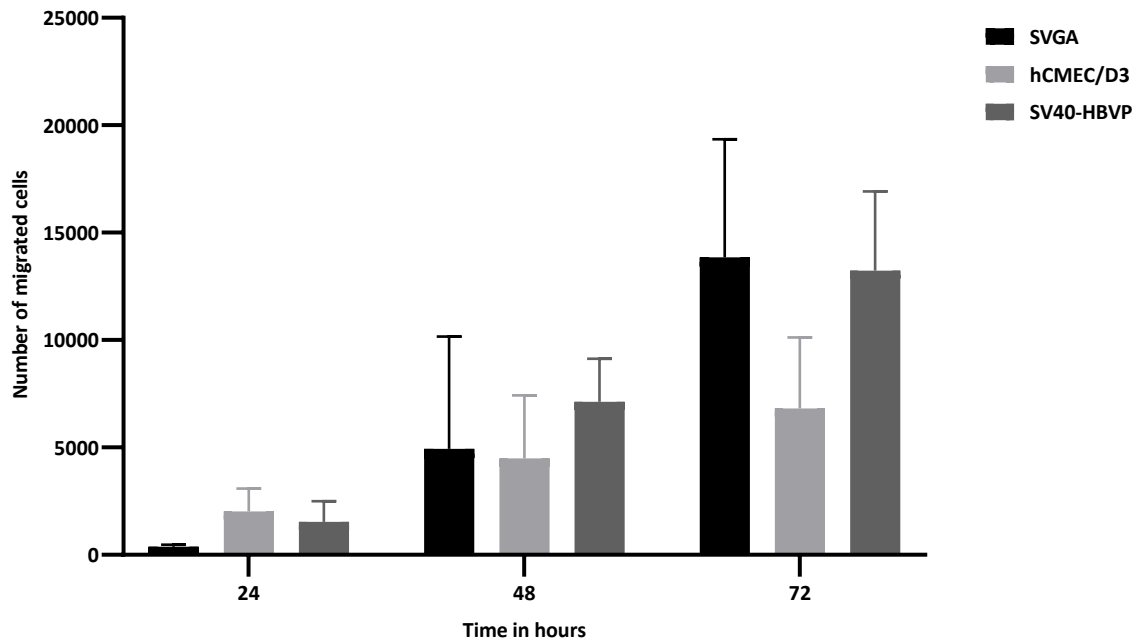


Figure 47 Invasion potential of the hicBBB cell lines

Invasion potential of the hicBBB cell lines on a PLL+FN coated membrane over 72 hours. Error bars represent SD.

4. MEAN VALUES OF TEER MEASUREMENTS DURING 72 HOURS OF COCULTURE

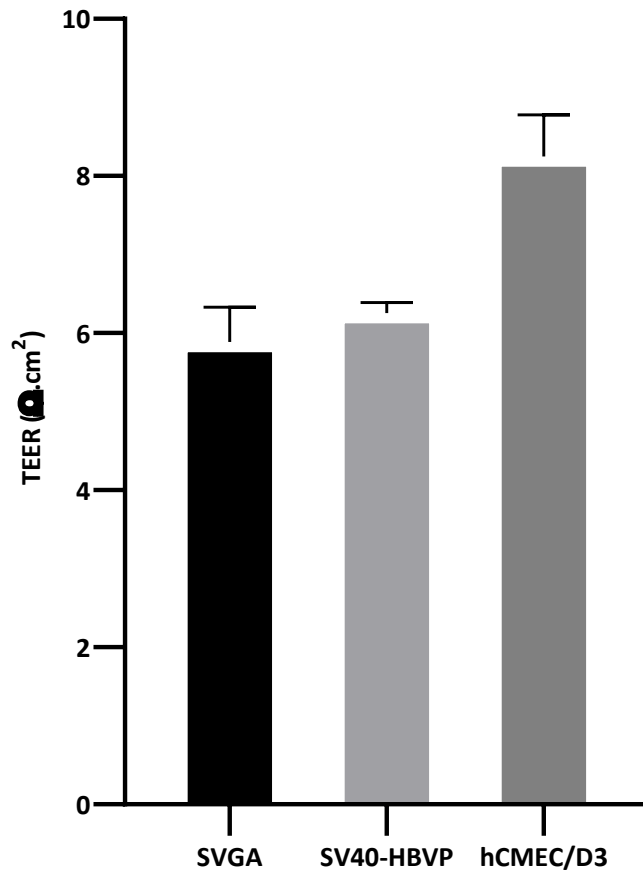


Figure 48 Mean values of TEER measurements during 72 hours of coculture

Mean values of TEER measurements of SVGA monoculture on membrane, SVGA+SV40-HBVP coculture and SVGA+SV40-HBVP+hCMEC/D3 triple coculture. Error bars represent SD.

5. EFFECT OF TNF α ON TEER

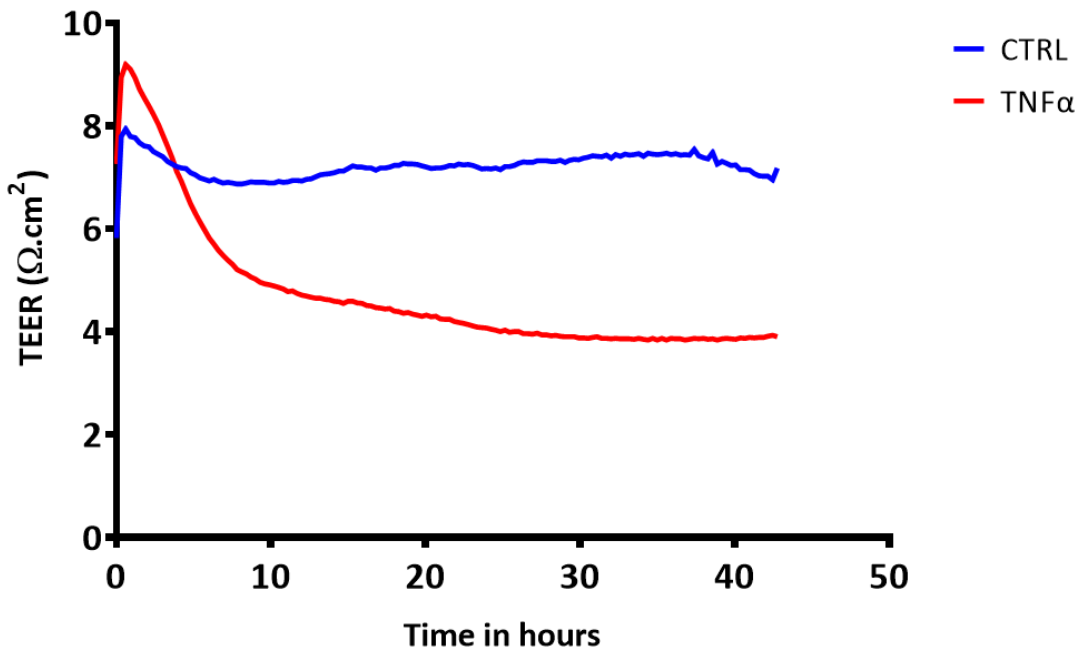


Figure 49 Disruption of hicBBB by TNFα
Impact of TNFα on the TEER of the hicBBB *in vitro* model.

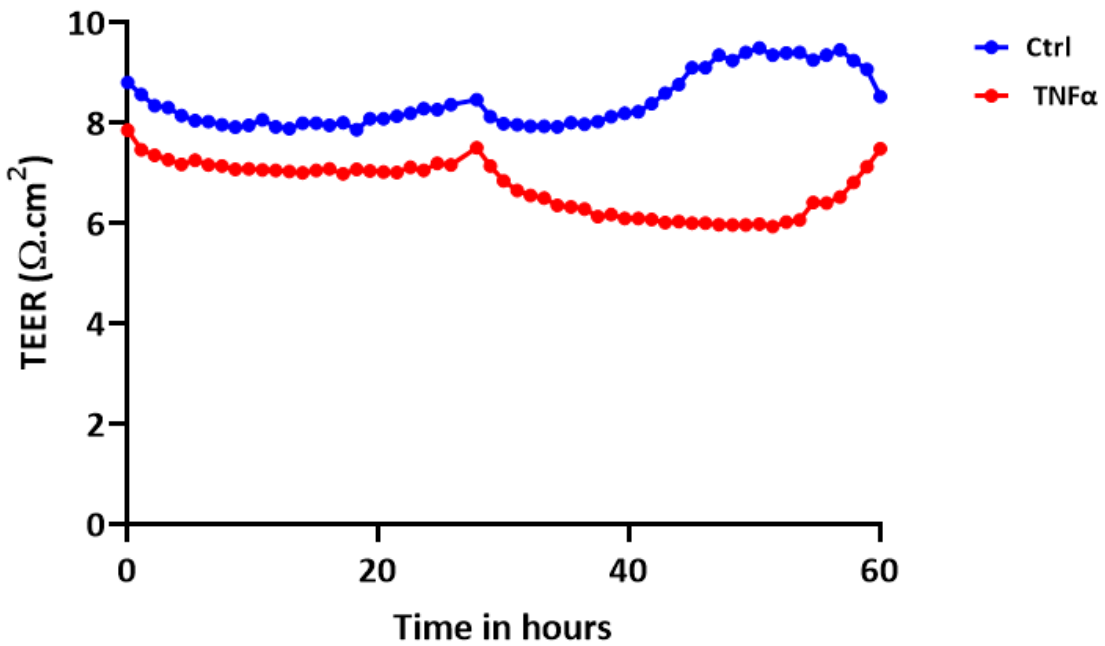


Figure 50 Disruption of hCMEC/D3 and SVGA coculture by TNFα
Impact of TNFα on the TEER of the hCMEC/D3 and SVGA coculture.

6. SAMPLES QC REPORT FOR 3' END mRNA-SEQUENCING

Dudelange, 05.09.2022

Name LIH, Luxembourg Center of Neuropathology Department of Cancer Research

Address 6, Rue Nicolas-Ernest Barblé City L-1210 Luxembourg

Country Luxembourg

Contact Name Rédouane Slimani / M. Mittelbronn

Samples QC Report for 3' end mRNA-Sequencing

1) Sample Processing Information

Species	Human
Number of Sample	13
Type of Sample	Total RNA extracted from Cells sorted in Versen + DMEM
Reception Date	16.08.2022
Library Processing	Poly(A) selection
Kit Used	Lexogen QuantSeq 3' mRNA-Seq Library Prep Kit FWD for Illumina
Add on Kit	UMI Second Strand Synthesis Module for QuantSeq FWD Lexogen i5 6 nt Unique Dual Indexing Add-on Kit (5001-5096)
Protocol	QUANT™ SEQ 3' mRNA-Seq Library Prep Kit User Guide 015UG009V0260

2) 3' end mRNA Library Processing

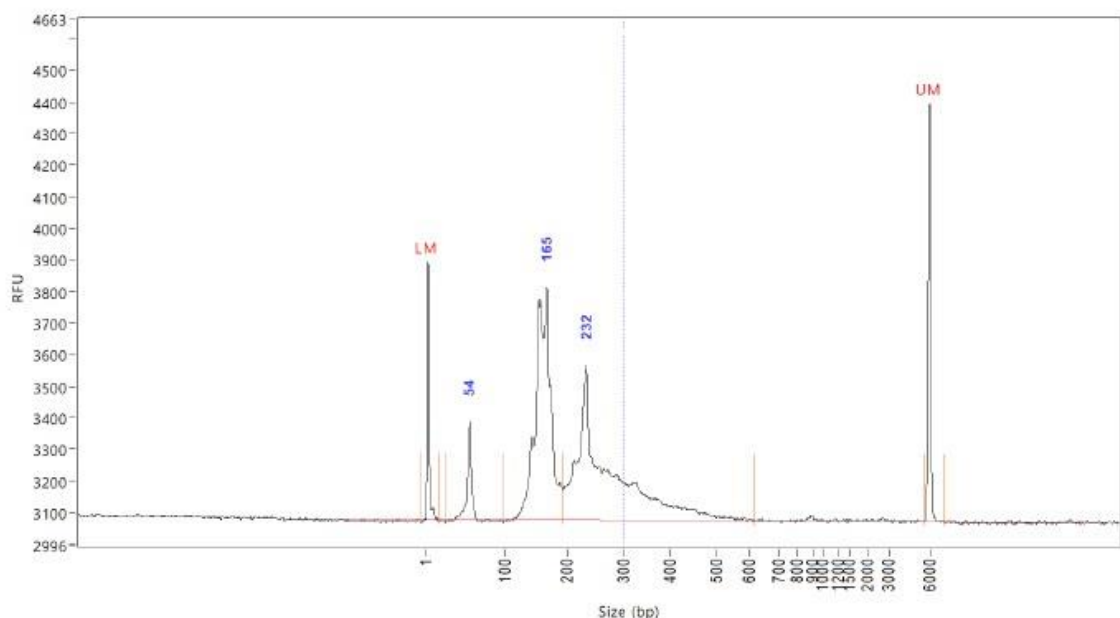
	QB hsRNA (ng/ul)	FA- hsRNA (ng/ul)	Input (ng)	i7 index	i7 Sequence	i5 index	i5 Sequence	Nb cycles	QB HS- dsDNA (ng/ul)	FA %primer	FA %dimer	FA %library	FA Avg Size (bp)
A375 CTRL1	259,2		1,2	7081	GCAGCC	5081	TATCAA	23	1,22	5,7	45,2	49,1	282
A375 CTRL2	588		1,2	7082	ACTCTT	5082	CGTGCT	23	1,61	1,5	28,3	70,3	321
A375 CTRL3	758,8		1,2	7083	TGCTAT	5083	GCGATC	23	2,1	0,6	39,5	59,9	272
M CTRL1	61		1,2	7084	AAGTGG	5084	GCATGC	23	2,28	0,8	24,2	75	259
M CTRL2	153		1,2	7085	CTCATA	5085	GAGGAA	23	2,53	0,4	20,5	79	276
M CTRL3		0,84	1,2	7086	CCGACC	5086	ATATAC	23	2,2	0,4	36	63,6	248
M2+		0,14	1,13	7089	CGCGGA	5089	CGGAGT	23	2,79	0,7	69,9	29,4	294

A375 wt mCherry	1,01	1,2	7090	CCTGCT	5090	TCCAGC	23	1,89	1,5	67	31,5	265
A375 wt tracer	0,75	1,2	7091	GCGCTG	5091	GGGTAG	23	3,45	2	37,5	60,4	252
A375 DR sample 2	0,65	1,2	7092	GAACCT	5092	AGATCG	23	2,34	0,9	47,1	52	262
A375 DR sample 3	0,15	1,2	7093	TTCGAG	5093	GCAGTA	23	3,61	0,7	47	52,3	268
A375 ER sample 2	2,37	1,2	7094	AGAATC	5094	GCCGGG	23	2,75	0,4	25,6	74,1	289
A375 ER sample 3	0,03	0,225	7095	AGGCAT	5095	AGTCAC	23	2,98	1,3	69,3	29,5	245

Sample: A375 ctrl1 E1

Well location: B1

Created: mardi, 27 septembre 2022 11:27:20



Electropherogram obtained for 1 library. It shows a high proportion of primer dimers (165bp fragment) which can interfere with library sequencing. As all libraries have a high proportion of primer dimers, all of them were repurified to remove a maximum of linker-linker artifacts.

3) 3' end mRNA Library Repurification

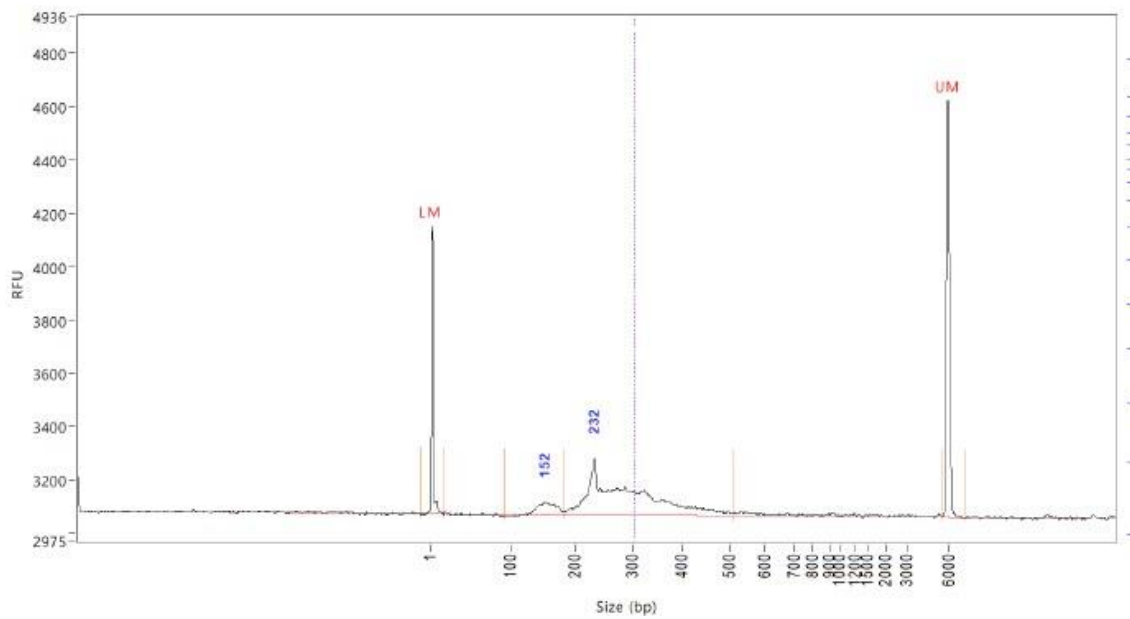
	qubit HS-dsDNA ng/ul	FA %dimer	FA %library	FA AvgSize lib	QB nM total
--	----------------------	-----------	-------------	----------------	-------------

A375 CTRL1	0,344	11,3	88,7	296	1,76
A375 CTRL2	0,503	5,0	95,0	342	2,23
A375 CTRL3	0,261	10,5	89,5	286	1,38
M CTRL1	0,114	0,0	100,0	264	0,65
M CTRL2	0,258	0,0	100,0	286	1,37
M CTRL3	0,526	13,5	86,5	263	3,03
M2+	0,435	30,4	69,6	331	1,99
A375 wt mCherry	0,081	41,5	58,5	253	0,49
A375 wt tracer	0,897	9,5	90,5	271	5,02
A375 DR sample 2	0,482	24,9	75,1	279	2,62
A375 DR sample 3	0,615	29,1	70,9	275	3,39
A375 ER sample 2	0,699	7,4	92,6	321	3,30
A375 ER sample 3	0,523	35,7	64,3	276	2,87

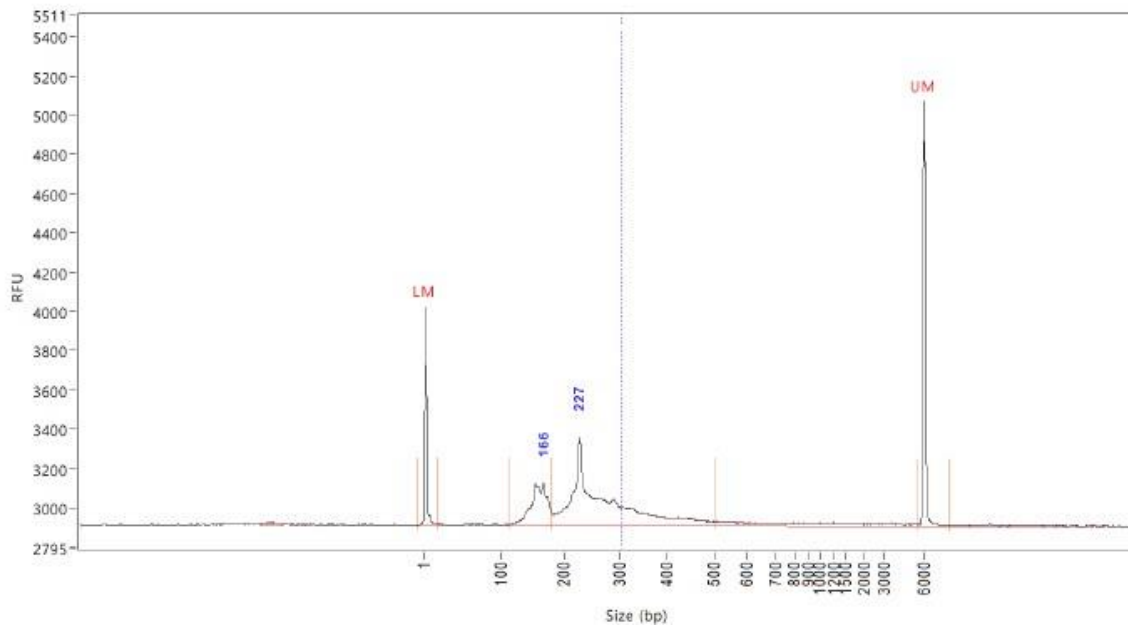
Sample: A375 ctrl1 G1

Well location: D1

Created: mercredi, 28 septembre 2022 14:17:53



Sample: A375 DR 2 H4
Well location: E4
Created: mercredi, 28 septembre 2022 15:24:24



Electropherogram obtained for 2 libraries after a second purification. It shows a decrease of the proportion of primer dimers. In 5 samples the primer dimers proportion is still high.

4) Library preparation Conclusion

For the library preparation, we adjusted the RNA input to the lowest sample quantity (1,2ng) except for sample A375 ER sample 3 which contained only 225pg of total RNA.

All libraries contained a high amount of dimers and have to be re-purified.

Despite a second round of purification the amount of primer-dimers decreased but remains high for 5 samples.

Among the 13 libraries prepared with UMI and dual indexing, 4 have a weak concentration and it was necessary to concentrate them before pooling all libraries prepared.

The 13 libraries were sequenced on a NovaSeq using 150bp single-end criteria.

5) Sequencing general statistics

This project includes 13 samples (NovaSeq – FC S1 200 RunID: 220930_A01275_0070_AHT7KTDRXY):

Sample Name	M Seqs
RS1-A375_CTRL1_S61_R1_001	20.1
RS10-A375_DR_sample_2_S70_R1_001	33.1
RS11-A375_DR_sample_3_S71_R1_001	29.2
RS12-A375_ER_sample_2_S72_R1_001	25.5
RS13-A375_ER_sample_3_S73_R1_001	37.3
RS2-A375_CTRL2_S62_R1_001	25.7
RS3-A375_CTRL3_S63_R1_001	23.5
RS4-M_CTRL1_S64_R1_001	13.6
RS5-M_CTRL2_S65_R1_001	23.1
RS6-M_CTRL3_S66_R1_001	26.1
RS7-M2_S67_R1_001	65.5
RS8-A375_wt_mCherry_S68_R1_001	30.2
RS9-A375_wt_tracer_S69_R1_001	25.5

6) Base quality along the read

In figure 1, the lines represent the mean quality at each position.

The y-axis shows the quality scores. The higher the score, the better the base call. The background of the graph divides the y-axis into very good quality scores (green), scores of reasonable quality (orange), and reads of poor quality (red).

It is normal with all Illumina sequencers for the mean quality score to start out lower over the first 5-7 bases and to then rise. The quality of reads on most platforms will drop at the end of the read. This is often due to signal decay or phasing during the sequencing run.

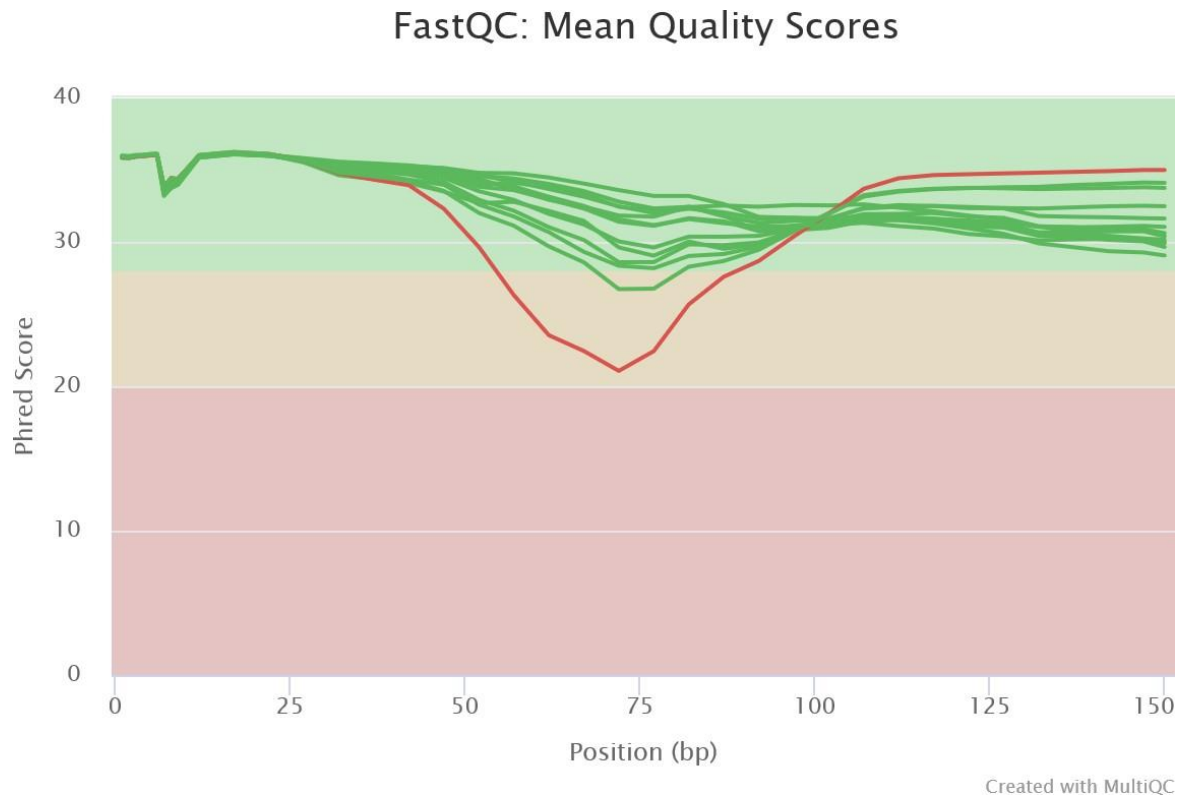


Figure 1: Per base sequence quality

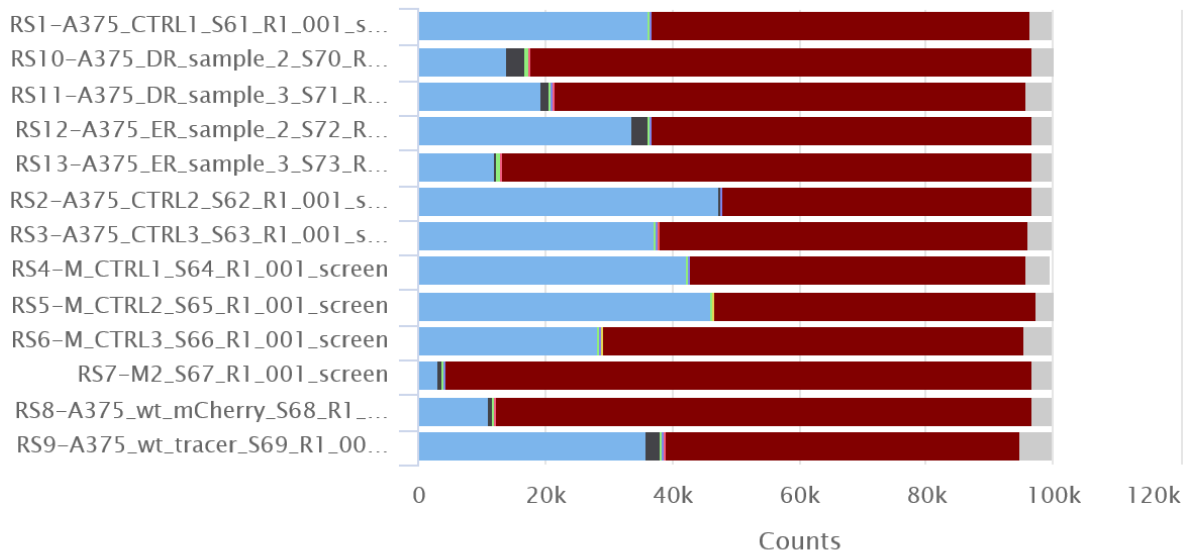
The red quality profiles corresponds to the sample RS7-M2_S67_R1_001 and it should be used with care for further analysis.

7) Contamination from other organisms

FastQ Screen allows you to screen a library of sequences in FastQ format against a set of sequence databases so you can see if the composition of the library matches with what you expect.

In figure 2 the samples match Human genomes as expected.

FastQ Screen: Mapped Reads



- Human
- Mouse
- Rat
- PhiX
- Arabidopsis
- Adapters
- Worm
- Vectors
- Drosophila
- Yeast
- Ecoli
- Multiple Genomes
- No hits

Created with MultiQC

VI. REFERENCES

Publication bibliography

Abaurrea, Andrea; Araujo, Angela M.; Caffarel, Maria M. (2021): The Role of the IL-6 Cytokine Family in Epithelial-Mesenchymal Plasticity in Cancer Progression. In *International journal of molecular sciences* 22 (15). DOI: 10.3390/ijms22158334.

Abbott, N. Joan; Patabendige, Adjanie A. K.; Dolman, Diana E. M.; Yusof, Siti R.; Begley, David J. (2010): Structure and function of the blood-brain barrier. In *Neurobiology of disease* 37 (1), pp. 13–25. DOI: 10.1016/j.nbd.2009.07.030.

Abbott, N. Joan; Rönnbäck, Lars; Hansson, Elisabeth (2006): Astrocyte–endothelial interactions at the blood–brain barrier. In *Nature Reviews Neuroscience* 7 (1), pp. 41–53. DOI: 10.1038/nrn1824.

Abbruscato, Thomas J.; Lopez, Steve P.; Mark, Karen S.; Hawkins, Brian T.; Davis, Thomas P. (2002): Nicotine and Cotinine Modulate Cerebral Microvascular Permeability and Protein Expression of ZO-1 through Nicotinic Acetylcholine Receptors Expressed on Brain Endothelial Cells. In *Journal of pharmaceutical sciences* 91 (12), pp. 2525–2538. DOI: 10.1002/jps.10256.

Ahluwalia, Manmeet; Metellus, Philippe; Soffiatti, Riccardo (2020): Central Nervous System Metastases. Cham: Springer International Publishing.

Albrechtsen, Reidar; Kveiborg, Marie; Stautz, Dorte; Vikeså, Jonas; Noer, Julie B.; Kotzsh, Alexander et al. (2013): ADAM12 redistributes and activates MMP-14, resulting in gelatin degradation, reduced apoptosis and increased tumor growth. In *Journal of cell science* 126 (20), pp. 4707–4720. DOI: 10.1242/jcs.129510.

Appelt-Menzel, Antje; Cubukova, Alevtina; Günther, Katharina; Edenhofer, Frank; Piontek, Jörg; Krause, Gerd et al. (2017): Establishment of a Human Blood-Brain Barrier Co-culture Model Mimicking the Neurovascular Unit Using Induced Pluri- and Multipotent Stem Cells. In *Stem cell reports* 8 (4), pp. 894–906. DOI: 10.1016/j.stemcr.2017.02.021.

Armulik, Annika; Abramsson, Alexandra; Betsholtz, Christer (2005): Endothelial/pericyte interactions. In *Circulation research* 97 (6), pp. 512–523. DOI: 10.1161/01.RES.0000182903.16652.d7.

Armulik, Annika; Genové, Guillem; Betsholtz, Christer (2011): Pericytes: developmental, physiological, and pathological perspectives, problems, and promises. In *Developmental cell* 21 (2), pp. 193–215. DOI: 10.1016/j.devcel.2011.07.001.

Arora, Rahul D.; Agarwal, Mohit S.; Maani, Elizabeth V.; Cascella, Marco (2022): Palliative Radiation Therapy For Brain Metastases. In : StatPearls. Treasure Island (FL).

Arvanitis, Costas D.; Ferraro, Gino B.; Jain, Rakesh K. (2020): The blood-brain barrier and blood-tumour barrier in brain tumours and metastases. In *Nature reviews. Cancer* 20 (1), pp. 26–41. DOI: 10.1038/s41568-019-0205-x.

Attwell, David; Mishra, Anusha; Hall, Catherine N.; O'Farrell, Fergus M.; Dalkara, Turgay (2016): What is a pericyte? In *Journal of cerebral blood flow and metabolism : official journal of the International Society of Cerebral Blood Flow and Metabolism* 36 (2), pp. 451–455. DOI: 10.1177/0271678X15610340.

Bachir, Alexia I.; Horwitz, Alan Rick; Nelson, W. James; Bianchini, Julie M. (2017): Actin-Based Adhesion Modules Mediate Cell Interactions with the Extracellular Matrix and Neighboring Cells. In *Cold Spring Harbor perspectives in biology* 9 (7). DOI: 10.1101/cshperspect.a023234.

Badaut, Jérôme; Lasbennes, François; Magistretti, Pierre J.; Regli, Luca (2002): Aquaporins in brain: distribution, physiology, and pathophysiology. In *Journal of cerebral blood flow and metabolism : official journal of the International Society of Cerebral Blood Flow and Metabolism* 22 (4), pp. 367–378. DOI: 10.1097/00004647-200204000-00001.

Baeten, Kim M.; Akassoglou, Katerina (2011): Extracellular matrix and matrix receptors in blood-brain barrier formation and stroke. In *Developmental neurobiology* 71 (11), pp. 1018–1039. DOI: 10.1002/dneu.20954.

Ballabh, Praveen; Braun, Alex; Nedergaard, Maiken (2004): The blood-brain barrier: an overview: structure, regulation, and clinical implications. In *Neurobiology of disease* 16 (1), pp. 1–13. DOI: 10.1016/j.nbd.2003.12.016.

Bander, Evan D.; Yuan, Melissa; Carnevale, Joseph A.; Reiner, Anne S.; Panageas, Katherine S.; Postow, Michael A. et al. (2021): Melanoma brain metastasis presentation, treatment, and outcomes in the age of targeted and immunotherapies. In *Cancer* 127 (12), pp. 2062–2073. DOI: 10.1002/cncr.33459.

Banerjee, Jayati; Shi, Yejiao; Azevedo, Helena S. (2016): In vitro blood-brain barrier models for drug research: state-of-the-art and new perspectives on reconstituting these models on artificial basement membrane platforms. In *Drug discovery today* 21 (9), pp. 1367–1386. DOI: 10.1016/j.drudis.2016.05.020.

Banerjee, Swati; Bhat, Manzoor A. (2007): Neuron-glia interactions in blood-brain barrier formation. In *Annual review of neuroscience* 30, pp. 235–258. DOI: 10.1146/annurev.neuro.30.051606.094345.

Banerji, Aniruddha; Das, Shamik; Chatterjee, Amitava (2008): Culture of human A375 melanoma cells in the presence of fibronectin causes expression of MMP-9 and activation of MMP-2 in culture supernatants. In *Journal of environmental pathology, toxicology and oncology : official organ of the International Society for Environmental Toxicology and Cancer* 27 (2), pp. 135–145. DOI: 10.1615/jenvironpatholtoxicoloncol.v27.i2.60.

Barnhill, Raymond L.; Benson, Peter J.; Lugassy, Claire (2009): Conspicuous angiotropism of malignant melanoma involving the brain: implications for extravascular migratory metastasis. In *The American Journal of dermatopathology* 31 (2), pp. 205–208. DOI: 10.1097/DAD.0b013e3181998e95.

Bauer, Katja; Mierke, Claudia; Behrens, Jürgen (2007): Expression profiling reveals genes associated with transendothelial migration of tumor cells: A functional role for $\alpha v \beta 3$ integrin. In *Int. J. Cancer* 121 (9), pp. 1910–1918. DOI: 10.1002/ijc.22879.

Bautch, Victoria L.; James, Jennifer M. (2009): Neurovascular development: The beginning of a beautiful friendship. In *Cell adhesion & migration* 3 (2), pp. 199–204. DOI: 10.4161/cam.3.2.8397.

Bazzoni, G.; Martinez-Estrada, O. M.; Orsenigo, F.; Cordenonsi, M.; Citi, S.; Dejana, E. (2000): Interaction of junctional adhesion molecule with the tight junction components ZO-1, cingulin, and occludin. In *The Journal of biological chemistry* 275 (27), pp. 20520–20526. DOI: 10.1074/jbc.M905251199.

Bazzoni, Gianfranco; Dejana, Elisabetta (2004): Endothelial cell-to-cell junctions: molecular organization and role in vascular homeostasis. In *Physiological reviews* 84 (3), pp. 869–901. DOI: 10.1152/physrev.00035.2003.

Bendayan, Reina; Ronaldson, Patrick T.; Gingras, Diane; Bendayan, Moise (2006): In situ localization of P-glycoprotein (ABCB1) in human and rat brain. In *The journal of histochemistry and cytochemistry : official journal of the Histochemistry Society* 54 (10), pp. 1159–1167. DOI: 10.1369/jhc.5A6870.2006.

Bentolila, Laurent A.; Prakash, Roshini; Mihic-Probst, Daniela; Wadehra, Madhuri; Kleinman, Hynda K.; Carmichael, Thomas S. et al. (2016): Imaging of angiotropism/vascular co-option in a murine model of brain melanoma: implications for melanoma progression along extravascular pathways. In *Scientific reports* 6 (1), pp. 1–11.

Bernatz, Simon; Ilina, Elena I.; Devraj, Kavi; Harter, Patrick N.; Mueller, Klaus; Kleber, Sascha et al. (2019): Impact of Docetaxel on blood-brain barrier function and formation of breast cancer brain metastases. In *Journal of experimental & clinical cancer research : CR* 38 (1), p. 434. DOI: 10.1186/s13046-019-1427-1.

Betz, A. L. (1986): Transport of ions across the blood-brain barrier. In *Federation proceedings* 45 (7), pp. 2050–2054.

Bhalerao, Aditya; Sivandzade, Farzane; Archie, Sabrina Rahman; Chowdhury, Ekram Ahmed; Noorani, Behnam; Cucullo, Luca (2020): In vitro modeling of the neurovascular unit: advances in the field. In *Fluids and barriers of the CNS* 17 (1), p. 22. DOI: 10.1186/s12987-020-00183-7.

Bicker, Joana; Alves, Gilberto; Fortuna, Ana; Falcão, Amílcar (2014): Blood-brain barrier models and their relevance for a successful development of CNS drug delivery systems: a review. In *European journal of pharmaceuticals and biopharmaceutics : official journal of Arbeitsgemeinschaft fur Pharmazeutische Verfahrenstechnik e.V* 87 (3), pp. 409–432. DOI: 10.1016/j.ejpb.2014.03.012.

Birbrair, Alexander; Zhang, Tan; Wang, Zhong-Min; Messi, Maria L.; Mintz, Akiva; Delbono, Osvaldo (2014): Pericytes: multitasking cells in the regeneration of injured, diseased, and aged skeletal muscle. In *Frontiers in aging neuroscience* 6, p. 245. DOI: 10.3389/fnagi.2014.00245.

Boche, D.; Perry, V. H.; Nicoll, J. A. R. (2013): Review: Activation patterns of microglia and their identification in the human brain. In *Neuropathology and applied neurobiology* 39 (1), pp. 3–18. DOI: 10.1111/nan.12011.

Bonkowski, Drew; Katyshev, Vladimir; Balabanov, Roumen D.; Borisov, Andre; Dore-Duffy, Paula (2011): The CNS microvascular pericyte: pericyte-astrocyte crosstalk in the regulation of tissue survival. In *Fluids and barriers of the CNS* 8 (1), p. 8. DOI: 10.1186/2045-8118-8-8.

Bonnans, Caroline; Chou, Jonathan; Werb, Zena (2014): Remodelling the extracellular matrix in development and disease. In *Nature reviews. Molecular cell biology* 15 (12), pp. 786–801. DOI: 10.1038/nrm3904.

Bracalente, Candelaria; Salguero, Noelia; Notcovich, Cintia; Müller, Carolina B.; Da Motta, Leonardo L.; Klamt, Fabio et al. (2016): Reprogramming human A375 amelanotic melanoma cells by catalase overexpression: Reversion or promotion of malignancy by inducing melanogenesis or metastasis. In *Oncotarget* 7 (27), pp. 41142–41153. DOI: 10.18632/oncotarget.9220.

Brahmkhatri, Varsha P.; Prasanna, Chinmayi; Atreya, Hanudatta S. (2015): Insulin-like growth factor system in cancer: novel targeted therapies. In *BioMed research international* 2015, p. 538019. DOI: 10.1155/2015/538019.

Breschi, Gian Luca; Cametti, Massimo; Mastropietro, Alfonso; Librizzi, Laura; Baselli, Giuseppe; Resnati, Giuseppe et al. (2013): Different permeability of potassium salts across the blood-brain barrier follows the Hofmeister series. In *PloS one* 8 (10), e78553. DOI: 10.1371/journal.pone.0078553.

Brown, Lachlan S.; Foster, Catherine G.; Courtney, Jo-Maree; King, Natalie E.; Howells, David W.; Sutherland, Brad A. (2019): Pericytes and Neurovascular Function in the Healthy and Diseased Brain. In *Frontiers in cellular neuroscience* 13, p. 282. DOI: 10.3389/fncel.2019.00282.

Cabezas, Ricardo; Avila, Marcos; Gonzalez, Janneth; El-Bachá, Ramon Santos; Báez, Eliana; García-Segura, Luis Miguel et al. (2014): Astrocytic modulation of blood brain barrier: perspectives on Parkinson's disease. In *Frontiers in cellular neuroscience* 8, p. 211. DOI: 10.3389/fncel.2014.00211.

Capper, David; Preusser, Matthias; Habel, Antje; Sahm, Felix; Ackermann, Ulrike; Schindler, Genevieve et al. (2011): Assessment of BRAF V600E mutation status by immunohistochemistry with a mutation-specific monoclonal antibody. In *Acta neuropathologica* 122 (1), pp. 11–19. DOI: 10.1007/s00401-011-0841-z.

Carpenter, Kevin J.; Weber, Peter K.; Davisson, M. Lee; Pett-Ridge, Jennifer; Haverty, Michael I.; Keeling, Patrick J. (2013): Correlated SEM, FIB-SEM, TEM, and NanoSIMS imaging of microbes from the hindgut of a lower termite: methods for in situ functional and ecological studies of uncultivable microbes. In *Microscopy and microanalysis : the official journal of Microscopy Society of America, Microbeam Analysis Society, Microscopical Society of Canada* 19 (6), pp. 1490–1501. DOI: 10.1017/S1431927613013482.

Carr, Stephanie; Smith, Christy; Wernberg, Jessica (2020): Epidemiology and Risk Factors of Melanoma. In *The Surgical clinics of North America* 100 (1), pp. 1–12. DOI: 10.1016/j.suc.2019.09.005.

Chambers, Ann F.; Groom, Alan C.; MacDonald, Ian C. (2002): Dissemination and growth of cancer cells in metastatic sites. In *Nature Reviews Cancer* 2 (8), pp. 563–572. DOI: 10.1038/nrc865.

Chambers, Ann F.; Naumov, George N.; Varghese, Hemanth J.; Nadkarni, Kishore V.; MacDonald, Ian C.; Groom, Alan C. (2001): Critical Steps in Hematogenous Metastasis: An Overview. In *Surgical Oncology Clinics of North America* 10 (2), pp. 243–255. DOI: 10.1016/S1055-3207(18)30063-2.

Cisternino, Salvatore; Mercier, Claire; Bourasset, Fanchon; Roux, Françoise; Scherrmann, Jean-Michel (2004): Expression, Up-Regulation, and Transport Activity of the Multidrug-Resistance Protein Abcg2 at the Mouse Blood-Brain Barrier. In *Cancer research* 64 (9), pp. 3296–3301. DOI: 10.1158/0008-5472.CAN-03-2033.

Coomber, B. L.; Stewart, P. A. (1985): Morphometric analysis of CNS microvascular endothelium. In *Microvascular research* 30 (1), pp. 99–115. DOI: 10.1016/0026-2862(85)90042-1.

Cordenonsi, Michelangelo; D'Atri, Fabio; Hammar, Eva; Parry, David A.D.; Kendrick-Jones, John; Shore, David; Citi, Sandra (1999): Cingulin Contains Globular and Coiled-Coil Domains and Interacts with Zo-1, Zo-2, Zo-3, and Myosin. In *J Cell Biol* 147 (7), pp. 1569–1582. DOI: 10.1083/jcb.147.7.1569.

Czupalla, Cathrin J.; Liebner, Stefan; Devraj, Kavi (2014): In vitro models of the blood-brain barrier. In *Methods in molecular biology (Clifton, N.J.)* 1135, pp. 415–437. DOI: 10.1007/978-1-4939-0320-7_34.

da Fonseca, Anna Carolina Carvalho; Matias, Diana; Garcia, Celina; Amaral, Rackele; Geraldo, Luiz Henrique; Freitas, Catarina; Lima, Flavia Regina Souza (2014): The impact of microglial activation on blood-brain barrier in brain diseases. In *Frontiers in cellular neuroscience* 8, p. 362. DOI: 10.3389/fncel.2014.00362.

Dalvi, Siddhartha; On, Ngoc; Nguyen, Hieu; Pogorzelec, Michael; W., Donald; M., Grant (2014): The Blood Brain Barrier — Regulation of Fatty Acid and Drug Transport. In Thomas Heinbockel (Ed.): *Neurochemistry*: InTech.

Daneman, Richard; Prat, Alexandre (2015): The blood-brain barrier. In *Cold Spring Harbor perspectives in biology* 7 (1), a020412. DOI: 10.1101/cshperspect.a020412.

Daneman, Richard; Zhou, Lu; Kebede, Amanuel A.; Barres, Ben A. (2010): Pericytes are required for blood-brain barrier integrity during embryogenesis. In *Nature* 468 (7323), pp. 562–566. DOI: 10.1038/nature09513.

Danen, Erik H.J.; Sonneveld, Petra; Brakebusch, Cord; Fässler, Reinhard; Sonnenberg, Arnoud (2002): The fibronectin-binding integrins $\alpha 5\beta 1$ and $\alpha v\beta 3$ differentially modulate RhoA–GTP loading, organization of cell matrix adhesions, and fibronectin fibrillogenesis. In *J Cell Biol* 159 (6), pp. 1071–1086. DOI: 10.1083/jcb.200205014.

Daphu, Inderjit; Sundstrøm, Terje; Horn, Sindre; Huszthy, Peter C.; Niclou, Simone P.; Sakariassen, Per Ø. et al. (2013): In vivo animal models for studying brain metastasis: value and limitations. In *Clinical & experimental metastasis* 30 (5), pp. 695–710. DOI: 10.1007/s10585-013-9566-9.

Daryanani, Deepak; Plukker, John Th; Jong, Mirjam A. de; Haaxma-Reiche, Hannie; Nap, Raoul; Kuiper, Hilde; Hoekstra, Harald J. (2005): Increased incidence of brain metastases in cutaneous head and neck melanoma. In *Melanoma research* 15 (2), pp. 119–124. DOI: 10.1097/00008390-200504000-00006.

Declèves, X.; Regina, A.; Laplanche, J.-L.; Roux, F.; Boval, B.; Launay, J.-M.; Scherrmann, J.-M. (2000): Functional expression of p-glycoprotein and multidrug resistance-associated protein (mrp1) in primary cultures of rat astrocytes. In *J. Neurosci. Res.* 60 (5), pp. 594–601. DOI: 10.1002/(SICI)1097-4547(20000601)60:5<594::AID-JNR4>3.0.CO;2-6.

Dehouck, B.; Dehouck, M. P.; Fruchart, J. C.; Cecchelli, R. (1994): Upregulation of the low density lipoprotein receptor at the blood-brain barrier: intercommunications between brain

capillary endothelial cells and astrocytes. In *J Cell Biol* 126 (2), pp. 465–473. DOI: 10.1083/jcb.126.2.465.

Dejana, Elisabetta; Corada, Monica; Lampugnani, Maria Grazia (1995): Endothelial cell-to-cell junctions. In *The FASEB Journal* 9 (10), pp. 910–918. DOI: 10.1096/fasebj.9.10.7615160.

Del Zoppo, G. J.; Milner, R.; Mabuchi, T.; Hung, S.; Wang, X.; Koziol, J. A. (2006): Vascular matrix adhesion and the blood-brain barrier. In *Biochemical Society transactions* 34 (Pt 6), pp. 1261–1266. DOI: 10.1042/BST0341261.

Deng, Jiangshan; Zhao, Fei; Yu, Xiaoyan; Zhao, Yuwu; Li, Dawei; Shi, Hong; Sun, Yongning (2014): Expression of Aquaporin 4 and Breakdown of the Blood-Brain Barrier after Hypoglycemia-Induced Brain Edema in Rats. In *PloS one* 9 (9), e107022. DOI: 10.1371/journal.pone.0107022.

Devraj, Kavi; Klinger, Marianne E.; Myers, Roland L.; Mokashi, Ashwini; Hawkins, Richard A.; Simpson, Ian A. (2011): GLUT-1 glucose transporters in the blood-brain barrier: differential phosphorylation. In *J. Neurosci. Res.* 89 (12), pp. 1913–1925. DOI: 10.1002/jnr.22738.

Dore-Duffy, Paula; Cleary, Kristen (2011): Morphology and properties of pericytes. In *Methods in molecular biology (Clifton, N.J.)* 686, pp. 49–68. DOI: 10.1007/978-1-60761-938-3_2.

Doyle, D. A.; Morais Cabral, J.; Pfuetzner, R. A.; Kuo, A.; Gulbis, J. M.; Cohen, S. L. et al. (1998): The structure of the potassium channel: molecular basis of K⁺ conduction and selectivity. In *Science (New York, N.Y.)* 280 (5360), pp. 69–77. DOI: 10.1126/science.280.5360.69.

Drioli, Enrico; Giorno, Lidietta (Eds.) (2016): *Encyclopedia of Membranes*. Berlin, Heidelberg: Springer Berlin Heidelberg.

Ebnet, Klaus; Kummer, Daniel; Steinbacher, Tim; Singh, Amrita; Nakayama, Masanori; Matis, Maja (2018): Regulation of cell polarity by cell adhesion receptors. In *Seminars in cell & developmental biology* 81, pp. 2–12. DOI: 10.1016/j.semcd.2017.07.032.

Ebnet, Klaus; Suzuki, Atsushi; Ohno, Shigeo; Vestweber, Dietmar (2004): Junctional adhesion molecules (JAMs): more molecules with dual functions? In *Journal of cell science* 117 (Pt 1), pp. 19–29. DOI: 10.1242/jcs.00930.

Engelhardt, Britta; Sorokin, Lydia (2009): The blood-brain and the blood-cerebrospinal fluid barriers: function and dysfunction. In *Seminars in immunopathology* 31 (4), pp. 497–511. DOI: 10.1007/s00281-009-0177-0.

Erickson, Michelle A.; Wilson, Miranda L.; Banks, William A. (2020): In vitro modeling of blood-brain barrier and interface functions in neuroimmune communication. In *Fluids and barriers of the CNS* 17 (1), p. 26. DOI: 10.1186/s12987-020-00187-3.

Escrig, Anna; Canal, Carla; Sanchis, Paula; Fernández-Gayol, Olaya; Montilla, Alejandro; Comes, Gemma et al. (2019): IL-6 trans-signaling in the brain influences the behavioral and physio-pathological phenotype of the Tg2576 and 3xTgAD mouse models of Alzheimer's disease. In *Brain, Behavior, and Immunity* 82, pp. 145–159. DOI: 10.1016/j.bbi.2019.08.005.

Evani, Shankar J.; Prabhu, Rajesh G.; Gnanaruban, V.; Finol, Ender A.; Ramasubramanian, Anand K. (2013): Monocytes mediate metastatic breast tumor cell adhesion to endothelium under flow. In *The FASEB Journal* 27 (8), pp. 3017–3029. DOI: 10.1096/fj.12-224824.

Fanning, A. S.; Jameson, B. J.; Jesaitis, L. A.; Anderson, J. M. (1998): The tight junction protein ZO-1 establishes a link between the transmembrane protein occludin and the actin cytoskeleton. In *The Journal of biological chemistry* 273 (45), pp. 29745–29753. DOI: 10.1074/jbc.273.45.29745.

Farahani, Ensieh; Patra, Hira K.; Jangamreddy, Jaganmohan R.; Rashedi, Iran; Kawalec, Marta; Rao Pariti, Rama K. et al. (2014): Cell adhesion molecules and their relation to (cancer) cell stemness. In *Carcinogenesis* 35 (4), pp. 747–759. DOI: 10.1093/carcin/bgu045.

Fazakas, Csilla; Wilhelm, Imola; Nagyoszi, Péter; Farkas, Attila E.; Haskó, János; Molnár, Judit et al. (2011): Transmigration of melanoma cells through the blood-brain barrier: role of endothelial tight junctions and melanoma-released serine proteases. In *PloS one* 6 (6), e20758. DOI: 10.1371/journal.pone.0020758.

Fidler, Isaiah J. (1970): Metastasis: Quantitative Analysis of Distribution and Fate of Tumor Emboli Labeled With ¹²⁵I-5-Iodo-2'-deoxyuridine²³. In *Journal of the National Cancer Institute* 45 (4), pp. 773–782. DOI: 10.1093/jnci/45.4.773.

Fidler, Isaiah J.; Yano, Seiji; Zhang, Ruo-dan; Fujimaki, Takahashi; Bucana, Corazon D. (2002): The seed and soil hypothesis: vascularisation and brain metastases. In *The Lancet Oncology* 3 (1), pp. 53–57. DOI: 10.1016/S1470-2045(01)00622-2.

Figueira, Inês; Tavares, Lucélia; Jardim, Carolina; Costa, Inês; Terrasso, Ana P.; Almeida, Andreia F. et al. (2019): Blood-brain barrier transport and neuroprotective potential of blackberry-digested polyphenols: an in vitro study. In *European journal of nutrition* 58 (1), pp. 113–130. DOI: 10.1007/s00394-017-1576-y.

Furuse, M.; Hirase, T.; Itoh, M.; Nagafuchi, A.; Yonemura, S.; Tsukita, S. (1993): Occludin: a novel integral membrane protein localizing at tight junctions. In *J Cell Biol* 123 (6), pp. 1777–1788. DOI: 10.1083/jcb.123.6.1777.

Furuse, Mikio (2010): Molecular basis of the core structure of tight junctions. In *Cold Spring Harbor perspectives in biology* 2 (1), a002907. DOI: 10.1101/cshperspect.a002907.

Gasic, G. J.; Gasic, T. B.; Stewart, C. C. (1968): Antimetastatic effects associated with platelet reduction. In *Proceedings of the National Academy of Sciences* 61 (1), pp. 46–52. DOI: 10.1073/pnas.61.1.46.

Gentil, Benoît J.; Benaud, Christelle; Delphin, Christian; Remy, Chantal; Berezowski, Vincent; Cecchelli, Roméo et al. (2005): Specific AHNAK expression in brain endothelial cells with barrier properties. In *Journal of cellular physiology* 203 (2), pp. 362–371. DOI: 10.1002/jcp.20232.

Giard, D. J.; Aaronson, S. A.; Todaro, G. J.; Arnstein, P.; Kersey, J. H.; Dosik, H.; Parks, W. P. (1973): In vitro cultivation of human tumors: establishment of cell lines derived from a series of solid tumors. In *Journal of the National Cancer Institute* 51 (5), pp. 1417–1423. DOI: 10.1093/jnci/51.5.1417.

Gifre-Renom, Laia; Daems, Margo; Lutun, Aernout; Jones, Elizabeth A. V. (2022): Organ-Specific Endothelial Cell Differentiation and Impact of Microenvironmental Cues on Endothelial Heterogeneity. In *International journal of molecular sciences* 23 (3). DOI: 10.3390/ijms23031477.

Ginhoux, Florent; Garel, Sonia (2018): The mysterious origins of microglia. In *Nature neuroscience* 21 (7), pp. 897–899. DOI: 10.1038/s41593-018-0176-3.

Ginhoux, Florent; Lim, Shawn; Hoeffel, Guillaume; Low, Donovan; Huber, Tara (2013): Origin and differentiation of microglia. In *Frontiers in cellular neuroscience* 7, p. 45. DOI: 10.3389/fncel.2013.00045.

Goaillard, Jean-Marc; Moubarak, Estelle; Tapia, Mónica; Tell, Fabien (2019): Diversity of Axonal and Dendritic Contributions to Neuronal Output. In *Frontiers in cellular neuroscience* 13, p. 570. DOI: 10.3389/fncel.2019.00570.

Goel, Vikas K.; Lazar, Alexander J. F.; Warneke, Carla L.; Redston, Mark S.; Haluska, Frank G. (2006): Examination of mutations in BRAF, NRAS, and PTEN in primary cutaneous melanoma. In *The Journal of investigative dermatology* 126 (1), pp. 154–160. DOI: 10.1038/sj.jid.5700026.

Goldmann, Edwin Ellen (1909): Die aussere und innere Sekretion des gesunden und kranken Organismus im Lichte der "vitalen Färbung". In *Beitr. Klin. Chir.* 64, pp. 192–265.

Goldmann, Edwin Ellen (1913): Vitalfärbung am Zentralnervensystem: Beitrag zur Physiopathologie des Plexus chorioideus und der Hirnhäute: Königl. Akademie der Wissenschaften (1).

González-Mariscal, L.; Betanzos, A.; Nava, P.; Jaramillo, B.E (2003): Tight junction proteins. In *Progress in Biophysics and Molecular Biology* 81 (1), pp. 1–44. DOI: 10.1016/S0079-6107(02)00037-8.

González-Mariscal, Lorenza; Tapia, Rocio; Chamorro, David (2008): Crosstalk of tight junction components with signaling pathways. In *Biochimica et biophysica acta* 1778 (3), pp. 729–756. DOI: 10.1016/j.bbamem.2007.08.018.

Gottardi, C. J.; Arpin, M.; Fanning, A. S.; Louvard, D. (1996): The junction-associated protein, zonula occludens-1, localizes to the nucleus before the maturation and during the remodeling of cell-cell contacts. In *Proceedings of the National Academy of Sciences* 93 (20), pp. 10779–10784. DOI: 10.1073/pnas.93.20.10779.

Greene, Chris; Hanley, Nicole; Campbell, Matthew (2019): Claudin-5: gatekeeper of neurological function. In *Fluids and barriers of the CNS* 16 (1), p. 3. DOI: 10.1186/s12987-019-0123-z.

Gumbiner, B.; Lowenkopf, T.; Apatira, D. (1991): Identification of a 160-kDa polypeptide that binds to the tight junction protein ZO-1. In *Proceedings of the National Academy of Sciences* 88 (8), pp. 3460–3464. DOI: 10.1073/pnas.88.8.3460.

Gumusay, Ozge; Coskun, Ugur; Akman, Tülay; Ekinci, Ahmet Siyar; Kocar, Muharrem; Erceleb, Ozlem Balvan et al. (2014): Predictive factors for the development of brain

metastases in patients with malignant melanoma: a study by the Anatolian society of medical oncology. In *Journal of cancer research and clinical oncology* 140 (1), pp. 151–157. DOI: 10.1007/s00432-013-1553-7.

Gutiérrez-Castañeda, Luz D.; Gamboa, Mauricio; Nova, John A.; Pulido, Leonardo; Tovar-Parra, Jose D. (2020): Mutations in the BRAF, NRAS, and C-KIT Genes of Patients Diagnosed with Melanoma in Colombia Population. In *BioMed research international*, p. 2046947. DOI: 10.1155/2020/2046947.

Haas, Alexis J.; Zihni, Ceniz; Ruppel, Artur; Hartmann, Christian; Ebnet, Klaus; Tada, Masazumi et al. (2020): Interplay between Extracellular Matrix Stiffness and JAM-A Regulates Mechanical Load on ZO-1 and Tight Junction Assembly. In *Cell reports* 32 (3), p. 107924. DOI: 10.1016/j.celrep.2020.107924.

Haqqani, Arsalan S.; Delaney, Christie E.; Brunette, Eric; Baumann, Ewa; Farrington, Graham K.; Sisk, William et al. (2018): Endosomal trafficking regulates receptor-mediated transcytosis of antibodies across the blood brain barrier. In *Journal of cerebral blood flow and metabolism : official journal of the International Society of Cerebral Blood Flow and Metabolism* 38 (4), pp. 727–740. DOI: 10.1177/0271678X17740031.

Harder, David R.; Zhang, Chenyang; Gebremedhin, Debebe (2002): Astrocytes function in matching blood flow to metabolic activity. In *News in physiological sciences : an international journal of physiology produced jointly by the International Union of Physiological Sciences and the American Physiological Society* 17, pp. 27–31. DOI: 10.1152/physiologyonline.2002.17.1.27.

Haskins, J.; Gu, L.; Wittchen, E. S.; Hibbard, J.; Stevenson, B. R. (1998): ZO-3, a novel member of the MAGUK protein family found at the tight junction, interacts with ZO-1 and occludin. In *The Journal of cell biology* 141 (1), pp. 199–208. DOI: 10.1083/jcb.141.1.199.

Hawkins, Brian T.; Davis, Thomas P. (2005): The blood-brain barrier/neurovascular unit in health and disease. In *Pharmacological reviews* 57 (2), pp. 173–185. DOI: 10.1124/pr.57.2.4.

Hawkins, Richard A.; O'Kane, Robyn L.; Simpson, Ian A.; Viña, Juan R. (2006): Structure of the blood-brain barrier and its role in the transport of amino acids. In *The Journal of nutrition* 136 (1 Suppl), 218S–26S. DOI: 10.1093/jn/136.1.218S.

Helms, Hans C.; Abbott, N. Joan; Burek, Malgorzata; Cecchelli, Romeo; Couraud, Pierre-Olivier; Deli, Maria A. et al. (2016): In vitro models of the blood-brain barrier: An overview of commonly used brain endothelial cell culture models and guidelines for their use. In *Journal of cerebral blood flow and metabolism : official journal of the International Society of Cerebral Blood Flow and Metabolism* 36 (5), pp. 862–890. DOI: 10.1177/0271678X16630991.

Herman, Hildegard; Fazakas, Csilla; Haskó, János; Molnár, Kinga; Mészáros, Ádám; Nyúl-Tóth, Ádám et al. (2019): Paracellular and transcellular migration of metastatic cells through the cerebral endothelium. In *Journal of cellular and molecular medicine* 23 (4), pp. 2619–2631. DOI: 10.1111/jcmm.14156.

Herwig, Nadine; Belter, Birgit; Pietzsch, Jens (2016): Extracellular S100A4 affects endothelial cell integrity and stimulates transmigration of A375 melanoma cells. In *Biochemical and biophysical research communications* 477 (4), pp. 963–969. DOI: 10.1016/j.bbrc.2016.07.009.

Hirase, T.; Staddon, J. M.; Saitou, M.; Ando-Akatsuka, Y.; Itoh, M.; Furuse, M. et al. (1997): Occludin as a possible determinant of tight junction permeability in endothelial cells. In *Journal of cell science* 110 (Pt 14), pp. 1603–1613. DOI: 10.1242/jcs.110.14.1603.

Hladky, Stephen B.; Barrand, Margery A. (2016): Fluid and ion transfer across the blood-brain and blood-cerebrospinal fluid barriers; a comparative account of mechanisms and roles. In *Fluids and barriers of the CNS* 13 (1), p. 19. DOI: 10.1186/s12987-016-0040-3.

Hodis, Eran; Watson, Ian R.; Kryukov, Gregory V.; Arold, Stefan T.; Imielinski, Marcin; Theurillat, Jean-Philippe et al. (2012): A landscape of driver mutations in melanoma. In *Cell* 150 (2), pp. 251–263. DOI: 10.1016/j.cell.2012.06.024.

Homem, Catarina C. F.; Repic, Marko; Knoblich, Jürgen A. (2015): Proliferation control in neural stem and progenitor cells. In *Nature reviews. Neuroscience* 16 (11), pp. 647–659. DOI: 10.1038/nrn4021.

Huang, Royston-Luke; Teo, Ziqiang; Chong, Han Chung; Zhu, Pengcheng; Tan, Ming Jie; Tan, Chek Kun et al. (2011): ANGPTL4 modulates vascular junction integrity by integrin signaling and disruption of intercellular VE-cadherin and claudin-5 clusters. In *Blood* 118 (14), pp. 3990–4002. DOI: 10.1182/blood-2011-01-328716.

- Huber, J. D.; Witt, K. A.; Hom, S.; Egleton, R. D.; Mark, K. S.; Davis, T. P. (2001): Inflammatory pain alters blood-brain barrier permeability and tight junctional protein expression. In *American journal of physiology. Heart and circulatory physiology* 280 (3), H1241-8. DOI: 10.1152/ajpheart.2001.280.3.H1241.
- Hussain, Basharat; Fang, Cheng; Huang, Xiaowen; Feng, Ziyang; Yao, Yuxuan; Wang, Yu; Chang, Junlei (2022): Endothelial β -Catenin Deficiency Causes Blood-Brain Barrier Breakdown via Enhancing the Paracellular and Transcellular Permeability. In *Frontiers in molecular neuroscience* 15, p. 895429. DOI: 10.3389/fnmol.2022.895429.
- Illina, Elena I.; Cialini, Camille; Gerloff, Dietlind L.; Duarte Garcia-Escudero, Maitane; Jeanty, Céline; Thézénas, Marie-Laëtitia et al. (2022): Enzymatic activity of glycosyltransferase GLT8D1 promotes human glioblastoma cell migration. In *iScience* 25 (2), p. 103842. DOI: 10.1016/j.isci.2022.103842.
- In, Gino K.; Poorman, Kelsey; Saul, Michelle; O'Day, Steven; Farma, Jeffrey M.; Olszanski, Anthony J. et al. (2020): Molecular profiling of melanoma brain metastases compared to primary cutaneous melanoma and to extracranial metastases. In *Oncotarget* 11 (33), pp. 3118–3128. DOI: 10.18632/oncotarget.27686.
- Itoh, M.; Furuse, M.; Morita, K.; Kubota, K.; Saitou, M.; Tsukita, S. (1999): Direct binding of three tight junction-associated MAGUKs, ZO-1, ZO-2, and ZO-3, with the COOH termini of claudins. In *The Journal of cell biology* 147 (6), pp. 1351–1363. DOI: 10.1083/jcb.147.6.1351.
- Itoh, Masahiko; Bissell, Mina J. (2003): The organization of tight junctions in epithelia: implications for mammary gland biology and breast tumorigenesis. In *Journal of mammary gland biology and neoplasia* 8 (4), pp. 449–462. DOI: 10.1023/B:JOMG.0000017431.45314.07.
- Janavicius, Mantas; Lachej, Nadezda; Anglickiene, Giedre; Vincerzevskiene, Ieva; Brasiuniene, Birute (2020): Outcomes of Treatment for Melanoma Brain Metastases. In *Journal of skin cancer* 2020, p. 7520924. DOI: 10.1155/2020/7520924.
- Jia, Wang; Lu, Runchun; Martin, Tracey A.; Jiang, Wen G. (2014): The role of claudin-5 in blood-brain barrier (BBB) and brain metastases (review). In *Molecular medicine reports* 9 (3), pp. 779–785. DOI: 10.3892/mmr.2013.1875.

Jo, Dong Hyun; Kim, Jin Hyoung; Heo, Jong-Ik; Kim, Jeong Hun; Cho, Chung-Hyun (2013): Interaction between pericytes and endothelial cells leads to formation of tight junction in hyaloid vessels. In *Molecules and cells* 36 (5), pp. 465–471. DOI: 10.1007/s10059-013-0228-1.

Johnson, Zachary Lee; Chen, Jue (2017): Structural Basis of Substrate Recognition by the Multidrug Resistance Protein MRP1. In *Cell* 168 (6), 1075-1085.e9. DOI: 10.1016/j.cell.2017.01.041.

Jouve, Nathalie; Bachelier, Richard; Despoix, Nicolas; Blin, Muriel G.; Matinzadeh, Maryam Khalili; Poitevin, Stéphane et al. (2015): CD146 mediates VEGF-induced melanoma cell extravasation through FAK activation. In *Int. J. Cancer* 137 (1), pp. 50–60. DOI: 10.1002/ijc.29370.

Juliano, R. L.; Ling, V. (1976): A surface glycoprotein modulating drug permeability in Chinese hamster ovary cell mutants. In *Biochimica et biophysica acta* 455 (1), pp. 152–162. DOI: 10.1016/0005-2736(76)90160-7.

Kadry, Hossam; Noorani, Behnam; Cucullo, Luca (2020): A blood-brain barrier overview on structure, function, impairment, and biomarkers of integrity. In *Fluids and barriers of the CNS* 17 (1), p. 69. DOI: 10.1186/s12987-020-00230-3.

Kakadia, Sunilkumar; Yarlagadda, Naveen; Awad, Ramez; Kundranda, Madappa; Niu, Jiaxin; Naraev, Boris et al. (2018): Mechanisms of resistance to BRAF and MEK inhibitors and clinical update of US Food and Drug Administration-approved targeted therapy in advanced melanoma. In *Oncotargets and therapy* 11, pp. 7095–7107. DOI: 10.2147/OTT.S182721.

Kaplan, Luke; Chow, Brian W.; Gu, Chenghua (2020): Neuronal regulation of the blood-brain barrier and neurovascular coupling. In *Nature reviews. Neuroscience* 21 (8), pp. 416–432. DOI: 10.1038/s41583-020-0322-2.

Karamchandani, Jason R.; Nielsen, Torsten O.; van de Rijn, Matt; West, Robert B. (2012): Sox10 and S100 in the diagnosis of soft-tissue neoplasms. In *Applied immunohistochemistry & molecular morphology : AIMM* 20 (5), pp. 445–450. DOI: 10.1097/PAI.0b013e318244ff4b.

Kartner, Norbert; Riordan, John R.; Ling, Victor (1983): Cell Surface P-Glycoprotein Associated with Multidrug Resistance in Mammalian Cell Lines. In *Science (New York, N.Y.)* 221 (4617), pp. 1285–1288. DOI: 10.1126/science.6137059.

Kashani-Sabet, M. (2014): Molecular markers in melanoma. In *The British journal of dermatology* 170 (1), pp. 31–35. DOI: 10.1111/bjd.12493.

Kaur, Charanjit; Hao, Ai-Jun; Wu, Ching-Hsiang; Ling, Eng-Ang (2001): Origin of microglia.

Kido, Y.; Tamai, I.; Okamoto, M.; Suzuki, F.; Tsuji, A. (2000): Functional clarification of MCT1-mediated transport of monocarboxylic acids at the blood-brain barrier using in vitro cultured cells and in vivo BUI studies. In *Pharmaceutical research* 17 (1), pp. 55–62. DOI: 10.1023/a:1007518525161.

Kim, K-J; Kwon, S-H; Yun, J-H; Jeong, H-S; Kim, H-R; Lee, E. H. et al. (2017): STAT3 activation in endothelial cells is important for tumor metastasis via increased cell adhesion molecule expression. In *Oncogene* 36 (39), pp. 5445–5459. DOI: 10.1038/onc.2017.148.

Kim, Young J.; Borsig, Lubor; Varki, Nissi M.; Varki, Ajit (1998): P-selectin deficiency attenuates tumor growth and metastasis. In *Proceedings of the National Academy of Sciences* 95 (16), pp. 9325–9330. DOI: 10.1073/pnas.95.16.9325.

Kiss, Anna L.; Botos, Erzsébet (2009): Endocytosis via caveolae: alternative pathway with distinct cellular compartments to avoid lysosomal degradation? In *Journal of cellular and molecular medicine* 13 (7), pp. 1228–1237. DOI: 10.1111/j.1582-4934.2009.00754.x.

Klemke, Martin; Weschenfelder, Tatjana; Konstandin, Mathias H.; Samstag, Yvonne (2007): High affinity interaction of integrin $\alpha 4\beta 1$ (VLA-4) and vascular cell adhesion molecule 1 (VCAM-1) enhances migration of human melanoma cells across activated endothelial cell layers. In *Journal of cellular physiology* 212 (2), pp. 368–374. DOI: 10.1002/jcp.21029.

Kluge, Matthew A.; Fetterman, Jessica L.; Vita, Joseph A. (2013): Mitochondria and endothelial function. In *Circulation research* 112 (8), pp. 1171–1188. DOI: 10.1161/CIRCRESAHA.111.300233.

Knox, Emily G.; Aburto, Maria R.; Clarke, Gerard; Cryan, John F.; O'Driscoll, Caitriona M. (2022): The blood-brain barrier in aging and neurodegeneration. In *Molecular psychiatry* 27 (6), pp. 2659–2673. DOI: 10.1038/s41380-022-01511-z.

Korc, M.; Friesel, R. E. (2009): The role of fibroblast growth factors in tumor growth. In *Current cancer drug targets* 9 (5), pp. 639–651. DOI: 10.2174/156800909789057006.

Kotliarova, Anastasiia; Sidorova, Yulia A. (2021): Glial Cell Line-Derived Neurotrophic Factor Family Ligands, Players at the Interface of Neuroinflammation and Neuroprotection: Focus

Onto the Glia. In *Frontiers in cellular neuroscience* 15, p. 679034. DOI: 10.3389/fncel.2021.679034.

Kugler, Elisabeth C.; Greenwood, John; MacDonald, Ryan B. (2021): The “Neuro-Glial-Vascular” Unit: The Role of Glia in Neurovascular Unit Formation and Dysfunction. In *Front. Cell Dev. Biol.* 9, Article 732820. DOI: 10.3389/fcell.2021.732820.

Kusuhara, Hiroyuki; Sugiyama, Yuichi (2005): Efflux transport systems at the blood–brain barrier and blood CSF barrier. In *International Congress Series* 1277, pp. 111–122. DOI: 10.1016/j.ics.2005.02.015.

Labelle, Myriam; Begum, Shahinoor; Hynes, Richard O. (2011): Direct signaling between platelets and cancer cells induces an epithelial-mesenchymal-like transition and promotes metastasis. In *Cancer cell* 20 (5), pp. 576–590. DOI: 10.1016/j.ccr.2011.09.009.

Lai, Char-Huei; Kuo, Kuo-Hsing; Leo, Joyce M. (2005): Critical role of actin in modulating BBB permeability. In *Brain research. Brain research reviews* 50 (1), pp. 7–13. DOI: 10.1016/j.brainresrev.2005.03.007.

Lammert, Eckhard; Axnick, Jennifer (2012): Vascular lumen formation. In *Cold Spring Harbor perspectives in medicine* 2 (4), a006619. DOI: 10.1101/cshperspect.a006619.

Langen, Urs H.; Ayloo, Swathi; Gu, Chenghua (2019): Development and Cell Biology of the Blood-Brain Barrier. In *Annual review of cell and developmental biology* 35, pp. 591–613. DOI: 10.1146/annurev-cellbio-100617-062608.

Langer, Harald F.; Orlova, Valeria V.; Xie, Changping; Kaul, Sunil; Schneider, Darius; Lonsdorf, Anke S. et al. (2011): A Novel Function of Junctional Adhesion Molecule-C in Mediating Melanoma Cell Metastasis. In *Cancer research* 71 (12), pp. 4096–4105. DOI: 10.1158/0008-5472.CAN-10-2794.

Larochelle, Catherine; Lécuyer, Marc-André; Alvarez, Jorge Ivan; Charabati, Marc; Saint-Laurent, Olivia; Ghannam, Soufiane et al. (2015): Melanoma cell adhesion molecule-positive CD8 T lymphocytes mediate central nervous system inflammation. In *Annals of neurology* 78 (1), pp. 39–53. DOI: 10.1002/ana.24415.

Larribère, Lionel; Utikal, Jochen (2016): Multiple roles of NF1 in the melanocyte lineage. In *Pigment cell & melanoma research* 29 (4), pp. 417–425. DOI: 10.1111/pcmr.12488.

- León, Gerardo (2016): Carrier-Mediated Transport. In Enrico Drioli, Lidietta Giorno (Eds.): *Encyclopedia of Membranes*. Berlin, Heidelberg: Springer Berlin Heidelberg, pp. 308–310.
- Lewandowsky, Max (1909): Zur lehre der cerebrospinalflussigkeit. In *Z. klin. Med.* 40, pp. 480–494.
- Liddel, Shane A. (2011): Fluids and barriers of the CNS: a historical viewpoint. In *Fluids and barriers of the CNS* 8 (1), p. 2. DOI: 10.1186/2045-8118-8-2.
- Lidonnici, Jacopo; Santoro, Massimo M.; Oberkersch, Roxana E. (2022): Cancer-Induced Metabolic Rewiring of Tumor Endothelial Cells. In *Cancers* 14 (11). DOI: 10.3390/cancers14112735.
- Lin, Qingtang; Balasubramanian, Krishnakumar; Fan, Dominic; Kim, Sun-Jin; Guo, Lixia; Wang, Hua et al. (2010): Reactive Astrocytes Protect Melanoma Cells from Chemotherapy by Sequestering Intracellular Calcium through Gap Junction Communication Channels. In *Neoplasia* 12 (9), pp. 748–754. DOI: 10.1593/neo.10602.
- Linton, Kenneth J.; Higgins, Christopher F. (2007): Structure and function of ABC transporters: the ATP switch provides flexible control. In *Pflügers Archiv : European journal of physiology* 453 (5), pp. 555–567. DOI: 10.1007/s00424-006-0126-x.
- Lippoldt, Andrea; Liebner, Stefan; Andbjør, Beth; Kalbacher, Hubert; Wolburg, Hartwig; Haller, Hermann; Fuxe, Kjell (2000): Organization of choroid plexus epithelial and endothelial cell tight junctions and regulation of claudin-1, -2 and -5 expression by protein kinase C. In *NeuroReport* 11 (7). Available online at https://journals.lww.com/neuroreport/Fulltext/2000/05150/Organization_of_choroid_plexus_epithelial_and.15.aspx.
- Liu, Jie; Wang, Caihong; Ma, Xuhui; Tian, Yang; Wang, Chunying; Fu, Yan; Luo, Yongzhang (2019): High expression of CCR5 in melanoma enhances epithelial-mesenchymal transition and metastasis via TGFβ1. In *The Journal of pathology* 247 (4), pp. 481–493. DOI: 10.1002/path.5207.
- Liu, Pei; Hu, Yaotian; Ma, Ling; Du, Min; Xia, Lin; Hu, Zhensheng (2015): miR-425 inhibits melanoma metastasis through repression of PI3K-Akt pathway by targeting IGF-1. In *Biomedicine & pharmacotherapy = Biomedecine & pharmacotherapie* 75, pp. 51–57. DOI: 10.1016/j.biopha.2015.08.010.

Loontjens, Siebe; Depestel, Lisa; Vanhauwaert, Suzanne; Dewyn, Givani; Gistelincq, Charlotte; Verboom, Karen et al. (2019): Purification of high-quality RNA from a small number of fluorescence activated cell sorted zebrafish cells for RNA sequencing purposes. In *BMC Genomics* 20 (1), p. 228. DOI: 10.1186/s12864-019-5608-2.

Löscher, Wolfgang; Potschka, Heidrun (2005a): Blood-brain barrier active efflux transporters: ATP-binding cassette gene family. In *NeuroRx : the journal of the American Society for Experimental NeuroTherapeutics* 2 (1), pp. 86–98. DOI: 10.1602/neurorx.2.1.86.

Löscher, Wolfgang; Potschka, Heidrun (2005b): Drug resistance in brain diseases and the role of drug efflux transporters. In *Nature reviews. Neuroscience* 6 (8), pp. 591–602. DOI: 10.1038/nrn1728.

Lu, Pengfei; Takai, Ken; Weaver, Valerie M.; Werb, Zena (2011): Extracellular matrix degradation and remodeling in development and disease. In *Cold Spring Harbor perspectives in biology* 3 (12). DOI: 10.1101/cshperspect.a005058.

Ludwig, Thomas; Ossig, Rainer; Graessel, Susanne; Wilhelmi, Marianne; Oberleithner, Hans; Schneider, Stefan W. (2002): The electrical resistance breakdown assay determines the role of proteinases in tumor cell invasion. In *American Journal of Physiology-Renal Physiology* 283 (2), F319-F327. DOI: 10.1152/ajprenal.00327.2001.

Luebker, Stephen A.; Koepsell, Scott A. (2019): Diverse Mechanisms of BRAF Inhibitor Resistance in Melanoma Identified in Clinical and Preclinical Studies. In *Frontiers in oncology* 9, p. 268. DOI: 10.3389/fonc.2019.00268.

Lugassy, Claire; Péault, Bruno; Wadehra, Madhuri; Kleinman, Hynda K.; Barnhill, Raymond L. (2013): Could pericytic mimicry represent another type of melanoma cell plasticity with embryonic properties? In *Pigment cell & melanoma research* 26 (5), pp. 746–754.

Luissint, Anny-Claude; Artus, Cédric; Glacial, Fabienne; Ganeshamoorthy, Kayathiri; Couraud, Pierre-Olivier (2012): Tight junctions at the blood brain barrier: physiological architecture and disease-associated dysregulation. In *Fluids and barriers of the CNS* 9 (1), p. 23. DOI: 10.1186/2045-8118-9-23.

Lund-Andersen, H. (1979): Transport of glucose from blood to brain. In *Physiological reviews* 59 (2), pp. 305–352. DOI: 10.1152/physrev.1979.59.2.305.

Madsen, Chris D.; Sahai, Erik (2010): Cancer dissemination--lessons from leukocytes. In *Developmental cell* 19 (1), pp. 13–26. DOI: 10.1016/j.devcel.2010.06.013.

Mamdouh, Zahra; Mikhailov, Alexei; Muller, William A. (2009): Transcellular migration of leukocytes is mediated by the endothelial lateral border recycling compartment. In *The Journal of experimental medicine* 206 (12), pp. 2795–2808. DOI: 10.1084/jem.20082745.

Marchetti, Luca; Engelhardt, Britta (2020): Immune cell trafficking across the blood-brain barrier in the absence and presence of neuroinflammation. In *Vascular biology (Bristol, England)* 2 (1), H1-H18. DOI: 10.1530/VB-19-0033.

Marcinowski, Filip (2020): Max Lewandowsky (1876–1918). In *Journal of Neurology* 267 (4), pp. 1223–1224. DOI: 10.1007/s00415-019-09393-y.

Mark, Karen S.; Davis, Thomas P. (2002): Cerebral microvascular changes in permeability and tight junctions induced by hypoxia-reoxygenation. In *American journal of physiology. Heart and circulatory physiology* 282 (4), H1485-94. DOI: 10.1152/ajpheart.00645.2001.

Martìn-Padura, I.; Lostaglio, S.; Schneemann, M.; Williams, L.; Romano, M.; Fruscella, P. et al. (1998): Junctional adhesion molecule, a novel member of the immunoglobulin superfamily that distributes at intercellular junctions and modulates monocyte transmigration. In *The Journal of cell biology* 142 (1), pp. 117–127. DOI: 10.1083/jcb.142.1.117.

Matsudaira, Tatsuyuki; Prinz, Marco (2022): Life and death of microglia: Mechanisms governing microglial states and fates. In *Immunology letters* 245, pp. 51–60. DOI: 10.1016/j.imlet.2022.04.001.

Mehnert, Janice M.; Kluger, Harriet M. (2012): Driver mutations in melanoma: lessons learned from bench-to-bedside studies. In *Curr Oncol Rep* 14 (5), pp. 449–457. DOI: 10.1007/s11912-012-0249-5.

Melnikova, Vladislava O.; Bar-Eli, Menashe (2009): Inflammation and melanoma metastasis. In *Pigment cell & melanoma research* 22 (3), pp. 257–267. DOI: 10.1111/j.1755-148X.2009.00570.x.

Miarka, Lauritz; Valiente, Manuel (2021): Animal models of brain metastasis. In *Neuro-oncology advances* 3 (Suppl 5), v144-v156. DOI: 10.1093/noajnl/vdab115.

Michael Bachmann; Sampo Kukkurainen; Vesa P. Hytönen; and Bernhard Wehrle-Haller (2019): Cell Adhesion by Integrins.

Michinaga, Shotaro; Koyama, Yutaka (2019): Dual Roles of Astrocyte-Derived Factors in Regulation of Blood-Brain Barrier Function after Brain Damage. In *International journal of molecular sciences* 20 (3). DOI: 10.3390/ijms20030571.

Mkrtchyan, H.; Scheler, S.; Klein, I.; Fahr, A.; Couraud, P. O.; Romero, I. A. et al. (2009): Molecular cytogenetic characterization of the human cerebral microvessel endothelial cell line hCMEC/D3. In *Cytogenetic and genome research* 126 (4), pp. 313–317. DOI: 10.1159/000253080.

Morris, Marilyn E.; Rodriguez-Cruz, Vivian; Felmler, Melanie A. (2017): SLC and ABC Transporters: Expression, Localization, and Species Differences at the Blood-Brain and the Blood-Cerebrospinal Fluid Barriers. In *The AAPS journal* 19 (5), pp. 1317–1331. DOI: 10.1208/s12248-017-0110-8.

Moser, B.; Clark-Lewis, I.; Zwahlen, R.; Baggiolini, M. (1990): Neutrophil-activating properties of the melanoma growth-stimulatory activity. In *The Journal of experimental medicine* 171 (5), pp. 1797–1802. DOI: 10.1084/jem.171.5.1797.

Murtas, Daniela; Maxia, Cristina; Diana, Andrea; Pilloni, Luca; Corda, Claudia; Minerba, Luigi et al. (2017): Role of epithelial-mesenchymal transition involved molecules in the progression of cutaneous melanoma. In *Histochemistry and cell biology* 148 (6), pp. 639–649. DOI: 10.1007/s00418-017-1606-0.

Nassoy, Pierre; Lamaze, Christophe (2012): Stressing caveolae new role in cell mechanics. In *Trends in cell biology* 22 (7), pp. 381–389. DOI: 10.1016/j.tcb.2012.04.007.

Nielsen, Søren; Arnulf Nagelhus, Erlend; Amiry-Moghaddam, Mahmood; Bourque, Charles; Agre, Peter; Petter Ottersen, Ole (1997): Specialized Membrane Domains for Water Transport in Glial Cells: High-Resolution Immunogold Cytochemistry of Aquaporin-4 in Rat Brain. In *The Journal of Neuroscience* 17 (1), p. 171. DOI: 10.1523/JNEUROSCI.17-01-00171.1997.

Nitta, Takehiro; Hata, Masaki; Gotoh, Shimpei; Seo, Yoshiteru; Sasaki, Hiroyuki; Hashimoto, Nobuo et al. (2003): Size-selective loosening of the blood-brain barrier in claudin-5-

deficient mice. In *The Journal of cell biology* 161 (3), pp. 653–660. DOI: 10.1083/jcb.200302070.

Nuñez, Jamie; Renslow, Ryan; Cliff, John B.; Anderton, Christopher R. (2017): NanoSIMS for biological applications: Current practices and analyses. In *Biointerphases* 13 (3), 03B301. DOI: 10.1116/1.4993628.

Odenwald, Matthew A.; Choi, Wangsun; Buckley, Aaron; Shashikanth, Nitesh; Joseph, Nora E.; Wang, Yitang et al. (2017): ZO-1 interactions with F-actin and occludin direct epithelial polarization and single lumen specification in 3D culture. In *Journal of cell science* 130 (1), pp. 243–259. DOI: 10.1242/jcs.188185.

Ogiso, Hideo; Suno, Ryoji; Kobayashi, Takuya; Kawami, Masashi; Takano, Mikiyoshi; Ogasawara, Masaru (2022): A Liquid Chromatography-Mass Spectrometry Method to Study the Interaction between Membrane Proteins and Low-Molecular-Weight Compound Mixtures. In *Molecules (Basel, Switzerland)* 27 (15). DOI: 10.3390/molecules27154889.

Ohtsuki, Sumio; Yamaguchi, Hirofumi; Katsukura, Yuki; Asashima, Tomoko; Terasaki, Tetsuya (2008): mRNA expression levels of tight junction protein genes in mouse brain capillary endothelial cells highly purified by magnetic cell sorting. In *J Neurochem* 104 (1), pp. 147–154. DOI: 10.1111/j.1471-4159.2007.05008.x.

Okada, Hideshi; Takemura, Genzou; Suzuki, Kodai; Oda, Kazumasa; Takada, Chihiro; Hotta, Yasuaki et al. (2017): Three-dimensional ultrastructure of capillary endothelial glycocalyx under normal and experimental endotoxemic conditions. In *Critical care (London, England)* 21 (1), p. 261. DOI: 10.1186/s13054-017-1841-8.

Ostrom, Quinn T.; Wright, Christina Huang; Barnholtz-Sloan, Jill S. (2018): Chapter 2 - Brain metastases: epidemiology. In David Schiff, Martin J. van den Bent (Eds.): *Handbook of Clinical Neurology : Metastatic Disease of the Nervous System*, vol. 149: Elsevier, pp. 27–42. Available online at <https://www.sciencedirect.com/science/article/pii/B9780128111611000025>.

Padua, David; Zhang, Xiang H-F; Wang, Qiongqing; Nadal, Cristina; Gerald, William L.; Gomis, Roger R.; Massagué, Joan (2008): TGFbeta primes breast tumors for lung metastasis seeding through angiopoietin-like 4. In *Cell* 133 (1), pp. 66–77. DOI: 10.1016/j.cell.2008.01.046.

Padua, R. A.; Barrass, N.; Currie, G. A. (1984): A novel transforming gene in a human malignant melanoma cell line. In *Nature* 311 (5987), pp. 671–673. DOI: 10.1038/311671a0.

Palade, George E. (1953): The fine structure of blood capillaries. In *J Appl phys* 24, p. 1424.

Pan, Weihong; Stone, Kirsten P.; Hsuchou, Hung; Manda, Vamshi K.; Zhang, Yan; Kastin, Abba J. (2011): Cytokine signaling modulates blood-brain barrier function. In *Current pharmaceutical design* 17 (33), pp. 3729–3740. DOI: 10.2174/138161211798220918.

Papadopoulos, Marios C.; Verkman, Alan S. (2007): Aquaporin-4 and brain edema. In *Pediatric nephrology (Berlin, Germany)* 22 (6), pp. 778–784. DOI: 10.1007/s00467-006-0411-0.

Pardridge, W. M.; Boado, R. J.; Farrell, C. R. (1990): Brain-type glucose transporter (GLUT-1) is selectively localized to the blood-brain barrier. Studies with quantitative western blotting and in situ hybridization. In *The Journal of biological chemistry* 265 (29), pp. 18035–18040. DOI: 10.1016/S0021-9258(18)38267-X.

Pardridge, William M. (2007): Blood-brain barrier delivery. In *Drug discovery today* 12 (1-2), pp. 54–61. DOI: 10.1016/j.drudis.2006.10.013.

Parkar, Nihal S.; Akpa, Belinda S.; Nitsche, Ludwig C.; Wedgewood, Lewis E.; Place, Aaron T.; Sverdlov, Maria S. et al. (2009): Vesicle formation and endocytosis: function, machinery, mechanisms, and modeling. In *Antioxidants & redox signaling* 11 (6), pp. 1301–1312. DOI: 10.1089/ars.2008.2397.

Peppiatt, Claire M.; Howarth, Clare; Mobbs, Peter; Attwell, David (2006): Bidirectional control of CNS capillary diameter by pericytes. In *Nature* 443 (7112), pp. 700–704. DOI: 10.1038/nature05193.

Petty, M.A; Wettstein, J.G (2001): Elements of cerebral microvascular ischaemia. In *Brain Research Reviews* 36 (1), pp. 23–34. DOI: 10.1016/S0165-0173(01)00062-5.

Petzold, Gabor C.; Murthy, Venkatesh N. (2011): Role of astrocytes in neurovascular coupling. In *Neuron* 71 (5), pp. 782–797. DOI: 10.1016/j.neuron.2011.08.009.

Pisani, Paolo; Airoidi, Mario; Allais, Anastasia; Aluffi Valletti, Paolo; Battista, Mariapina; Benazzo, Marco et al. (2020 Apr): Metastatic disease in head & neck oncology.

Poggioli, Tommaso; Sarathchandra, Padmini; Rosenthal, Nadia; Santini, Maria P. (2014): Intramyocardial cell delivery: observations in murine hearts. In *Journal of visualized experiments : JoVE* (83), e51064. DOI: 10.3791/51064.

Potschka, Heidrun (2010): Transporter hypothesis of drug-resistant epilepsy: challenges for pharmacogenetic approaches. In *Pharmacogenomics* 11 (10), pp. 1427–1438. DOI: 10.2217/pgs.10.126.

Prat, A.; Biernacki, K.; Becher, B.; Antel, J. P. (2000): B7 expression and antigen presentation by human brain endothelial cells: requirement for proinflammatory cytokines. In *Journal of neuropathology and experimental neurology* 59 (2), pp. 129–136. DOI: 10.1093/jnen/59.2.129.

Prendiville, Terence W.; Ma, Qing; Lin, Zhiqiang; Zhou, Pingzhu; He, Aibin; Pu, William T. (2014): Ultrasound-guided transthoracic intramyocardial injection in mice. In *Journal of visualized experiments : JoVE* (90), e51566. DOI: 10.3791/51566.

Prieto, Pilar; Blaauboer, Bas J.; Boer, Albertus Gerrit de; Boveri, Monica; Cecchelli, Romeo; Clemenson, Cecilia et al. (2004): Blood-brain barrier in vitro models and their application in toxicology. The report and recommendations of ECVAM Workshop 49. In *Alternatives to laboratory animals : ATLA* 32 (1), pp. 37–50. DOI: 10.1177/026119290403200107.

Pulgar, Victor M. (2018): Transcytosis to Cross the Blood Brain Barrier, New Advancements and Challenges. In *Frontiers in neuroscience* 12, p. 1019. DOI: 10.3389/fnins.2018.01019.

Pytlak, Beata; Prochorec-Sobieszek, Monika; Szumera-Ciećkiewicz, Anna (2019): SOX10 as an immunohistochemical marker in cancer diagnostics. In *Nowotwory. Journal of Oncology* 69 (2), pp. 58–64. DOI: 10.5603/NJO.2019.0011.

Qiu, Yan-Mei; Zhang, Chun-Lin; Chen, An-Qi; Wang, Hai-Ling; Zhou, Yi-Fan; Li, Ya-Nan; Hu, Bo (2021): Immune Cells in the BBB Disruption After Acute Ischemic Stroke: Targets for Immune Therapy? In *Frontiers in immunology* 12, p. 678744. DOI: 10.3389/fimmu.2021.678744.

Redmer, Torben (2018): Deciphering mechanisms of brain metastasis in melanoma - the gist of the matter. In *Molecular cancer* 17 (1), p. 106. DOI: 10.1186/s12943-018-0854-5.

Reese, T. S.; Karnovsky, M. J. (1967): Fine structural localization of a blood-brain barrier to exogenous peroxidase. In *J Cell Biol* 34 (1), pp. 207–217. DOI: 10.1083/jcb.34.1.207.

Ren, Min; Zhang, Jing; Kong, Yunyi; Bai, Qianming; Qi, Peng; Zhang, Ling et al. (2022): BRAF, C-KIT, and NRAS mutations correlated with different clinicopathological features: an analysis of 691 melanoma patients from a single center. In *Annals of translational medicine* 10 (2), p. 31. DOI: 10.21037/atm-21-4235.

Reymond, Nicolas; d'Água, Bárbara Borda; Ridley, Anne J. (2013): Crossing the endothelial barrier during metastasis. In *Nature Reviews Cancer* 13 (12), pp. 858–870. DOI: 10.1038/nrc3628.

Rubin, L. L.; Hall, D. E.; Porter, S.; Barbu, K.; Cannon, C.; Horner, H. C. et al. (1991): A cell culture model of the blood-brain barrier. In *J Cell Biol* 115 (6), pp. 1725–1735. DOI: 10.1083/jcb.115.6.1725.

Saginala, Kalyan; Barsouk, Adam; Aluru, John Sukumar; Rawla, Prashanth; Barsouk, Alexander (2021): Epidemiology of Melanoma. In *Medical sciences (Basel, Switzerland)* 9 (4). DOI: 10.3390/medsci9040063.

Saitou, M.; Furuse, M.; Sasaki, H.; Schulzke, J. D.; Fromm, M.; Takano, H. et al. (2000): Complex phenotype of mice lacking occludin, a component of tight junction strands. In *Molecular biology of the cell* 11 (12), pp. 4131–4142. DOI: 10.1091/mbc.11.12.4131.

Sakakibara, A.; Furuse, M.; Saitou, M.; Ando-Akatsuka, Y.; Tsukita, S. (1997): Possible involvement of phosphorylation of occludin in tight junction formation. In *The Journal of cell biology* 137 (6), pp. 1393–1401. DOI: 10.1083/jcb.137.6.1393.

Salimi, Hamid; Klein, Robyn S. (2019): Disruption of the Blood-Brain Barrier During Neuroinflammatory and Neuroinfectious Diseases. In Hiroshi Mitoma, Mario Manto (Eds.): *Neuroimmune Diseases*. Cham: Springer International Publishing (Contemporary Clinical Neuroscience), pp. 195–234.

Sampson, J. H.; Carter, J. H., JR; Friedman, A. H.; Seigler, H. F. (1998): Demographics, prognosis, and therapy in 702 patients with brain metastases from malignant melanoma. In *Journal of neurosurgery* 88 (1), pp. 11–20. DOI: 10.3171/jns.1998.88.1.0011.

Sanchez-Covarrubias, Lucy; Slosky, Lauren M.; Thompson, Brandon J.; Davis, Thomas P.; Ronaldson, Patrick T. (2014): Transporters at CNS barrier sites: obstacles or opportunities for drug delivery? In *Current pharmaceutical design* 20 (10), pp. 1422–1449. DOI: 10.2174/13816128113199990463.

Sandoval, Karin E.; Witt, Ken A. (2008): Blood-brain barrier tight junction permeability and ischemic stroke. In *Neurobiology of disease* 32 (2), pp. 200–219. DOI: 10.1016/j.nbd.2008.08.005.

Santos, Gabryella S. P.; Magno, Luiz A. V.; Romano-Silva, Marco A.; Mintz, Akiva; Birbrair, Alexander (2019): Pericyte Plasticity in the Brain. In *Neuroscience bulletin* 35 (3), pp. 551–560. DOI: 10.1007/s12264-018-0296-5.

Satoh, H.; Zhong, Y.; Isomura, H.; Saitoh, M.; Enomoto, K.; Sawada, N.; Mori, M. (1996): Localization of 7H6 tight junction-associated antigen along the cell border of vascular endothelial cells correlates with paracellular barrier function against ions, large molecules, and cancer cells. In *Experimental cell research* 222 (2), pp. 269–274. DOI: 10.1006/excr.1996.0034.

Schey, Kevin L.; Grey, Angus C.; Nicklay, Joshua J. (2013): Mass spectrometry of membrane proteins: a focus on aquaporins. In *Biochemistry* 52 (22), pp. 3807–3817. DOI: 10.1021/bi301604j.

Schiff, David; van den Bent, Martin J. (Eds.) (2018): *Handbook of Clinical Neurology : Metastatic Disease of the Nervous System*: Elsevier.

Schulz, Michael; Salamero-Boix, Anna; Niesel, Katja; Alekseeva, Tijna; Sevenich, Lisa (2019): Microenvironmental Regulation of Tumor Progression and Therapeutic Response in Brain Metastasis. In *Frontiers in immunology* 10, p. 1713. DOI: 10.3389/fimmu.2019.01713.

Scolyer, Richard A.; Long, Georgina V.; Thompson, John F. (2011): Evolving concepts in melanoma classification and their relevance to multidisciplinary melanoma patient care. In *Molecular Oncology* 5 (2), pp. 124–136. DOI: 10.1016/j.molonc.2011.03.002.

Seelig, Anna (2020): P-Glycoprotein: One Mechanism, Many Tasks and the Consequences for Pharmacotherapy of Cancers. In *Frontiers in oncology* 10, p. 576559. DOI: 10.3389/fonc.2020.576559.

SEIJI, M.; FITZPATRICK, T. B.; SIMPSON, R. T.; BIRBECK, M. S. C. (1963): Chemical Composition and Terminology Of Specialized Organelles (Melanosomes and Melanin Granules) in Mammalian Melanocytes. In *Nature* 197 (4872), pp. 1082–1084. DOI: 10.1038/1971082a0.

Settergren, G.; Lindblad, B. S.; Persson, B. (1976): Cerebral blood flow and exchange of oxygen, glucose, ketone bodies, lactate, pyruvate and amino acids in infants. In *Acta paediatrica Scandinavica* 65 (3), pp. 343–353. DOI: 10.1111/j.1651-2227.1976.tb04896.x.

Shain, A. Hunter; Bastian, Boris C. (2016): From melanocytes to melanomas. In *Nature reviews. Cancer* 16 (6), pp. 345–358. DOI: 10.1038/nrc.2016.37.

Sharma, Hari Shanker; Westman, Jan (Eds.) (2004): Blood-Spinal Cord and Brain Barriers in Health and Disease. San Diego: Academic Press.

Simpson, Ian A.; Carruthers, Anthony; Vannucci, Susan J. (2007): Supply and Demand in Cerebral Energy Metabolism: The Role of Nutrient Transporters. In *Journal of Cerebral Blood Flow & Metabolism* 27 (11), pp. 1766–1791. DOI: 10.1038/sj.jcbfm.9600521.

Skoniecka, A.; Cichorek, M.; Tyminska, A.; Pelikant-Malecka, I.; Dziewiatkowski, J. (2021): Melanization as unfavorable factor in amelanotic melanoma cell biology. In *Protoplasma* 258 (5), pp. 935–948. DOI: 10.1007/s00709-021-01613-5.

Smith, David F.; Galkina, Elena; Ley, Klaus; Huo, Yuqing (2005): GRO family chemokines are specialized for monocyte arrest from flow. In *American journal of physiology. Heart and circulatory physiology* 289 (5), H1976-84. DOI: 10.1152/ajpheart.00153.2005.

Song, Jinna; Wang, Jun; Yang, Jianli; Jiang, Chunhua; Shen, Wei; Wang, Li (2006): Influence of angiogenin on the growth of A375 human melanoma cells and the expression of basic fibroblast growth factor. In *Melanoma research* 16 (2), pp. 119–126. DOI: 10.1097/01.cmr.0000215029.62199.4c.

Sorani, Marco D.; Zador, Zsolt; Hurowitz, Evan; Yan, Donghong; Giacomini, Kathleen M.; Manley, Geoffrey T. (2008): Novel variants in human Aquaporin-4 reduce cellular water permeability. In *Hum Mol Genet* 17 (15), pp. 2379–2389. DOI: 10.1093/hmg/ddn138.

Srinivasan, Balaji; Kolli, Aditya Reddy; Esch, Mandy Brigitte; Abaci, Hasan Erbil; Shuler, Michael L.; Hickman, James J. (2015): TEER measurement techniques for in vitro barrier model systems. In *Journal of laboratory automation* 20 (2), pp. 107–126. DOI: 10.1177/2211068214561025.

Stamatovic, Svetlana M.; Johnson, Allison M.; Keep, Richard F.; Andjelkovic, Anuska V. (2016): Junctional proteins of the blood-brain barrier: New insights into function and dysfunction. In *Tissue barriers* 4 (1), e1154641. DOI: 10.1080/21688370.2016.1154641.

Stan, R. V. (2007): Endothelial stomatal and fenestral diaphragms in normal vessels and angiogenesis. In *Journal of cellular and molecular medicine* 11 (4), pp. 621–643. DOI: 10.1111/j.1582-4934.2007.00075.x.

Staud, Frantisek; Ceckova, Martina; Micuda, Stanislav; Pavek, Petr (2010): Expression and Function of P-Glycoprotein in Normal Tissues: Effect on Pharmacokinetics. In Jun Zhou (Ed.): *Multi-Drug Resistance in Cancer*. Totowa, NJ: Humana Press, pp. 199–222.

Staud, Frantisek; Pavek, Petr (2005): Breast cancer resistance protein (BCRP/ABCG2). In *The international journal of biochemistry & cell biology* 37 (4), pp. 720–725. DOI: 10.1016/j.biocel.2004.11.004.

Strilic, Boris; Yang, Lida; Albarrán-Juárez, Julián; Wachsmuth, Laurens; Han, Kang; Müller, Ulrike C. et al. (2016): Tumour-cell-induced endothelial cell necroptosis via death receptor 6 promotes metastasis. In *Nature* 536 (7615), pp. 215–218. DOI: 10.1038/nature19076.

Summers, Lauren; Kangwantas, Korakoch; Rodriguez-Grande, Beatriz; Denes, Adam; Penny, Jeffrey; Kielty, Cay; Pinteaux, Emmanuel (2013): Activation of brain endothelial cells by interleukin-1 is regulated by the extracellular matrix after acute brain injury. In *Molecular and Cellular Neuroscience* 57, pp. 93–103. DOI: 10.1016/j.mcn.2013.10.007.

Sun, Xiaoyan; Li, Jun; Sun, Yanhong; Zhang, Yi; Dong, Liyun; Shen, Chen et al. (2016): miR-7 reverses the resistance to BRAFi in melanoma by targeting EGFR/IGF-1R/CRAF and inhibiting the MAPK and PI3K/AKT signaling pathways. In *Oncotarget* 7 (33), pp. 53558–53570. DOI: 10.18632/oncotarget.10669.

Sundararaj, Srinivasan; Ravindran, Agin; Casarotto, Marco G. (2021): AHNAK: The quiet giant in calcium homeostasis. In *Cell calcium* 96, p. 102403. DOI: 10.1016/j.ceca.2021.102403.

Sweeney, Melanie D.; Ayyadurai, Shiva; Zlokovic, Berislav V. (2016): Pericytes of the neurovascular unit: key functions and signaling pathways. In *Nature neuroscience* 19 (6), pp. 771–783. DOI: 10.1038/nn.4288.

Sweeney, Melanie D.; Sagare, Abhay P.; Zlokovic, Berislav V. (2018): Blood–brain barrier breakdown in Alzheimer disease and other neurodegenerative disorders. In *Nature Reviews Neurology* 14 (3), pp. 133–150. DOI: 10.1038/nrneuro.2017.188.

- Sweeney, Melanie D.; Zhao, Zhen; Montagne, Axel; Nelson, Amy R.; Zlokovic, Berislav V. (2019): Blood-Brain Barrier: From Physiology to Disease and Back. In *Physiological reviews* 99 (1), pp. 21–78. DOI: 10.1152/physrev.00050.2017.
- Szokol, Karolina; Heuser, Kjell; Tang, Wannan; Jensen, Vidar; Enger, Rune; Bedner, Peter et al. (2015): Augmentation of Ca(2+) signaling in astrocytic endfeet in the latent phase of temporal lobe epilepsy. In *Frontiers in cellular neuroscience* 9, p. 49. DOI: 10.3389/fncel.2015.00049.
- Tawbi, Hussein A.; Boutros, Celine; Kok, David; Robert, Caroline; McArthur, Grant (2018): New Era in the Management of Melanoma Brain Metastases. In *American Society of Clinical Oncology Educational Book* (38), pp. 741–750. DOI: 10.1200/EDBK_200819.
- Tenreiro, M. M.; Ferreira, R.; Bernardino, L.; Brito, M. A. (2016): Cellular response of the blood-brain barrier to injury: Potential biomarkers and therapeutic targets for brain regeneration. In *Neurobiology of disease* 91, pp. 262–273. DOI: 10.1016/j.nbd.2016.03.014.
- Thompson, Anthony; Nessler, Randy; Wisco, Dolora; Anderson, Eric; Winckler, Bettina; Sheff, David (2007): Recycling Endosomes of Polarized Epithelial Cells Actively Sort Apical and Basolateral Cargos into Separate Subdomains. In *Molecular biology of the cell* 18 (7), pp. 2687–2697. DOI: 10.1091/mbc.e05-09-0873.
- Thurgur, Hannah; Pinteaux, Emmanuel (2019): Microglia in the Neurovascular Unit: Blood-Brain Barrier-microglia Interactions After Central Nervous System Disorders. In *Neuroscience* 405, pp. 55–67. DOI: 10.1016/j.neuroscience.2018.06.046.
- Tontsch, Ulrike; Bauer, Hans-Christian (1991): Glial cells and neurons induce blood-brain barrier related enzymes in cultured cerebral endothelial cells. In *Brain research* 539 (2), pp. 247–253. DOI: 10.1016/0006-8993(91)91628-E.
- Tremblay, P-L; Auger, F. A.; Huot, J. (2006): Regulation of transendothelial migration of colon cancer cells by E-selectin-mediated activation of p38 and ERK MAP kinases. In *Oncogene* 25 (50), pp. 6563–6573. DOI: 10.1038/sj.onc.1209664.
- Uemura, Maiko T.; Maki, Takakuni; Ihara, Masafumi; Lee, Virginia M. Y.; Trojanowski, John Q. (2020): Brain Microvascular Pericytes in Vascular Cognitive Impairment and Dementia. In *Frontiers in aging neuroscience* 12, p. 80. DOI: 10.3389/fnagi.2020.00080.

Valent, P.; Groner, B.; Schumacher, U.; Superti-Furga, G.; Busslinger, M.; Kralovics, R. et al. (2016): Paul Ehrlich (1854-1915) and His Contributions to the Foundation and Birth of Translational Medicine. In *J Innate Immun* 8 (2), pp. 111–120. DOI: 10.1159/000443526.

Vandenhoute, Elodie; Drolez, Aurore; Sevin, Emmanuel; Gosselet, Fabien; Mysiorek, Caroline; Dehouck, Marie-Pierre (2016): Adapting coculture in vitro models of the blood-brain barrier for use in cancer research: maintaining an appropriate endothelial monolayer for the assessment of transendothelial migration. In *Laboratory investigation; a journal of technical methods and pathology* 96 (5), pp. 588–598. DOI: 10.1038/labinvest.2016.35.

Vasileva, Ekaterina; Rouaud, Florian; Spadaro, Domenica; Huang, Wenmao; Colom, Adai; Flinois, Arielle et al. (2020): Cingulin unfolds ZO-1 and organizes myosin-2B and γ -actin to mechanoregulate apical and tight junction membranes. In *bioRxiv*, 2020.05.14.095364. DOI: 10.1101/2020.05.14.095364.

Vasiliou, Vasilis; Vasiliou, Konstandinos; Nebert, Daniel W. (2009): Human ATP-binding cassette (ABC) transporter family. In *Human genomics* 3 (3), pp. 281–290. DOI: 10.1186/1479-7364-3-3-281.

Verkhratsky, Alexei; Matteoli, Michela; Parpura, Vladimir; Mothet, Jean-Pierre; Zorec, Robert (2016): Astrocytes as secretory cells of the central nervous system: idiosyncrasies of vesicular secretion. In *The EMBO journal* 35 (3), pp. 239–257. DOI: 10.15252/embj.201592705.

Vestweber, Dietmar; Winderlich, Mark; Cagna, Giuseppe; Nottebaum, Astrid F. (2009): Cell adhesion dynamics at endothelial junctions: VE-cadherin as a major player. In *Trends in cell biology* 19 (1), pp. 8–15. DOI: 10.1016/j.tcb.2008.10.001.

Voura, Evelyn B.; English, Jane L.; Yu, Hoi-Ying E.; Ho, Andrew T.; Subarsky, Patrick; Hill, Richard P. et al. (2013): Proteolysis during tumor cell extravasation in vitro: metalloproteinase involvement across tumor cell types. In *PLoS one* 8 (10), e78413. DOI: 10.1371/journal.pone.0078413.

Walts, A. E.; Said, J. W.; Shintaku, I. P. (1988): Cytodiagnosis of malignant melanoma. Immunoperoxidase staining with HMB-45 antibody as an aid to diagnosis. In *American journal of clinical pathology* 90 (1), pp. 77–80. DOI: 10.1093/ajcp/90.1.77.

Wang, Zhaoqing; Xu, Qingji; Zhang, Nengwei; Du, Xuemei; Xu, Guangzhong; Yan, Xiyun (2020): CD146, from a melanoma cell adhesion molecule to a signaling receptor. In *Signal transduction and targeted therapy* 5 (1), p. 148. DOI: 10.1038/s41392-020-00259-8.

Weber, Martin R.; Zuka, Masahiko; Lorgier, Mihaela; Tschan, Mario; Torbett, Bruce E.; Zijlstra, Andries et al. (2016): Activated tumor cell integrin $\alpha\beta3$ cooperates with platelets to promote extravasation and metastasis from the blood stream. In *Thrombosis research* 140 Suppl 1 (Suppl 1), S27-36. DOI: 10.1016/S0049-3848(16)30095-0.

Weidenfeller, Christian; Svendsen, Clive N.; Shusta, Eric V. (2007): Differentiating embryonic neural progenitor cells induce blood–brain barrier properties. In *J Neurochem* 101 (2), pp. 555–565. DOI: 10.1111/j.1471-4159.2006.04394.x.

Weinstein, David; Leininger, Jennifer; Hamby, Carl; Safai, Bijan (2014): Diagnostic and prognostic biomarkers in melanoma. In *The Journal of clinical and aesthetic dermatology* 7 (6), pp. 13–24.

Weinstein, Jonathan R.; Koerner, Ines P.; Möller, Thomas (2010): Microglia in ischemic brain injury. In *Future neurology* 5 (2), pp. 227–246. DOI: 10.2217/fnl.10.1.

Weksler, B. B.; Subileau, E. A.; Perrière, N.; Charneau, P.; Holloway, K.; Leveque, M. et al. (2005): Blood-brain barrier-specific properties of a human adult brain endothelial cell line. In *The FASEB Journal* 19 (13), pp. 1872–1874. DOI: 10.1096/fj.04-3458fje.

Weksler, Babette; Romero, Ignacio A.; Couraud, Pierre-Olivier (2013): The hCMEC/D3 cell line as a model of the human blood brain barrier. In *Fluids and barriers of the CNS* 10 (1), p. 16. DOI: 10.1186/2045-8118-10-16.

Wolburg, Hartwig; Lippoldt, Andrea (2002): Tight junctions of the blood–brain barrier: development, composition and regulation. In *Vascular Pharmacology* 38 (6), pp. 323–337. DOI: 10.1016/S1537-1891(02)00200-8.

Wolburg, Hartwig; Noell, Susan; Mack, Andreas; Wolburg-Buchholz, Karen; Fallier-Becker, Petra (2009): Brain endothelial cells and the glio-vascular complex. In *Cell and tissue research* 335 (1), pp. 75–96. DOI: 10.1007/s00441-008-0658-9.

Wolf, Monika Julia; Hoos, Alexandra; Bauer, Judith; Boettcher, Steffen; Knust, Markus; Weber, Achim et al. (2012): Endothelial CCR2 signaling induced by colon carcinoma cells

enables extravasation via the JAK2-Stat5 and p38MAPK pathway. In *Cancer cell* 22 (1), pp. 91–105. DOI: 10.1016/j.ccr.2012.05.023.

Yamada, Eichi (1955): The Fine Structure of the Renal Glomerulus of the Mouse. In *The Journal of Biophysical and Biochemical Cytology* 1 (6), pp. 551–566. Available online at <http://www.jstor.org/stable/1602923>.

Yan, Serena L. S.; Hwang, Il-Young; Kamenyeva, Olena; Kehrl, John H. (2019): In Vivo F-Actin Filament Organization during Lymphocyte Transendothelial and Interstitial Migration Revealed by Intravital Microscopy. In *iScience* 16, pp. 283–297. DOI: 10.1016/j.isci.2019.05.040.

Zakrzewski, Jan; Geraghty, Laurel N.; Rose, Amy E.; Christos, Paul J.; Mazumdar, Madhu; Polsky, David et al. (2011): Clinical variables and primary tumor characteristics predictive of the development of melanoma brain metastases and post-brain metastases survival. In *Cancer* 117 (8), pp. 1711–1720. DOI: 10.1002/cncr.25643.

Zaragozá, Rosa (2020): Transport of Amino Acids Across the Blood-Brain Barrier. In *Frontiers in physiology* 11, p. 973. DOI: 10.3389/fphys.2020.00973.

Zhang, Chenyu; Lowery, Frank J.; Yu, Dihua (2017): Intracarotid Cancer Cell Injection to Produce Mouse Models of Brain Metastasis. In *Journal of visualized experiments : JoVE* (120). DOI: 10.3791/55085.

Zhang, Yue; Ding, Xiaowei; Miao, Changhong; Chen, Jiawei (2019): Propofol attenuated TNF- α -modulated occludin expression by inhibiting Hif-1 α / VEGF/ VEGFR-2/ ERK signaling pathway in hCMEC/D3 cells. In *BMC Anesthesiology* 19 (1), p. 127. DOI: 10.1186/s12871-019-0788-5.

Zhao, Zhen; Nelson, Amy R.; Betsholtz, Christer; Zlokovic, Berislav V. (2015): Establishment and Dysfunction of the Blood-Brain Barrier. In *Cell* 163 (5), pp. 1064–1078. DOI: 10.1016/j.cell.2015.10.067.

Zhong, Y.; Saitoh, T.; Minase, T.; Sawada, N.; Enomoto, K.; Mori, M. (1993): Monoclonal antibody 7H6 reacts with a novel tight junction-associated protein distinct from ZO-1, cingulin and ZO-2. In *J Cell Biol* 120 (2), pp. 477–483. DOI: 10.1083/jcb.120.2.477.

Zhou, Heling; Zhao, Dawen (2014): Ultrasound imaging-guided intracardiac injection to develop a mouse model of breast cancer brain metastases followed by longitudinal MRI. In *Journal of visualized experiments : JoVE* (85). DOI: 10.3791/51146.

Zhou, Min; Shi, Samuel X.; Liu, Ning; Jiang, Yinghua; Karim, Mardeen S.; Vodovoz, Samuel J. et al. (2021): Caveolae-Mediated Endothelial Transcytosis across the Blood-Brain Barrier in Acute Ischemic Stroke. In *Journal of clinical medicine* 10 (17). DOI: 10.3390/jcm10173795.

Zimmermann, K. W. (1923): Der feinere Bau der Blutcapillaren. In *Zeitschrift für Anatomie und Entwicklungsgeschichte* 68 (1), pp. 29–109. DOI: 10.1007/BF02593544.